DISTINCT FUNCTIONAL PROPERTIES OF PERINATAL VERSUS ADULT ADIPOSE PROGENITOR SUBPOPULATIONS

APPROVED BY SUPERVISORY COMMITTEE

Rana K. Gupta, Ph.D., Advisor

Philipp Scherer, Ph.D.

Joel K. Elmquist, D.V.M. Ph.D.

Perry E. Bickel, M.D.

Gary Hon, Ph.D.

Dayoung Oh, Ph.D. （Chair）

DEDICATION

To my fiancé Yang (Antony) Liu,

My parents Bojun Zhang and Zhishu Huang,

and our two Japanese Akita Inus, Kanna and Kilua

# DISTINCT FUNCTIONAL PROPERTIES OF PERINATAL VERSUS ADULT ADIPOSE PROGENITOR SUBPOPULATIONS

by

QIANBIN ZHANG

DISSERTATION

Presented to the Faculty of the Graduate School of Biomedical Sciences

The University of Texas Southwestern Medical Center at Dallas

In Partial Fulfillment of the Requirements

For the Degree of

DOCTOR OF PHILOSOPHY

The University of Texas Southwestern Medical Center at Dallas

Dallas, Texas

May, 2022

ACKNOWLEDGEMENT

I am very grateful to come this far and achieve more than I have ever wished for. This was only possible with the support of those to whom I would like to express my sincere gratitude.

I want to thank my mentor Dr. Rana K. Gupta. He provided me with extraordinary guidance, support, opportunities, and trust throughout my four and half years in the lab. I received tremendous training here, from experimental skills, to thinking, expressing, and writing in a scientific manner. He also built a lab that is the most ideal place to work in, lab members exchange thoughts, collaborate on experiments, help out when others needed- like friends, like families. Chelsea was the first graduate student in the lab, and I was very fortunate to shadow her during my rotation. She taught me the magic trick of "time"—be fast and you will find everything working out. Besides many experimental techniques, she also set a great example for me regarding how to communicate with Rana. I started with feeling a gap between a mentor and a student, but Chelsea proved to me that I can walk up to Rana and talk to him in a straightforward manner. Mengle and Bo, the two greatest researchers I have worked with, provided me detailed guidance on almost every experiment I did, from genotyping to cell transplantation surgeries. Lavanya, we call her Lavy, is the sweetest of all. She is always patient when teaching me new things and accompanies me when I am working on frustrating experiments. Mengle, Bo and Lavy are the three lab members that I've sticked with for the entire time. Best of all, we have been good friends outside the lab. Special thanks to George, who was assigned to me as my "technician" for the last year. He helped me with

massive amounts of genotyping as well as mouse husbandry. Thanks to Ashley, Pablo, Maggie, Jasmine, Bethany and Jessica- I very much enjoyed working with all of you.

I want to thank the Touchstone Diabetes Center. My discussions with members of the center and the Tuesday Seminars really broadened my knowledge about the field, especially at the beginning of my graduate school career. I also want to thank the core facilities of UTSW Medical Center: Vanessa and the McDermott Sequencing Core, John and the Histopathology Core, Andy and the Proteomics Core, and the most special one to me: Angie and the Flow Cytometry Core. Angie, Alyssa, Debora, and Mason, together helped me with hundreds of sorting hours, which is the foundation of my work. Moreover, chatting and sharing things around us have always been a necessary pleasure for me while waiting for the sort to be done.

I would also like to thank the Genes, Development, and Diseases graduate program; especially Amy for graduate school administrative supports. I also thank Drs. Oh, Scherer, Bickel, Elmquist, and Hon, for their time and commitment as committee members, and for their suggestions that advanced my studies.

I have learned here that life is equally important to work, and being happy and healthy is a must. I want to thank my friends and families in China; apparently distance and time-zones were not able to keep us apar. Special thanks to Oliva, who I have known for 19 years. The fact that we can go straight into any conversation no matter how long it's been since we met assures me whenever I feel lost. Thank you, mom and dad. I feel guided by them no matter how far I am from home. Heartful thanks to my grandparents Meichu Zhao and Jichun Huang, as well as my grandmother Shifeng Li. They supported me regardless of

not having a clue what I am pursuing. I want to also express gratitude to Mr. and Mrs. Glock in Austin TX. Mrs. Glock was my kindergarten teacher in 2000. We built our strong bound from there, and I felt blessed being able to attend family events and spend holidays with them. It always made me feel strong to know that I have a local family.

I am also very grateful to the friends I have made during my time in Dallas. I am very fortunate to have Yujing as my first roommate; we have been best friends ever since. With her, I was able to make the best of entering a new environment. I am also very lucky to find companions for boardgames, script-games, League of Legends, camping, etc. They all contributed to a bright and beautiful living experience.

Finally, I come to my core personal family: Yang and our two Japanese Akita Inus, Kanna and Kilua. I have to use the word “indescribable” for Yang. He is my beloved significant other. I couldn’t ask for anyone better; we share the same attitude towards many things, including food, science, family, and the future. We also collide on many other topics but always ends up knowing each other better. Thank you for taking my hand and I am very delighted to have you in the future. Kanna is the world’s most perfect dog ever. She is beautiful, elegant, calm, and strong. Kilua is a newly introduced puppy to the family. He is handsome, smart, active, and always happy. Their greetings wash away everything negative from me, and light up the warmth in where I call home.

If there is anything I would praise myself for, it is my genuineness. I sincerely thank all of you for guiding me to keep this personality as I chase after my desires.

DISTINCT FUNCTIONAL PROPERTIES OF PERINATAL VERSUS ADULT ADIPOSE PROGENITOR SUBPOPULATIONS

Qianbin Zhang, Ph.D.

The University of Texas Southwestern Medical Center at Dallas, 2022

Supervising Professor: Rana K. Gupta, Ph.D.

The manner in which energy-storing white adipose tissue (WAT) expands and remodels in obesity is tightly linked to the development of metabolic syndrome. The recruitment of new fat cells ensures adequate energy storage in WAT and prevents against ectopic lipid accumulation and is therefore considered as “healthy expansion”. Pathologic WAT expansion is characterized by chronic tissue inflammation and fibrosis, and is tightly linked to the development of diabetes.

Our lab previously identified functionally distinct subpopulations of PDGFRβ+ perivascular progenitor cells within adult WAT depots that differentially impact tissue remodeling in obesity. PDGFRb+ APCs contribute to adipocyte hyperplasia associated with

diet-induced obesity, whereas PDGFRb+ fibro-inflammatory progenitors, or "FIPs," regulate collagen deposition and inflammation in pathophysiological settings.

My work aims to understand when and where these distinct cells emerge during the initial period of WAT development, and how manipulating the fate and function of these progenitors during the perinatal period can influence metabolism in adulthood. I used single-cell transcriptomics to unveil the cellular landscape of the perinatal murine epididymal WAT (eWAT) primordium. I reveal that adipocyte precursor cells (APCs) and fibro-inflammatory progenitors (FIPs) emerge as functionally distinct PDGFRb+ subpopulations within the eWAT anlagen prior to adipocyte accrual, at postnatal day 3 (P3). Importantly, I identify important molecular and functional differences between perinatal and adult FIPs, including differences in their pro-inflammatory response, adipogenic capacity, and anti-adipogenic behavior. Additionally, I found that transient overexpression of *Pparg* in PDGFRβ+ cells only during postnatal day 0.5 to 7.5 leads to hyperplastic WAT development, durable progenitor cell reprogramming, and protection against pathologic wat remodeling and glucose intolerance in adult-onset obesity. Thus, factors that alter the adipogenic capacity of perinatal adipose progenitors can have long-lasting effects on progenitor plasticity, tissue expandability, and metabolic health into adulthood.

TABLE OF CONTENTS

PRIOR PUBLICATIONS

1. **Qianbin Zhang**, Bo Shan*, Lei Guo*, Mengle Shao, Lavanya Vishvanath, Lin Xu & Rana K. Gupta. “Distinct Functional Properties of Perinatal versus Adult Adipose Progenitor Subpopulations.” *Nature metabolism (Under revision)*
2. Bo Shan*, Clive S. Barker*, Mengle Shao*, **Qianbin Zhang**, Rana K. Gupta, Yibo Wu. “Multilayered omics Reveal Sex- and Depot-Dependent Adipose Progenitor Cell Heterogeneity.” *Cell metabolism (Accepted)*
3. Shao Mengle*, **Qianbin Zhang***, Ashley Truong, Bo Shan, Lavanya Vishvanath, Lin Li, Patrick Seale, and Rana K. Gupta. "ZFP423 controls EBF2 coactivator recruitment and PPARγ occupancy to determine the thermogenic plasticity of adipocytes." *Genes & Development* 35, no. 21-22 (2021): 1461-1474.
4. Shan Bo*, Mengle Shao*, **Qianbin Zhang**, Yu A. An, Lavanya Vishvanath, and Rana K. Gupta. "Cold-responsive adipocyte progenitors couple adrenergic signaling to immune cell activation to promote beige adipocyte accrual." *Genes & Development* 35, no. 19-20 (2021): 1333-1338.
5. Shao Mengle*, Chelsea Hepler*, **Qianbin Zhang**, Bo Shan, Lavanya Vishvanath, Gervaise H. Henry, Shangang Zhao, Yu A. An, Yibo Wu, Douglas W. Strand, Rana K. Gupta. "Pathologic HIF1α signaling drives adipose progenitor dysfunction in obesity." *Cell Stem Cell* 28, no. 4 (2021): 685-701.
6. Joffin Nolwenn, Vivian A. Paschoal, Christy M. Gliniak, Clair Crewe, Abdallah Elnwasany, Luke I. Szweda, **Qianbin Zhang**， Chelsea Hepler, Christine M. Kusminski, Ruth Gordillo, Da Young Oh, Rana K. Gupta, Philipp E. Scherer. "Mitochondrial metabolism is a key regulator of the fibro-inflammatory and adipogenic stromal subpopulations in white adipose tissue." *Cell Stem Cell* 28, no. 4 (2021): 702-717.
7. Shan Bo*, Mengle Shao*, **Qianbin Zhang**, Chelsea Hepler, Vivian A. Paschoal, Spencer D. Barnes, Lavanya Vishvanath, Yu A. An, Lin Jia, Venkat S. Malladi, Douglas W. Strand, Olga T. Gupta, Joel K. Elmquist, Dayoung Oh & Rana K. Gupta. "Perivascular mesenchymal cells control adipose-tissue macrophage accrual in obesity." *Nature metabolism* 2, no. 11 (2020): 1332-1349.
8. Peics Julia*, Lavanya Vishvanath*, **Qianbin Zhang**, Bo Shan, Thomas Å. Pedersen, and Rana K. Gupta. "Isolation of adipogenic and fibro-inflammatory stromal cell subpopulations from murine intra-abdominal adipose depots." *JoVE (Journal of Visualized Experiments)* 162 (2020): e61610.
9. Hepler Chelsea, Bo Shan, **Qianbin Zhang**, Gervaise H. Henry, Mengle Shao, Lavanya Vishvanath, Alexandra L. Ghaben et al. "Identification of functionally distinct fibro-inflammatory and adipogenic stromal subpopulations in visceral adipose tissue of adult mice." *Elife* 7 (2018): e39636.

LIST OF FIGURES

**CHAPTER ONE**



**CHAPTER TWO**



**CHAPTER THREE**

**CHAPTER FOUR**

LIST OF TABLES

**CHAPTER TWO**



**CHAPTER THREE**

LIST OF ABBREVIATIONS

APCs – Adipocyte precursor cells

BAT – brown adipose tissue

ChIP –chromatin immunoprecipitation

DMI – dexamethasone, 3-isobutyl-1-methylxanthine, and insulin

DOX – doxycycline

eWAT – epididymal white adipose tissue

FACS – fluorescence-activated cell sorting

FIPs – fibro-inflammatory progenitors

HFD – high fat diet

IL33 – interleukin33

iWAT – inguinal white adipose tissue

MLCs – mesothelial like cells

PDGFRβ – platelet derived growth factor receptor beta

PPARγ – peroxisome proliferator- activated receptor gamma

Rosi – rosiglitazone

rtTA – reverse tetracycline transactivator

scRNA-seq – singlr-cell RNA-sequencing

SMCs – smooth muscle cells

SVF – stromal vascular fraction

vWAT– visceral white adipose tissue

# CHAPTER ONE

## INTRODUCTION

*(This section contains content from a manuscript in preparation for Cell Metabolism)*

### The Role of Adipose tissue in the Regulation of Energy Balance

Throughout evolution, organisms have evolved mechanisms for energy storage that ensure nutrient availability in times of energy deficit. The evolution of fat cells, or "adipocytes," in mammals provided a safe compartment for the storage of excess energy in the form of triglyceride. Placental mammals possess two classes of adipocytes. "White" adipocytes are characterized by the presence of a single large lipid droplet. These cells have the capacity to convert glucose and fatty acids to triglyceride in times of nutrient excess. Adipocytes also can hydrolyze stored lipids to free fatty acids in times to increased energy demand. "Brown" and "beige" adipocytes represent a distinct class of energy-burning, heat-producing (or "thermogenic") fat cells. Thermogenic fat cells are characterized by their multi-locular fat droplet appearance, high mitochondrial content, and presence of cellular mechanisms that enable futile energy cycling (e.g. UCP1). These cells likely evolved as a mechanism to defend against cold environmental temperatures. Importantly, adipose tissue is an endocrine organ; adipocyte secrete hormones and peptides ("adipokines") that enable cross talk with other organs such as the brain, liver, heart, and pancreas (Rosen and Spiegelman 2014). For example, Leptin is secreted almost exclusively by adipocytes, generally in proportion to adiposity. This hormone serves as a major regulator of food intake and promotes energy expenditure through central mechanisms. Animals and humans with

mutations in either Leptin or the Leptin Receptor are obese (Unger 2005). The initial discovery of leptin and its role in regulating food intake revealed the ability of adipose tissue to regulate energy balance in ways other than energy storage. Leptin also acts on peripheral tissues (muscle, adipose, liver) to regulate glucose and lipid homeostasis. Adiponectin is another well-characterized adipokine (Scherer, Williams et al. 1995, Hu, Liang et al. 1996). Adiponectin secretion from adipocytes promotes insulin sensitivity and prevents against ectopic lipid accumulation in non-adipose tissues. The importance of functional adipose tissue is highlighted by the condition of lipodystrophy (Mann and Savage 2019). Lipodystrophy can occur because of failure in the development of adipocytes ("adipogenesis") or inability to synthesize triglyceride (lipogenesis). When excess energy is not stored in adipose due to lipodystrophy, fatty acids will overflow into non-adipose tissues, including skeletal muscle, heart, pancreas, and liver. This ectopic lipid deposition is deleterious, as accumulated lipid species (e.g. ceramides and diacylglycerols) can interfere with insulin signaling pathways and other functions of the tissues (initially termed, "lipotoxicity" by the late Dr. Unger)(Unger 2005). Therefore, individuals with lipodystrophy have dys-functional adipocytes and are generally quite thin and develop hepatic steatosis and severe diabetes. As such, adipocytes are essential. They play a critical role in the regulation of all aspects of energy balance; functioning as a metabolic sensor that controls energy storage, energy utilization, and food intake.

**The Obesity Pandemic**

Obesity is a disorder of energy balance resulting in the excessive expansion of energy-storing white adipose tissue. Obesity is diagnosed when body mass index (BMI) exceeds 30 or higher (Engin 2017). The condition of obesity highlights the tremendous and unique ability of energy storing white WAT to expand in mass. The expansion of adipose tissue in the face of overnutrition is a necessary consequence of the increased demand for energy storage (Cohen and Spiegelman 2016). Nevertheless, the condition of obesity is closely linked to the development of *Metabolic Syndrome*: a cluster of chronic conditions including dyslipidemia, hypertension, and hyperglycemia (Ghaben and Scherer 2019).

Today, obesity is a global epidemic and a major contributor to many leading causes of death including heart disease, stroke, diabetes, and cancers. Moreover, the condition of obesity significantly increases risk for severe complications resulting from SARS Co-V2 infection (Stefan, Birkenfeld et al. 2021). According to the CDC, over one-third (~35%) of adults in the United States are obese. It is predicted that by 2030 nearly 42% of the population will be obese, with rates above 60% in 12 states (Hales, Carroll et al. 2020). Strikingly, obesity is not only a concern in adults, but is increasingly evidence in more and more children and even infants. The rise of childhood obesity has linked hypertension and type II diabetes, to earlier and earlier onset ages, which was not thought to be common (Flynn 2013). More importantly, obese children are likely to stay obese into adulthood (Gordon-Larsen, The et al. 2010), which results in a longer progression and higher risks of more severe disease conditions (Bass and Eneli 2015). The estimated medical costs for treating obesity and associated illnesses is between $147-$210 billion a year.

**Adipose Tissue Distribution and the Development of Metabolic Disease**

Interestingly, not all individuals with obesity develop metabolic disease. In fact, a large proportion of individuals with obesity remain insulin sensitive, at least for a period of time (Kloting, Fasshauer et al. 2010, Smith, Mittendorfer et al. 2019). This suggests that factors outside of increased BMI *per se* trigger metabolic disease. Great effort is now placed on understanding all aspects of adipose tissue biology, including the function of adipocytes, how adipose tissue expands in obesity, and how expanded adipose tissues in adults can impact physiology.

Epidemiological studies have focused on elucidating better predictors of metabolic syndrome in the setting of obesity. These efforts have led to the concepts that *WHERE* adipose tissue expands is a key determinant of metabolic health. White adipocytes can be found throughout the body but is invariably organized into anatomically distinct "depots". In general, white adipose depots appear in subcutaneous regions or within the intra-abdominal area while BAT accumulates in distinct regions (Figure 1). Subcutaneous white adipose depots in part provide support and cushioning to surrounding organs include orbital fat, cranial fat, and fat in heel pad (Hepler and Gupta 2017, Cypess 2022). The mostly studied subcutaneous depot in humans is the gluteofemoral fat depot, whose expansion results of in a "pear-shaped" body fat distribution (Jensen 2008). On the other hand, preferential expansion of intrabdominal, or visceral, WAT depots results in an "apple-shaped" body fat distribution. It is widely appreciated that in obesity, "apple-shaped" fat distribution is closely linked with metabolic complications, while "pear-shaped" obese individuals appear relatively protected against the development of insulin resistance, at least for a period of time (termed

"metabolically healthy"). The exact reasons why body fat distribution impacts disease susceptibility is still unclear; however, it may be due to location of the depots (e.g. portal delivery of pro-inflammatory cytokines) or intrinsic properties of subcutaneous vs. visceral adipocytes. Another important factor in body fat distribution is sex hormone; however, recent human GWAS studies implicate genetics in the determination of body fat distribution (Shungin, Winkler et al. 2015, Lotta, Wittemans et al. 2018). A notable finding from the work of O'Rahilly and colleagues is that those genes linked to body fat distribution and insulin resistance encode factors controlling adipogenesis and adipocyte function. This highlights the need to better understand the biology of adipocyte progenitor cells and the mechanisms controlling their differentiation in anatomically distinct regions.

The expansion of adipose tissue mass is driven by an increased in both adipocyte number (cellular hyperplasia) and adipocyte size (adipocyte hypertrophy). Adipocytes are post mitotic; therefore, an increase in adipocyte number is dependent on de novo adipocyte differentiation from adipocyte precursor cells, or "APCs." Moreover, WAT expansion in obesity is accompanied by extensive tissue remodeling, including alterations in immune cell composition and extracellular matrix reorganization. It is now widely appreciated that the manner by which adipose expands and remodels is tightly linked to the development of metabolic syndrome (Sun, Kusminski et al. 2011). Pathologic WAT expansion, associated with insulin resistance, is characterized the presence of large hypertrophic adipocytes. This suggests that there is an inadequate level of de novo adipogenesis while the existing adipocytes enlarge to store more lipid. The prevailing hypothesis is that enlarged adipocytes eventually become uncapable to store more lipid and lipid subsequently accumulates into

other organs and tissues such as muscle, liver and heart (Ghaben and Scherer 2019). Hypertrophic WAT is also linked with tissue hypoxia, inflammation, and fibrosis, which further accelerate the loss of tissue function. On the other hand, WAT in the "metabolically healthy" obese exhibits a healthier tissue phenotype, characterized by the presence of smaller and more numerous adipocytes. It is widely postulated that the recruitment of additional adipocytes through "adipogenesis" from adipocyte progenitor cells ensures safe energy storage in adipose, preserves tissue health (less inflammation and fibrosis), and protects against ectopic lipid deposition (Ghaben and Scherer 2019). As such, the activity of adipocyte precursor cells in adults in an important determinant of metabolic health in obesity. Understanding the identity of adipocyte precursor cells and their molecular and functional properties remains a high priority for the field of adipose tissue biology.

**Evolving methodologies to study adipocyte progenitors**

Much of our knowledge regarding of the cellular aspects of adipocyte differentiation and functional properties of mature adipocytes was derived from studies of immortalized fibroblast cell lines capable of undergoing adipocyte differentiation in vitro and upon transplantation in vivo. In the 1970's, Howard Green and colleagues derived clonal sublines of immortalized Swiss 3T3 mouse embryonic fibroblasts that exhibited potential to accumulate lipid and adopt an adipocyte-like morphology (Green and Meuth 1974). This discovery suggested that adipocytes arise from fibroblast-like cells through multiple steps, including lineage determination (the formation of "preadipocytes") and then terminal differentiation (transformation of a preadipocyte into a mature fat cell). One of these

sublines, termed 3T3-L1 cells, had subsequently become the most widely used model for study of adipocyte differentiation. 3T3-L1 cells are viewed as being a "committed" preadipocyte cell line. These cells are morphologically indistinguishable from less- or non-adipogenic fibroblasts but are highly competent to undergo adipogenesis. Other useful cellular models were also developed, including preadipogenic OP9 cells (Wolins, Quaynor et al. 2006) and multi-potential C3H10T1/2 cells (Tang, Otto et al. 2004). In response to a hormonal/pharmacological cocktail consisting of dexamethasone, iso-butyl-methyl-xanthine, and insulin (generally referred to as "DMI medium"), 3T3-L1 cells can differentiate into lipid-laden adipocytes that exhibit a molecular and functional phenotype resembling native adipocytes. 3T3-L1 cells remain a powerful model for many critical aspects of adipocyte biology. In fact, the discoveries of many transcription factors controlling adipogenesis, including the master regulatory protein PPARγ, have been identified through analysis in 3T3 cells (Chawla and Lazar 1994, Tontonoz, Hu et al. 1994). Nevertheless, there are notable limitations to the use of immortalized cells lines. In particular, the relationship between these cultured preadipocytes and adipose progenitors found in adult and fetal animals *in vivo* remains uncertain. Moreover, to what extent 3T3-L1 adipocytes can resemble any of the anatomically distinct white adipocytes found *in vivo* remains unclear.

In more recent years, the field has leveraged primary cell cultures of adipose tissue-derived fibroblasts. Studies from the 1970's revealed that adherent fibroblast-like cells within cultures of the adipose stromal vascular fraction (SVF) can be differentiated into mature adipocytes *in vitro* using largely the same conditions utilized for immortalized cells (Poznanski, Waheed et al. 1973, Van, Bayliss et al. 1976, Van Robin and Roncari 1977).

Cultured stromal cells from human and mouse WAT give rise to adipocytes that molecularly resemble adipocytes located in their tissue of origin (Tchkonia, Giorgadze et al. 2006, Macotela, Emanuelli et al. 2012). Notably, these cells can be isolated from genetic mouse models of interest, enabling critical gain and loss of function studies. Nevertheless, there are still numerous limitations to the use of cultured SVF cells as a model of adipose precursor biology. First, it is not clear if only certain subpopulations of adipose precursor cells may be selected through the culture process, and how these cells may change during the growth/passage of these cultures. Moreover, the kind of cell types that these precursors represent *in vivo* cannot easily be inferred from these culture systems. Importantly, the abilities of cultured cells to differentiate in vitro do not always reflect their capacity to differentiate in vivo under different physiological conditions.

In 2013, Scherer and colleagues reported the derivation and use of the "AdipoChaser" model; a doxycycline-inducible genetic lineage tracing system that enables a precise analysis of adipocyte turnover in mice and a quantitative measure of de novo adipogenesis occurring *in vivo* (Wang, Tao et al. 2013). This study reported the surprising finding that high-fat diet feeding of mice triggers adipocyte differentiation in a depot-selective manner. In the murine inguinal WAT depot of C57BL/6 male mice, relatively little de novo adipogenesis occurs upon high fat diet feeding. This depot expands almost exclusively through cellular hypertrophy. This is notable since primary SVF cells from this depot have a strong capacity to differentiate in vitro upon isolation. On the other hand, the expansion of the epididymal WAT depot in the same mice involves an appreciable degree of de novo adipogenesis. Interestingly, plastic-adherent SVF cells from this depot are more resistant to undergo

differentiation in culture. These observations suggested that the plastic-adherent SVF cells obtained through common isolation protocols do not entirely reflect native progenitor cells found in vivo and/or the signals that drive or inhibit adipogenesis in vivo are not recapitulated in a dish.

In 2008, Friedman and colleagues developed a strategy to prospectively purify adipocyte progenitor cells (APCs) from freshly isolated murine adipose SVF (i.e. before cell culture) (Rodeheffer, Birsoy et al. 2008). These authors utilized antibodies raised against known mesenchymal stem cell cell-surface proteins to identify and separate distinct cell populations within the SVF by fluorescent-activated cell sorting (FACS). Through this approach, they isolated and characterized two functionally distinct SVF subpopulations with adipogenic potential. Both populations are devoid of endothelial and hematopoietic markers (CD31 and CD45, respectively), in support of most lineage tracing studies indicating that most adipocytes arise from non-endothelial and non-hematopoietic lineages. Instead, both cell populations were positive for common mesenchymal stem cell markers, SCA1, CD34, and CD29, but distinguishable by the expression of CD24. Follow-up studies by Rodeheffer and colleagues indicated that the $CD24^+$ APCs represent a proliferative stem cell-like adipose progenitor population, whereas $CD24^-$ APCs appear to represent a more committed "preadipocyte" population that expresses lineage-selective genes such as *Pparg* and *Cebpa*. Upon transplantation, $CD24^+$ APCs give rise to $CD24^-$ APCs in route to becoming mature adipocytes adipocytes (Berry and Rodeheffer 2013). These data were important because they revealed the existence of hierarchical populations of adipose precursors residing within adult adipose tissue.

The FACS-based method to isolate $CD24^+$ and $CD24^-$ APCs provides a convenient approach to purify and study adipose precursors from various rodent models, using commercially available antibodies. Within the following years, multiple cell separation strategies emerged based on the expression of different cell surface receptors (e.g. platelet derived growth factor receptor alpha (PDGFRα) (Berry and Rodeheffer 2013). Nevertheless, one limitation to the approach lies in the inability to visualize these cells *in vivo* in their natural environment since the identification of APCs will depend on the use of multiple cell surface markers. Contemporaneous studies from the Graff lab established a complementary approach to identifying native adipocyte precursors in their native localization. Tang et al. postulated that cells within the SVF with the greatest adipogenic potential will be those cells with the highest expression of *Pparg*. Indeed, using a genetic reporter system of *Pparg* expression, they demonstrated that functional APCs can be isolated on the basis of *Pparg* expression and that *Pparg*-expressing APCs reside within the adipose tissue vasculature as a subset of perivascular "mural" cells (pericytes and vascular smooth muscle cells)(Tang, Zeve et al. 2008). In fact, the hypothesis that committed APCs reside within the adipose tissue vasculature was first suggested many decades ago using microscopy approaches. My mentor's postdoctoral studies supported this hypothesis. Using a genetic reporter mouse strain, Gupta et al discovered that APCs can be isolated based on the expression of *Zfp423*, an upstream regulator of *Pparg* expression in adipogenesis (Gupta, Arany et al. 2010). *Zfp423*-expressing cells can also be identified within the adipose tissue vasculature, appearing as a subset of peri-endothelial mesenchymal cells expressing platelet derived growth factor receptor beta (PDGFRβ). In 2016, the Gupta lab at UTSW extended this

hypothesis by performing pulse-chase genetic lineage tracing of *Pdgfrb*-expressing cells in vivo using (the "MuralChaser" mouse). Vishvanath et al. demonstrated that adipocytes emerging in the gonadal WAT depots upon high fat diet feeding originate from *Pdgfrb*-expressing cells (Shao, Vishvanath et al. 2018). This model thus represents another model (complementary to the AdipoChaser model) that allows for a quantitative analysis of adipocyte formation in mice.

**Single-ing out adipocyte precursor cells through single-cell RNA sequencing**

By 2018, multiple strategies to isolate adipocyte precursor cells existed; however, to what degree these described populations are overlapping was unclear. Moreover, whether additional/multiple APC populations exist in adipose tissue was known. Beginning in 2018, our understanding of the identity, function, and heterogeneity of APCs, had begun to change drastically due to the emergence of robust single-cell RNA sequencing (scRNA-seq) technology. Over the past 4 years alone, we have learned a great deal about the functional and molecular heterogeneity of adipose precursor cells in adult mice and humans. In particular, it is now clear that exact identity and heterogeneity of adipocyte precursors is both depot and sex-dependent and varies between mice and humans. Moreover, the previously described FACS strategies to isolate APCs actually purified heterogeneous pools of cells containing subpopulations exerting opposing functions. In the following paragraphs, I summarize the current knowledge of adipose precursor cell heterogeneity in mice. Single-cell RNA sequencing studies of multiple anatomically distinct adipose tissue depots (both BAT and WAT) have now been reported. A detailed discussion of each depot is beyond the scope

of my dissertation work. As such, I focus here on the current knowledge of mesenchymal stromal cell heterogeneity in the two best-characterized WAT depots in mice as examples: the subcutaneous inguinal WAT (iWAT) and intra-abdominal epididymal WAT (eWAT).

*Adipocyte Progenitor cell Hierarchy in iWAT*

The subcutaneous inguinal WAT depot in mice begins to develop in the late stages of fetal developed (~embryonic day 16.5) with primitive adipocytes emerging in proximity to a dense vascular network. Most adipocytes are differentiated in this depot by the time of birth, with lipid-filling occurring in the early postnatal period. As noted above, the SVF of this depot is a rich source of highly adipogenic fibroblasts. Contemporaneous studies from the laboratories of Granneman, Wolfrum, Depanke, and Seale, were the first to shed considerable insight the identity of APCs in this depot through scRNA-seq (Burl, Ramseyer et al. 2018, Schwalie, Dong et al. 2018, Merrick, Sakers et al. 2019). All three studies support the notion that adult iWAT harbors hierarchical subpopulations of adipocyte precursor cells that represent cells at different stages of lineage commitment. One subpopulation represents multipotent mesenchymal cells with stem cell-like characteristics. These cells have been referred to by many names, including “P1” (Wolfrum/Deplanke), “Group 1” or “interstitial progenitor cells” (Seale), and “APC2” (Granneman). In all three studies, in silico cell trajectory analysis predicted that these multipotent stem cells give rise to a lineage committed “preadipocyte” population termed as, “P2” (Wolfrum/Deplanke), “Group 2” or “Committed Preadipocytes” (Seale), and “APC1” (Granneman). Merrick et al. demonstrated that these multipotent cells can be identified based on DPP4 expression (DPP4+) and localize to the

interstitial region on the outer edge of the iWAT depot. The more committed preadipocytes (DPP4-) are enriched in the expression of *Pparg* and other lineage-selective genes and appear in proximity to the adipose vasculature. Functional studies of isolated cell subpopulations also supported this hypothesis. Both subpopulations exhibit adipogenic capacity *in vitro*; however, the committed preadipocytes (*Pparg*+) have a greater capacity to undergo adipocyte differentiation. Moreover, upon transplantation into mice, the multipotent cell subpopulation gives rise to more committed preadipocyte population in the process of forming adipocytes (Stefkovich, Traynor et al. 2021). These studies confirm and greatly extend the earlier findings by Rodeheffer that a progenitor cell hierarchy exists in adult iWAT. Importantly, human adipose tissue harbors stromal cell subpopulations closely resembling these murine APCs, suggesting that this progenitor cell hierarchy also exists in adult humans.

Our own work in the Gupta lab corroborates the findings of these scRNA-seq studies. We demonstrated that two distinct cell subpopulations reside amongst the pool of PDGFRβ+ cells in iWAT (Shao, Hepler et al. 2021). One subpopulation of cells, marked by DPP4 expression (DPP4+ PDGFRβ+ cells), is nearly identical to the multipotent progenitor cells described above. DPP4- PDGFRβ+ cells represent the committed preadipocyte fraction, enriched in the expression of *Pparg* and highly adipogenic in vitro and in vivo. Importantly, our analysis of scRNA-seq profiles revealed insight into the mechanisms restraining the ability of these subcutaneous adipose precursor cells to differentiate in vivo upon high fat diet feeding. We discovered that high fat diet feeding induces PPARγ S112 phosphorylation in PDGFRβ+ cells of the iWAT depot; this inhibitory phosphorylation event occurs to a

lower degree in eWAT progenitors, which retain adipogenesis capacity *in vivo*. We determined that this inhibitory PPARγ S112 phosphorylation is driven by HIF1α signaling, which drives APCs to adopt a fibrogenic, rather than adipogenic, phenotype. Remarkably, doxycycline-inducible inhibition of HIF1α signaling in *Pdgfrb*-expressing adipose progenitors of mice unlocks the adipogenic activity of iWAT APCs and promotes a metabolically healthy hyperplastic expansion of iWAT in obese mice.

*Non-adipogenic roles of adipocyte precursor cells subpopulations in iWAT*

Our group's expression analysis of these distinct PDGFRβ+ APC subpopulation identified an important non-adipogenic role for DPP4+ APCs in the context of cold-induced thermogenic remodeling (i.e. "browning") of iWAT. We observed that inguinal DPP4+ APCs, but not DPP4- APCs, exhibit a robust transcriptional response to acute cold challenge (Shan, Shao et al. 2021). This transcriptional response of DPP4+ APCs includes β-adrenergic receptor/CREB-dependent upregulation in the expression and secretion of the pro-thermogenic cytokine, IL33. scRNA-seq revealed that DPP4+ APCs represent the principal source of IL33 in iWAT. IL33 functions, at least in part, to promote eosinophil accumulation and the subsequent secretion of eosinophil-derived met-enkephalin peptides which promote beige adipocyte accumulation (Brestoff, Kim et al. 2015). Doxycyline-inducible deletion of *Il33* in *Pdgfrb*-expressing cells strongly diminished cold-induced beige cell recruitment. Collectively, these data reveal that distinct subpoulations in iWAT respond to adrenergic signaling events and couple adrenergic signaling to immune cell activity under physiological conditions.

*Anti-adipogenic regulatory cells in iWAT*

One of the most interesting and surprising findings from scRNA-seq studies is the presence of anti-adipogenic regulatory cells. The study by Schwalie et. al. defined a previously unrecognized population of iWAT stromal cells that exert an anti-adipogenic effect on APCs in vitro and upon transplantation in vivo. These adipogenesis-regulatory cells, termed "Aregs," inhibit adipogenesis through the production of secreted molecules. In a recent follow-up study, Dong et al searched for the identity of anti-adipogenic secreted factors, with a focus on genes that encoded for secreted proteins and were selectively expressed in Aregs vs. adipocytes and other progenitor cell subpopulations (Dong, Sun et al. 2022). This analysis led to the identification of *Rspo2* as an Areg-enriched secretory protein. Notably, co-culture assays indicate that the full anti-adipogenic effect of Aregs is dependent on *Rspo2*. *Rspo2* encodes R-spondin 2, a modulator of the WNT signaling pathway, a well-known suppressor of adipogenesis. Dong *et al*. revealed that R-spondin 2 targets the LGR4 receptor to exert an anti-adipogenic effect. Moreover, the study indicates that R-spondin 2 selectively inhibits the stem cell to committed preadipocyte transition, and thus commitment of multi-potent cells to the adipocyte lineage. Importantly, cells bearing the signature genes of Aregs are present in human WAT; however, the importance of these cells in controlling adipose tissue hyperplasia under physiological conditions still needs to be evaluated further.

The Sul laboratory also identified a unique population of regulatory stromal cells (Nguyen, Lin et al. 2021). Nguyen et al. compared the scRNA-seq profiles of stromal vascular cells of inguinal WAT from young and aging mice. They identified an aging-

asssociated subpopulation that is distinct from the aforementioned APC populations described above and termed these cells, "Aging-dependent regulatory cells" (ARCs, $CD36^{+}$ $LGALS3^{+}$). ARCs raised in numbers during aging in mice; this occurred only in the iWAT depot. ARCs could secrete CCL6 and other cytokines to inhibit the differentiation and proliferation of neighboring adipocyte precursors. The emergence of these cells may contribute, at least in part, to the well-known known age-related reduction of subcutaneous adipose tissue mass and plasticity observed in human aging.

*Distinct adipogenic and fibroinflammatory progenitor cells in adult eWAT*

When I first started in the laboratory, I helped a senior graduate student, Chelsea Hepler, complete her work that reported the discovery of functionally distinct adipogenic and fibroinflammatory progenitors in murine eWAT. eWAT was the initial focus of the lab's work since this depot expands through adipocyte hyperplasia. Using scRNA-seq analysis, she discovered three molecularly distinct PDGFRβ+ subpopulations in eWAT, now termed "adipocyte precursor cells" (APCs), "fibro-inflammatory progenitors" (FIPs), and "mesothelial-like cells" (MLCs) (Hepler, Shan et al. 2018). APCs, defined as LY6C- CD9- PDGFRβ+ cells, are enriched in the expression of *Pparg* and differentiate robustly *in vitro* in presence of growth media supplemented with insulin. These cells are highly committed to the adipocyte lineage; the differentiation of these cells does not require the full adipogenic cocktail ("DMI") used in studies of 3T3-L1 differentiation. Transplantation of APCs led to the formation of an ectopic fat depot in a mouse model of lipodystrophy (Adiponectin-Cre;

*Pparg*$^{loxP/loxP}$). On the other hand, FIPs from adult mice were refractory to pro-adipogenic stimuli, both *in vitro* and *in vivo*. MLCs represent a small subset of mesothelial cells that express both epithelial and mesenchymal markers. To date, the function of these cells is unclear; however, we have observed that these cells do not differentiate into adipocytes under any of the conditions we have examined. Interestingly, FIPs are not only "non-adipogenic." These cells exhibit an anti-adipogenic phenotype in which FIPs can inhibit the differentiation of APCs *in vitro* through the production of secreted factors. In this regard, FIPs are functionally similar to Aregs found in the iWAT depot; however, the gene expression profile of eWAT FIPs strongly differs from that of Aregs. Moreover, FIPs are enriched in the expression of genes associated with extracellular matrix remodeling and pro-inflammatory signaling. Upon HFD feeding, the expression of this fibroinflammatory gene expression profile increased in FIPs, to a much greater degree than observed in APCs. As such, our findings revealed the presence of functionally distinct adipogenic and fibro-inflammatory progenitor subpopulations that reside within the broader pool of PDGFRβ+ perivascular cells of adult eWAT.

Over the past three years, I have contributed to multiple projects that determined the functional significance of FIPs and APCs in obesity. The study from Shan et al. determined that the pro-inflammatory phenotype of FIPs is activated immediately (1-3 days) upon HFD feeding and drives macrophage accumulation in adipose tissue (Shan, Shao et al. 2020). Inducible disruption of *Tlr4* in *Pdgfrb*-expressing cells blocked the induction of this pro-inflammatory gene program in FIPs and diminished the overall degree of macrophage

accumulation in eWAT by 50%. These data indicate that FIPs are a stromal cell subpopulation that mediates activation of metabolic inflammation in obesity.

Our data align closely with scRNA-seq studies from other laboratories (Burl, Ramseyer et al. 2018, Spallanzani, Zemmour et al. 2019, Sarvari, Van Hauwaert et al. 2021). Shortly after our 2018 publication, the Mathis and Artis labs independently reported their own scRNA-seq analyses of eWAT, confirming the presence of molecularly distinct adipogenic and fibroinflammatory cell populations in this depot. Both groups note the selective expression of IL-33 in FIPs of lean adult mice. IL-33 regulates the activity of Tregs, immune cells that are critical to maintain an "anti-inflammatory" phenotype in adipose tissue under homeostatic conditions. As such, FIPs do not only play a pathogenic role but also play a role under homeostatic conditions.

When joining the Gupta laboratory, I became very interested in the heterogeneity of adipose precursor cells. Given my interest in developmental biology, I decided to address the following unresolved questions: When does the adipose precursor cell heterogeneity emerge during development? Do we have these distinct precursor populations from the time of birth? Do the properties of these cells change during life? What happens if the activity of these cells is altered early in life rather than in adulthood. In the chapters ahead, I describe my studies (currently under revision for *Nature Metabolism*) that aim to address these questions.

**Figure 1. Human Adipose-Tissue Depots (Cypess 2022)**

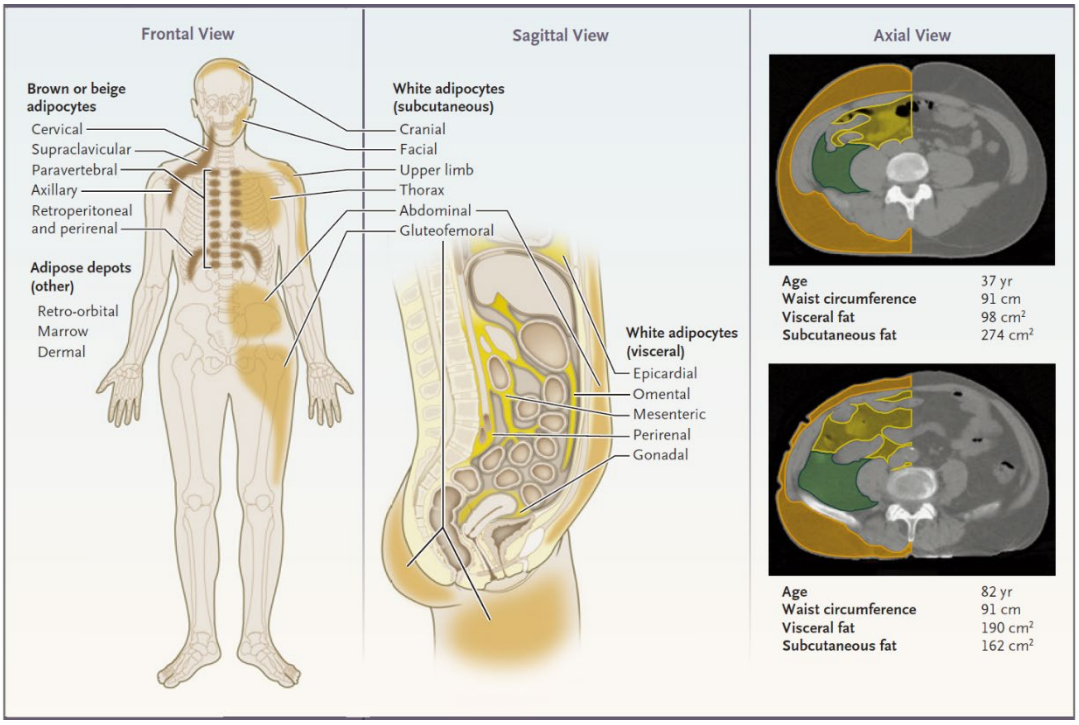

# CHAPTER TWO

## Distinct Functional Properties of Perinatal Versus Adult Adipose Progenitor Subpopulations

*(This section contains content from a manuscript in revision at Nature Metabolism)*


SUMMARY

Adult white adipose tissue (WAT) harbors distinct mesenchymal stromal cell subpopulations that differentially impact WAT function and plasticity. Here, we use single-cell transcriptomics to unveil the cellular landscape of the perinatal murine epididymal WAT (eWAT) primordium. We reveal that adipocyte precursor cells (APCs) and fibro-inflammatory progenitors (FIPs) emerge as functionally distinct PDGFRβ+ subpopulations within the eWAT anlagen prior to adipocyte accrual, at postnatal day 3 (P3). Importantly, we identify important molecular and functional differences between perinatal and adult FIPs, including differences in their pro-inflammatory response, adipogenic capacity, and anti-adipogenic behavior. These data reveal the complex changes that occur in adipose progenitor cell function over the course of tissue development.

# INTRODUCTION

White adipocytes are specialized lipid-storing cells that evolved as a safe and efficient compartment for long term energy storage in the form of triglyceride. These cells can appear throughout the body but are generally organized into distinct tissues, or "depots," with remarkable cellular heterogeneity. In fact, adipocytes comprise of only 30-60% of the cellular components in the tissue (Roh, Tsai et al. 2017). Under homeostatic conditions, the non-parenchymal fraction of adipose tissue (termed "stromal-vascular fraction") consists of a vast array of cell types, including immune cells, endothelial cells, mural cells, and fibroblast-like subpopulations. WAT expansion in the setting of obesity involves qualitative and quantitative changes in cellular composition of the tissue, including a shift from an anti-inflammatory phenotype to a low grade chronic pro-inflammatory state, alterations in adipocyte number and size, and extracellular matrix remodeling (Hepler and Gupta 2017, Ghaben and Scherer 2019). Activity within the adipose tissue microenvironment is critical as these various cell types interact with adipocytes to coordinate local and systemic adaptations to changing environmental and physiological conditions. The emergence of single-cell RNA-sequencing (scRNA-seq) has greatly facilitated the derivation of several cellular atlases of the mouse and human adipose tissue microenvironment (Corvera 2021). Of particular interest has been the murine perigonadal WAT depot. The perigonadal WAT depot of male mice (epididymal WAT, or "eWAT") is a well characterized site of immune cell residence, adipose progenitor heterogeneity, and robust tissue remodeling and expansion in obesity. As such, the eWAT depot of mice offers a model for many aspects of adipose tissue remodeling observed in human obesity.

Multiple groups have utilized scRNA-seq to unveil functionally distinct APC subpopulations in eWAT of adult mice (Burl, Ramseyer et al. 2018, Hepler, Shan et al. 2018, Spallanzani, Zemmour et al. 2019). Our own efforts have focused on two functionally distinct fibro-inflammatory and adipogenic PDGFRβ-expressing cell subpopulations within adult eWAT (Hepler, Shan et al. 2018, Shan, Shao et al. 2020). The LY6C- CD9- PDGFRβ+ subpopulation in eWAT represents functional APCs. These cells are enriched in the expression of *Pparg*, encoding the "master regulator" of adipocyte differentiation, and possess robust adipogenic capacity both *in vitro* and *in vivo* (Hepler, Shan et al. 2018). De novo differentiation from PDGFRb+ APCs drives adipocyte recruitment in the setting of diet-induced obesity and ensures healthy tissue remodeling and proper lipid storage in WAT (Shao, Vishvanath et al. 2018, Vishvanath and Gupta 2019, Shao, Hepler et al. 2021). In contrast, LY6C+ PDGFRβ+ cells represent fibro-inflammatory precursors, or "FIPs." FIPs exert strong pro-inflammatory, fibrogenic, and anti-adipogenic phenotypes (Hepler, Shan et al. 2018). These cells are activated upon high-fat diet (HFD) feeding and play an important role in controlling pro-inflammatory macrophage accrual and tissue collagen deposition associated with obesity (Shan, Shao et al. 2020, Joffin, Paschoal et al. 2021, Shao, Hepler et al. 2021).

There is now considerable consensus that the APC pool in adult WAT is molecularly heterogeneous (Rondini and Granneman 2020); however, it is unclear when functionally distinct adipose progenitor subpopulations emerge during development, where they are localized, and if/how their molecular and functional properties change over time. Here, we combined scRNA-seq, in silico cell trajectory analysis, and functional analyses in cells and

genetic mouse models to define the developmental origin of murine eWAT and the unique functional properties of perinatal adipose progenitor subpopulations. My results highlight the emergence of functionally distinct progenitor cell subpopulations prior to the formation of parenchymal adipocytes and reveal important molecular and functional differences between perinatal and adult progenitor cell subpopulations.

# RESULTS

**Progenitor cell heterogeneity emerges at the onset of eWAT development.**

Murine eWAT develops shortly after birth. The accumulation of lipid-laden epididymal adipocytes becomes readily apparent by approximately postnatal (P) day 7 (P7) (Han, Lee et al. 2011, Wang, Tao et al. 2013). I visualized the eWAT anlagen by histological analysis of transverse sections of the lower abdominal/inguinal region of newborn C57BL/6 mice at P0, P3, and P7 (Fig. 1a). At P0, the presumptive eWAT depot appears as an evagination of the caput epididymis. By P3, the eWAT anlagen appears as a thin, translucent structure surrounded by a continuous mesothelial layer expressing *Mesothelin* (MSLN+). At P7, unilocular PLIN1+ adipocytes are readily apparent within a distinct depot that is encapsulated by the surrounding mesothelium.

In adult mice, de novo differentiation of epididymal adipocytes originates from PDGFRβ + mesenchymal cells (Vishvanath, MacPherson et al. 2016). I asked whether the initial perinatal development of epididymal adipocytes involves differentiation from *Pdgfrb*-expressing cells present within the observed perinatal eWAT primordium. First, I utilized our previously developed genetic lineage tracing system that enables labeling and fate-mapping of *Pdgfrb*-expressing cells. In WAT, *Pdgfrb* expression is found in mural cells (pericytes and vascular smooth muscle cells) and adventitial fibroblasts, but not differentiated adipocytes. This doxycycline-inducible "MuralChaser" model consists of the *Pdgfrb*$^{rtTA}$ transgene, TRE-*Cre* transgene, and the CRE-dependent *Rosa26R*$^{mT/mG}$ membrane-bound GFP reporter (mGFP) allele (Fig. 1b) (Vishvanath, MacPherson et al. 2016). Newborn

MuralChaser pups were exposed to doxycycline at their time of birth (P0.5) through postpartum feeding of lactating mothers with doxycycline-containing chow diet (DOX-Chow). This enables permanent mGFP labeling of *Pdgfrb*-expressing cells in MuralChaser mice at the earliest stages of perinatal eWAT development. Upon tissue harvest at P28, I observed widespread labeling of lipid-laden adipocytes with mGFP (Fig. 1c). These data provide evidence that epididymal adipocytes develop from perinatal *Pdgfrb*-expressing cells.

I utilized single-cell RNA-Seq (scRNA-Seq) analysis to reveal the overall cellular landscape of the eWAT primordium and identified putative adipose progenitor subpopulations. Our earliest time point of analysis was P3, which was the earliest stage in which discernible eWAT could be reliably dissected. I also profiled the stromal-vascular fraction (SVF) of P7 eWAT, a stage when adipocytes are first readily apparent, as well as adult (P35) eWAT SVF. An integrated analysis of the three datasets identified the presence of endothelial cells, immune cells, mesenchymal stromal cells, epithelial (mesothelial) cells, and committed preadipocytes, across each stage of tissue development (Extended Data Fig. 1a-c). Upon further sub-clustering, I observed the vast array of immune cells that are known to reside within adult perigonadal WAT, including T cells, B cells, neutrophils, dendritic cells, and two main subtypes of macrophages (Perivascular macrophages and non-perivascular macrophages) (Fig. 2a). Remarkably, many of these hematopoietic lineage cells were present at the onset of eWAT development. Sub-clustering of the mesenchymal stromal cells (PDGFRα/β+) revealed the presence of distinct cell subpopulations in P3 and P7 eWAT that cluster together with those previously identified in adult eWAT. This includes cell types bearing the previously described molecular markers of adult APCs (e.g *Agt*, *Apoe*, *Fndc5*;

Cluster 9) and FIPs (e.g., *Ly6c1*, *Efhd1*, *Mfap5*, *Fn1;* Cluster 1). Our analysis also identified smooth muscle cells ("SMCs", Cluster 10) as well as a small population of mesothelial-like cells ("MLCs"; Cluster 17) expressing a mixed mesenchymal/epithelial phenotype and are distinct from the large cluster of classical mesothelial cells (Fig. 2a, b). Across all time points, I also observed a distinct cluster of cells expressing adipocyte lineage-selective transcripts, including *Pparg*, *Fabp4*, and low levels of *Adipoq* (Extended Data Figure 1c and Extended Data Figure 2a, b). Notably, expression of *Pparg* and *Fabp4* increases over time within this cell cluster, suggesting that these cells likely represent committed preadipocytes and/or immature adipocytes.

I developed a strategy to quantify and isolate these distinct perinatal PDGFRβ+ subpopulations using FACS (Extended Data Fig. 3a, b). Perinatal APCs and FIPs both reside amongst the PDGFRβ+ CD9- fraction of CD45- CD31- (Lin-) eWAT SVF cells and can be distinguished from one another based on LY6C expression (Perinatal FIPs= PDGFRβ+ LY6C+; Perinatal APCs= PDGFRβ+ CD9- LY6C-). SMCs and MLCs are enriched in the PDGFRβ+ CD9+ fraction of Lin- SVF cells and can be distinguished by the expression of DPP4 (Perinatal SMCs= PDGFRβ+ CD9+ DPP4-; Perinatal MLCs= PDGFRβ+ CD9+ DPP4+). At P7, APCs were the most abundant PDGFRβ+ subpopulation, followed by FIPs (Extended Data Fig. 4a). This differs from adult mice, where FIPs outnumber APCs in lean and obese eWAT (Hepler, Shan et al. 2018, Shan, Shao et al. 2020). Gene expression analysis of subpopulation-selective genes confirmed that the sorting strategy indeed enriched for the appropriate cell population (Extended Data Fig. 3c). I performed global bulk-RNA

sequencing to confirm that APCs, FIPs, MLCs, and SMCs, represent molecularly distinct subclusters of cells and to better define their molecular profiles. P7 cell subpopulations were isolated by FACS and lysed immediately for RNA extraction and library production. Principal component analysis and sample clustering based on global transcriptomes confirmed that these four subpopulations within perinatal eWAT are molecularly distinct, with APCs and FIPs bearing more resemblance to one another than to SMCs and MLCs (Extended Data Fig. 4b-d). I utilized Gene Set Enrichment Analysis to identify gene signatures that distinguish perinatal APCs and FIPs. Much like their adult counterparts, perinatal APCs are enriched in a gene signature of "adipogenesis," whereas FIPs are enriched in gene signatures reflecting heightened pro-inflammatory signaling (Extended Data Fig. 5a). All together, these data establish that the molecular heterogeneity of adipose progenitors observed in adult mice emerges at the onset of eWAT development.

**Peri-endothelial PDGFRβ+ LY6C- CD9- cells are the highly adipogenic subpopulation within perinatal eWAT.**

In adult mice, the LY6C- CD9- fraction of PDGFRβ+ cells (termed APCs) represent the highly adipogenic subpopulation within the eWAT SVF, whereas adult LY6C+ fraction of PDGFRβ+ cells (termed FIPs) lack adipogenic potential even in the presence of strong pro-adipogenic stimuli (e.g. PPARγ agonism) (Hepler, Shan et al. 2018). In silico cell trajectory analysis based on the single-cell transcriptomes predicted a direct developmental relationship between APCs and committed preadipocytes and suggested that APCs may be the only direct source of committed preadipocytes amongst these populations (Fig. 3a). I explored the

adipogenic capacity of perinatal APCs and FIPs directly by testing the ability of these subpopulations to undergo adipocyte differentiation in vitro and in vivo. I isolated and maintained these PDGFRβ+ subpopulations in growth medium containing 2% FBS and 1% ITS (insulin, transferrin, selenium). These represent culture conditions that I previously established for growth and differentiation of adult eWAT PDGFRβ+ cells (Vishvanath, MacPherson et al. 2016, Hepler, Shan et al. 2018). Under these conditions, perinatal LY6C-CD9- PDGFRβ+ cells (APCs) underwent adipocyte differentiation at a high efficiency within 6 days of reaching confluence (Day 6 after confluence) (Fig. 3b, c). Even by the time that APCs reach confluence (Day 0), the expression of several adipocyte-selective transcripts can be readily detected (Fig. 3c). On the contrary, very few adipocytes emerged within cultures of perinatal FIPs or MLCs, indicating that APCs are the subpopulation most committed to the adipocyte lineage (Fig. 3b, c).

I also tested the abilities of these perinatal progenitor subpopulations to undergo differentiation in response to the more commonly used hormonal adipogenic cocktail (dexamethasone, IBMX, and insulin) with the addition of the PPARγ agonist, Rosiglitazone. Under these very strong pro-adipogenic conditions both perinatal APCs and FIPs can undergo differentiation with high efficiency, whereas only occasional lipid-laden adipocytes were present in cultures of MLCs (Fig. 3b, c). The latent adipogenic potential of P7 FIPs is remarkably different from the potential of adult FIPs, which are largely refractory upon the same strong adipogenic stimuli. I also evaluated the ability of P7 APCs and FIPs to undergo adipocyte differentiation upon transplantation into the remnant subcutaneous WAT depots of *Adipoq*-Cre; *Pparg*$^{loxP/loxP}$ animals, a well-described model of lipodystrophy (Wang, Mullican

et al. 2013). Three weeks following cell transplantation, the WAT depot of *Adipoq*-Cre; *Pparg*$^{loxP/loxP}$ mice injected with P7 APCs contain numerous clusters of lipid-laden fat cells (Fig. 3d). The contralateral depots of the same animals injected with P7 FIPs, or matrigel alone, remained devoid of mature adipocytes. Collectively, these data indicate that perinatal APCs represent the highly adipogenic subpopulation of the developing eWAT. Importantly, these data also highlight the difference between perinatal FIPs and adult FIPs in their lineage plasticity.

In adult eWAT, committed preadipocytes and APCs reside within small blood vessels where they take on the appearance of PDGFRβ+ mural cells (pericytes or vascular smooth muscle) (Tang, Zeve et al. 2008, Gupta, Mepani et al. 2012). I performed indirect immunofluorescence assays to assess the localization of APCs and FIPs in perinatal eWAT. I utilized a commercially available antibody recognizing AGT (angiotensinogen), whose expression is selective to APCs (Figure 2b, Extended Data Figure 4d). I identified FIPs on the basis of EFHD1 (EF-hand domain family D1) protein expression. In P7 eWAT, AGT expression was readily detected within blood vessels, specifically within peri-endothelial cells resembling mural cells (Fig. 4a). The expression of EFHD1 was found in both perivascular cells and cells resembling interstitial fibroblasts (Fig. 4b). Moreover, I observed the occasional EHFD1+ in association with the tissue mesothelium (Fig. 4c). These histological data provide evidence that perinatal eWAT APCs reside in the vasculature as peri-endothelial cells; however, FIPs at this stage appear more broadly distributed within the tissue.

**Perinatal FIPs are less anti-adipogenic and pro-inflammatory than adult FIPs.**

A notable feature of adult FIPs is their capacity to block adipocyte differentiation from APCs through the production of paracrine factors. Given the difference between perinatal and adult FIPs in their abilities to undergo differentiation under strong adipogenic conditions, I asked whether these two populations also differed in their anti-adipogenic potential. As previously reported, adult APCs exposed to conditioned media from adult FIPs fail to undergo adipogenesis (Fig. 5a) (Hepler, Shan et al. 2018). On the other hand, adult APCs exposed to conditioned media from parallel cultures of APCs maintain their adipogenic potential (Fig. 5a). Remarkably, APCs exposed to conditioned media from perinatal FIPs also maintain nearly their full adipogenic potential (Fig. 5a). This indicates that perinatal FIPs are not anti-adipogenic, in contrast to their adult counterparts.

Another notable feature of adult FIPs is their ability to exert a pro-inflammatory phenotype in response to pro-inflammatory stimuli (Shan, Shao et al. 2020). GSEA indicated that perinatal FIPs are enriched in gene signatures reflecting heightened pro-inflammatory signaling when compared to perinatal APCs. I observed that cultured perinatal FIPs indeed exhibit a stronger pro-inflammatory gene expression response to LPS treatment than perinatal APCs (Extended Data Fig. 5b). Nevertheless, cross comparison of these data to the published data on adult FIPs and APCs caused us to speculate that the response of perinatal FIPs to pro-inflammatory stimuli may not be as robust as observed in adulthood. I examined the pro-inflammatory responses of perinatal vs adult FIPs more closely by first comparing their transcriptional response to LPS *in vitro*. Upon LPS stimulation, levels of several key pro-inflammatory cytokines were elevated to a greater degree in adult FIPs when compared

to P7 FIPs (Fig. 5b). Similar results were observed when cells were instead treated with TNFα (Extended Data Fig. 5c).

The NFκB signaling cascade is a classical signaling pathway that integrates both TNFα and LPS signaling. I previously demonstrated that adult FIPs differed from adult APCs in their transcriptional response to genetic NFκB activation (Shan, Shao et al. 2020). Thus, I asked whether the differential gene expression response of adult FIPs and perinatal FIPs to pro-inflammatory signals reflects an intrinsic difference in their potential to respond to NFκB activation. I utilized our previously described "*Pdgfrb-Ikk2*$^{CA}$" model in which the addition of doxycycline results in expression of a constitutively active form of IKK2 (IKK2$^{CA}$), an activator of NFκB, in PDGFRβ+ cells (Fig. 5c) (Shan, Shao et al. 2020). Following the addition of Dox in vitro, the induction in mRNA levels of all of the pro-inflammatory genes examined were 2-3 fold greater in adult FIPs than in perinatal FIPs (Fig. 5d). Taken together, data provide evidence that perinatal FIPs are less anti-adipogenic and less pro-inflammatory than adult FIPs.

# DISSCUSION

The development of scRNA-seq has enabled rapid progress in unraveling the molecular heterogeneity and complexity of the adipose tissue microenvironment. One key question that arises from these studies is whether cell subpopulations of interest emerge during the initial development of the tissue, or instead, emerge and adopt their unique phenotypes in adulthood. Here, I demonstrate that APCs and FIPs emerge at the earliest stages of murine eWAT development. Their presence within the eWAT primordium at P3 provides evidence that these distinct cell subpopulations emerge even prior to formation of lipid-laden adipocytes. The scRNA-seq data provide evidence of global transcriptomic similarities between perinatal and adult adipose progenitors; however, our functional studies reveal important differences that can be observed upon isolation of the cells. Most notably, perinatal FIPs lack the anti-adipogenic phenotype exhibited by adult FIPs. It is tempting to speculate that such a change in phenotype over time may be advantageous, at least for periods of time. The lack of anti-adipogenic signals in the early postnatal period may help enhance adipocyte differentiation during this key period of WAT development. In adults, the presence of such anti-adipogenic signals may help maintain APCs in a quiescent state under homeostatic conditions. Recent independent studies have highlighted the impact of aging on progenitor activity and the age-dependent accumulation of anti-adipogenic cells in subcutaneous WAT (Berry, Jiang et al. 2017, Wang, Ishibashi et al. 2019, Gao, Daquinag et al. 2020, Kodani and Tseng 2021, Nguyen, Lin et al. 2021). In aging, the imbalance between anti-adipogenic and pro-adipogenic signals may contribute to progenitor exhaustion and an inability to maintain WAT plasticity.

Our work here also sheds insight into the cellular origin of adipocytes during tissue development. The exact origin of adipocytes and the timing of their emergence varies with depot(Wang, Tao et al. 2013, Sebo and Rodeheffer 2019). Murine epididymal adipocytes differentiate during the early postnatal period. This stands in contrast to inguinal white adipocytes and classical brown adipocytes which emerge during the late stages of fetal development. Over the past few years, the prevailing view has been that epididymal adipocytes originate, at least in part, from a mesothelial cell origin (Chau, Bandiera et al. 2014, Gupta and Gupta 2015). This hypothesis is attractive given the presence of mesothelial cells in intra-abdominal, but not subcutaneous, WAT depots. Our lineage tracing, scRNA-seq analyses, and functional analyses, point to mesenchymal PDGFRβ+ cells as precursors to epididymal adipocytes during the early postnatal period. Given the limitations of all approaches utilized, further studies will be needed to understand the complexity of eWAT development and the inductive signals that initiate tissue development during the perinatal period.

# MATERIALS AND METHODS

## Animals and diets

All animal experiments were performed according to procedures approved by the UTSW Animal Care and Use Committee. MuralChaser mice were derived from breeding *Pdgfrb*$^{rtTA}$ (JAX 028570), TRE-Cre (JAX 006234), and *Rosa26R*$^{mT/mG}$ (JAX 007676) mice as previously described (Vishvanath, MacPherson et al. 2016). *Pdgfrb-Ikk2*$^{CA}$ mice were derived through intercrosses of *Pdgfrb*$^{rtTA}$, TRE-Cre, and *Rosa26R*$^{IKK2CA}$ (JAX008242) as previously described (Shan, Shao et al. 2020). Lipodystrophic Adiponectin-Cre; *Pparg*$^{loxP/loxP}$ animals were derived by crossing Adiponectin-Cre mice (JAX 028020) and *Pparg*$^{loxP/loxP}$ (JAX 004584) animals and were previously described (Wang, Mullican et al. 2013). C57BL/6 wildtype mice were obtained from Charles River Laboratories. Postnatal day 0.5, 3, and 7 (P0.5, P3, P7), 4-6 weeks old male mice were used in this study.

Mice were maintained on a 12 hr light/dark cycle in a temperature-controlled environment (22˚C) and given free access to water and diets as indicated in the manuscript. Diet utilized include, standard rodent chow diet, or doxycyline-containing chow diet (Dox-Chow, 600 mg/kg doxycycline, Bio-Serv, S4107).

## Histological analysis

Transverse cuts through the mid-thoracic to lower abdominal/inguinal region of P0, P3 and P7 pups were fixed in 4% paraformaldehyde for 24h and maintained in 50% ethanol solution. Paraffin embedding, perinatal tissue sectioning and H&E staining was performed by

the Molecular Pathology Core Facility at UTSW. Brightfield and fluorescent images were acquired using a Keyence BZ-X710 microscope. Indirect immunofluorescence was performed as previously described (Vishvanath, MacPherson et al. 2016). Primary antibodies used for immunofluorescence include: guinea pig anti-PERILIPIN 1:1000 (Fitzgerald #20R-PP004), rabbit anti-MESOTHELIN 1:1000 (LSBio #LS-C407883), rabbit anti-MAC-2 1:500 (Cedarlane #CL8942AP), rabbit anti-EFHD1 1:100 (Sigma #SAB3500392), mouse anti EFHD1 1:100 (Abnova #H00080303-M05), mouse anti-AGT 1:100 (Santa Cruz Biotechnology #sc-374511), rat anti-ENDOMUCIN 1:100 (Santa Cruz Biotechnology #sc-65495).

**Gene expression analysis by qPCR**

RNA was isolated using RNAqueous-Micro Total RNA Isolation Kit (Thermo Fisher Scientific). cDNA was synthesized using M-MLV Reverse Transcriptase (Invitrogen) and Random Primers (Invitrogen). Relative mRNA levels were determined by quantitative PCR using SYBR Green PCR Master Mix (Applied Biosystems). Values were normalized to *Rps18* levels using the $2\text{-}Ct^{\Delta\Delta}$ method. Unpaired Student's t-test was used to evaluate statistical significance. All primer sequences are listed within Supplementary Table 1.

**Isolation of adipose SVF and flow cytometry**

Adipose tissue from five P3 or P7 pups or one 6-8 weeks old male mouse were combined and minced with scissors in a 1.5 mL tube containing 100ul of digestion buffer (1X HBSS, 1.5% BSA, and 1 mg/mL collagenase D) and then transferred to a 50 mL Falcon

tube containing 5 mL digestion buffer. The mixture was incubated in a 37˚C shaking water bath for 30 mins or 1h. The solution of digested tissue was passed through a 100 □m cell strainer, diluted to 30 mL with 2% FBS/PBS, and centrifuged at 500 x g for 5 min. The supernatant was aspirated, and cells were washed once with 2% FBS/PBS and resuspended in blocking buffer (2% FBS/PBS containing anti-mouse CD16/CD32 Fc Block (1:200)). Primary antibodies were added to the cells in blocking buffer for 15 mins at 4˚C in the dark. After incubation, the cells were washed once with 2% FBS/PBS and resuspended in 200 □l of 2% FBS/PBS for sorting. Cells were sorted for collection into 100% FBS using a BD Biosciences FACSAria cytometer (UTSW Flow Cytometry Core Facility). Flow cytometry plots were generated using FlowJo.

Primary antibodies and the working concentrations were as follows: CD45–PerCP/Cyanine 5.5 1:400 (Biolegend, clone 30-F11, no. 103132), CD31–PerCP/Cyanine 5.5 1:400 (Biolegend, clone 390, no. 102420), PDGFRβ-PE 1:75 (Biolegend, clone APB5, no. 136006), LY6C–APC/Cyanine7 1:400 (Biolegend, clone HK1.4, no. 128026), CD9–FITC 1:400 (Biolegend, clone MZ3, no. 124808), CD26(DPP4)-APC 1:400 (Biolegend, clone H194-112, #137807).

**Isolation of adipose tissue associated mesothelial cells**

eWAT associated mesothelial cells were isolated using a protocol previously described (Darimont, Avanti et al. 2008). Dissected eWAT depots from P7 mice were placed in 10 mL of 0.25% trypsin for 20 min at 37˚C with continuous end over end rotation. The entire solution was passed through a 400 μm cell strainer to remove adipose tissue. Flow-through

cells were then centrifuged at 600 x g for 5 min. Cell pellets were then resuspended in appropriate solution for RNA-seq analysis or cell culture. For cell culture assays, cell pellets were resuspended in 2% ITS growth media [2% FBS in 60% pH7–7.4 low glucose DMEM, 40% pH 7.25 MCDB201 (Sigma M6770), 1% ITS premix (BD Bioscience 354352), 0.1 mM L-ascorbic acid-2- 2phosphate (Sigma A8960-5G), 10 ng/mL FGF basic (R and D Systems 3139-FB-025/CF), Pen/Strep, and gentamicin] and plated in a 12-well collagen-coated plate. The cells were incubated at 37˚C in 10 CO2 and the media was replaced daily.

**Single-cell RNA-sequencing and analysis**

eWAT SVF from P3 or P7 male pups or 5 weeks old male mice were isolated and digested as described above and used immediately for single-cell RNA library preparation using the 10X Genomics Single Cell 3' v3 kit according to the manufacturer's instructions and as previously described (Hepler, Shan et al. 2018). Sequencing was performed by the McDermott Center Next Generation Sequencing Core in UTSW. Cell Ranger software (v3.1.0) was used to perform demultiplexing, aligning reads, filtering, clustering, and gene expression analyses, using default parameters. GRCh38 was used as the genome reference for reads alignment and aggregation.Further analysis, including clustering, dimensionality reduction and differential gene expression analysis, was performed using Seurat (Hao, Hao et al. 2021). Cells with less than 200 genes and more than 6500 (P3), 5000 (P7) and 5500 (Adult) genes detected were removed. Genes expressed less than 3 cells were removed. Cells with percentage of mitochondrial gene expression greater than 20% and those with percentage of ribosome gene expression less than 5% were also removed. The final input

data for Seurat after the quality control and filtering were composed of 23320 cells for P3, 18585 cells for P7 and 11769 for adults. Data from different developmental stages were integrated using SCTransform (Hafemeister and Satija 2019). Cell clusters were then identified for the integrated data using the top 30 dimensions from the principal component analysis (PCA) at the resolution of 1. Cluster marker genes were identified using "FindAllMarkers" function in Seurat. Differential gene expression analysis between developmental stages or cell types was done using "FindMarkers" function in Seurat. Cell types were annotated manually using cell type specific marker genes collected from the literature (citations maybe). Clusters with ambiguous or unknown annotation were removed, resulting in 11553 cells for P3, 14538 cells for P7 and 10442 cells for adults. Trajectory analysis was performed for APC, FIP, SMLC, MLC, and committed preadipocytes using Slingshot (v1.8.0) (Street, Risso et al. 2018). All Single-cell mRNA-seq data have been deposit to GEO (Accession number: GSE180987).

**Bulk mRNA-sequencing and analysis**

RNA was isolated using RNAqueous-Micro Total RNA Isolation Kit (Thermo Fisher Scientific). mRNA libraries were prepared using the NEB Poly(A) mRNA Magnetic Isolation Module (NEB #E7490) and NEBNext Ultra II RNA Library Prep Kit for Illumina (NEB #E7770). Indices used were from NEBNext Multiplex Oligos for Illumina (NEB #7335, E7500, E7710). Sequencing was performed by the McDermott Center Next Generation Sequencing Core in UTSW. FASTQ files were aligned by HISAT2 and

differential gene expression was determined using DEseq2. All Bulk mRNA-seq data have been deposit to GEO (Accession number: GSE181245).

**Cell culture and cellular assays**

Sorted PDGFRβ+ sub-populations cells were plated at a density of 4 x $10^4$ cells/ well in a 48-well plate or 2 x $10^4$ cells/ well in a 96-well plate containing 2% ITS growth media [consisting of 60% low-glucose DMEM, 40% MCDB-201 medium, 2% FBS, 1% ITS premix (Insulin–Transferrin–Selenium) (BD Biosciences, no. 354352), 0.1 mM l-ascorbic acid-2-2phosphate (Sigma, no. A8960-5G), 10 ng ml–1 FGF basic (R&D systems, no.3139-FB-025/CF), penicillin–streptomycin and gentamicin] and incubated at 37˚C in 10% $CO_2$.

For in vitro adipocyte differentiation assay, cells were grown to confluence in 2% ITS growth media and switched to induction media (growth media supplemented with 1 mM dexamethasone, 0.5 mM isobutylmethyxanthine, ±1 mM rosiglitazone) for 48 hrs. After 48 hrs., cultures were maintained in 2% ITS growth media. Media were changed every two days until harvesting.

For conditioned media assay, donor cells and recipient cells were derived simultaneously using FACS and plated in separate plates. Media from equally confluent cultures of APCs, FIPs, P7 APCs, P7 FIPs was harvested and placed onto APCs or P7 APCs beginning 48 hrs. after initial plating in a 1:1 ratio with 2% FBS in ITS media. Cells were harvested at the indicated time points for RNA expression analysis. Images were obtained using a Leica DMIL LED microscope and a Leica DFC3000g camera. For LPS treatment, cells were grown to confluence and starved overnight with serum-free ITS medium. Cells were then

treated with 100ng/ml LPS or PBS for 2 hrs. prior to harvest. For TNFα treatment, cells were grown to confluence and starved overnight with serum-free ITS medium. Cells were then treated with 20ng/ml TNFa or PBS, for 2 hrs. prior to harvest. For in vitro *Ikk2*$^{CA}$ expression, cells were grown to confluence and then serum starved starved overnight in serum-free ITS medium. Cells were then treated with 5 μM Doxcycline or PBS for 8 hrs prior to harvest.

**Oil red O staining**

Cells were pre-fixed in 4% PFA for 15 min at room temperature and then washed twice with ddH2O. Following 1 hour of additional fixation, cells were rinsed with ddH2O six times and then incubated in Oil Red O working solution (2 g Oil red O in 60% isopropanol) for 10 minures. Stained cells were then washed three times with ddH2O and then bright field images were acquired using Keyence BZ-X710 Microscope.

**Cell transplantation assays**

0.8~1 x $10^5$ cells (P7 APCs or P7 FIPs) collected by FACS were suspended in 100 mL transplantation media (50% Matrigel in PBS, supplemented with 2 ng/mL FGF) and injected subcutaneously into the remnant inguinal WAT region of 3-month-old lipodystrophic mice (*Adiponectin-Cre*; *Pparg*$^{loxP/loxP}$). Three weeks later, the remnant inguinal WAT depots were harvested for histological analysis.

**Statistical analysis**

Statistical methods were not used to predetermine sample size. The experiments were not randomized, and the investigators were not blinded. All data were expressed as the mean ±SEM. GraphPad Prism 9.1.2 (GraphPad Software, Inc., La Jolla, CA, USA) were used to perform the statistical analyses. For comparisons between two independent groups, unpaired Student's t-test was used and $p<0.05$ was considered statistically significant. All statistical analyses were performed using Microsoft Excel or GraphPad Prism 9.1.2 (GraphPad Software). All statistical information, including P values, samples sizes and repetitions, are provided in the Source Data associated with each figure.

ACKNOWLEDGEMENTS

The authors are grateful to members of the UTSW Touchstone Diabetes Center for critical reading of the manuscript and B. Evers for useful discussions. The authors thank C. Lee, the UTSW Animal Resource Center, Metabolic Phenotyping Core, Pathology Core, Live Cell Imaging Core, Flow Cytometry Core, and McDermott Sequencing Center for excellent guidance and assistance with experiments performed here. This study and/or personnel were supported in part by the NIH NIDDK R01 DK104789, R01 DK119163, and RC2 DK118620 to R.K.G., the American Heart Association postdoctoral fellowship 16POST26420136 and Career Development Award 19CDA34670007 from the American Heart Association and the Harry S. Moss Heart Trust to M.S, and Research Award from Rally Foundation (20IC37), NIH P30 CA142543, NIH R21CA259771 and CPRIT award RP180805 to L.X.

FIGURE LEGENDS

**Figure 1. Postnatal emergence of epididymal WAT from the *Pdgfrb* lineage.**

**a)** Histological analysis of perinatal eWAT development. Top two rows: representative H&E staining of transverse sections of the lower abdominal region of mice at postnatal (P) day 0 (P0), day 3 (P3), and day 7 (P7). First row H&E images are captured at 4x magnification. Second row H&E images are 10x magnifications of the dotted-lined boxes shown in the top row. Bottom two rows: indirect immunofluorescence (IF) assay of PLIN1 (Green) and MSLN (Red) expression within the presumptive eWAT at P0, P3, and P7. First row IF images are captured at 10x magnification. Second row IF images are 20x magnifications of the dotted-lined boxes shown directly above. EP = epididymis, T = testis, iWAT = subcutaneous inguinal WAT.

**b)** Genetic alleles of the "MuralChaser" lineage tracing system. In the presence of doxycycline (Dox), rtTA activates *Cre* expression in *Pdgfrb*-expressing cells. CRE excises the *loxP*-flanked membrane *tdTomato* cassette and allows constitutive activation of membrane GFP *(mGFP)* reporter expression in *Pdgfrb*-expressing cells and cells subsequently descending from this lineage.

**c)** Representative whole mount 63x confocal image of direct GFP and tdTomato expression in P28 eWAT of Control (*Cre*-) or "MuralChaser" mice. Lactating mice were administrated Dox-containing chow diet from P0 to P28.

**Figure 2. Cellular heterogeneity of perinatal and adult eWAT.**

a) UMAP analyses of transcriptional profiles of eWAT stromal-vascular cells harvested at P3 (n= 11553 cells), P7 (n= 14538 cells) and 5-weeks old (adult) (n= 10442 cells).

b) Heatmap depicting expression of 10 selected signature genes for PDGFR□+ sub-populations: APCs (cluster 9), FIPs (cluster 1), MLCs (cluster 17) and SMCs (cluster 10). Scaled by cluster mean expression and normalized by z-score.

**Figure 3. PDGFRβ+ LY6C- CD9- cells are the highly adipogenic subpopulation within perinatal eWAT.**

a) Cell lineage trajectory analysis using Slingshot. Committed preadipocytes (Preads), APCs, FIPs, MLCs and SMCs from merged datasets were subclustered as input for Slingshot, indicated by panels "Cell Origin" and "Cell Type". Committed Preads was specified as the end state, and either APCs ("APCs as origin") or FIPs ("FIPs as origin") was set as the root for pseudotime analysis.

b) Representative 10x magnification brightfield images of P7 APCs, P7 FIPs, Adult (5 weeks old) FIPs, and P7 MLCs, 6 days following the induction of in vitro adipocyte differentiation. Cultures are stained with oil red-O to visualize lipid accumulation.

c) mRNA levels of adipocyte-selective genes in P7 APCS and P7 FIPs at confluence (Day 0) or 6 days following the induction of in vitro adipocyte differentiation (Day 6). Bars represent ± SEM. * denotes $p<0.05$ by student t-test, ** denotes $p<0.01$, *** denotes $p<0.001$.

d) Representative 10x magnification image of H&E stained sections of the remnant inguinal WAT depot from lipodystrophic *Adipoq-Cre*, *Pparg*$^{loxP/loxP}$ mice 3 weeks after transplantion of either matrigel (vehicle control), 100,000 P7 APCs or 100,000 P7 FIPs.

Exact p values and numbers of repetitions can be found in Supplementary Table 2.

**Figure 4. Localization of APCs and FIPs in P7 eWAT.**

a) Representative 63x magnification confocal image of CD31, ANGIOTENSINOGEN (AGT), and PERILIPIN (PLIN) in P7 eWAT sections. Nuclei were counterstained with DAPI.

b) Representative 63x magnification confocal image of ENDOMUCIN (EMCN), EFHD1, and PLIN, in P7 eWAT sections. Nuclei were counterstained with DAPI.

c) Representative 63x magnification confocal image of MESOTHELIN (MSLN), EFHD1, and PLIN, in P7 eWAT sections. Nuclei were counterstained with DAPI.

**Figure 5. Perinatal FIPs are less anti-adipogenic and pro-inflammatory than adult FIPs.**

a) Representative 10x brightfield images of adult (5 weeks-old) APCs after 8 days of culture in conditioned media from parallel cultures of adult APCs, adult FIPs and P7 FIPs. Cultures are stained with oil red-O to visualize lipid accumulation.

b) mRNA levels of indicated proinflammatory genes in P7 FIPs and adult (5 weeks-old) FIPs treated with PBS or LPS (100ng/ml) for 2 hours. n=3 for each group. Bars represent ± SEM. * denotes $p<0.05$ by student t-test, ** denotes $p<0.01$, *** denotes $p<0.001$.

c) Scheme of *Pdgfrb-Ikk2*$^{CA}$ mice. Derived by breeding *Pdgfrb*$^{rtTA}$ transgenic mice to animals expressing *Cre* recombinase under the control of the tetracycline-response element (*TRE-Cre*) and carrying the *Rosa26RIkk2*$^{CA}$ allele. Littermates carrying only *Pdgfrb*$^{rtTA}$ and *Rosa26R*$^{Ikk2CA}$ alleles were used as the control animals. The addition of doxycycline leads to activation of the *Rosa26RIkk2*$^{CA}$ allele and constitutively active (CA) *IKK2* in *Pdgfrb*-expressing cells which leads to activation of NF-κB signaling.

d) mRNA levels of indicated proinflammatory genes in cultured P7 FIPs and adult (5 weeks-old) FIPs 24 hours the addition of doxycycline (1μg/ml). n=3 for each group. Bars represent ± SEM. * denotes $p<0.05$ by student t-test, ** denotes $p<0.01$, *** denotes $p<0.001$.

Exact p values and numbers of repetitions can be found in Supplementary Table 2.

**Extended Data Figure 1. Cellular composition of developing eWAT**

a) Cell clusters of merged transcriptional profiles of eWAT stromal-vascular cells harvested at P3 (n= 11553), P7 (n= 14538) and Adult (5-weeks old, n= 10442). Unsupervised clustering identifies distinct lineages corresponding to mesenchymal stromal cells (MSC), mesothelial cells, immune cells, endothelial cells, and committed preadipocytes (Preads).

b) Cell clusters from a at each developmental stage.

c) Expression of selected signature genes defining each cell cluster depicted in a and b.

Exact p values and numbers of repetitions can be found in Supplementary Table 2.

**Extended Data Figure 2. Expression of preadipocyte markers in perinatal PDGFR□+ subpopulations and committed preadipocytes.**

a) *Pparg* expression in *Pdgfrb*+ sub-populations and committed preadipocytes.

b) *Fabp4* expression in *Pdgfrb*+ sub-populations and committed preadipocytes.

c) *Dlk1* expression in *Pdgfrb*+ sub-populations and committed preadipocytes.

d) *Wt1* expression in *Pdgfrb*+ sub-populations and committed preadipocytes.

**Extended Data Figure 3. FACS strategy for the isolation of perinatal eWAT *Pdgfrb*+ sub-populations.**

a) Expression of marker genes used for FACS in the single cell clusters.

b) Gating strategy for isolating P7 *Pdgfrb*+ sub-populations. After live cell and singlet selection, CD31-Cd45- (Lin-) PDGFRβ+ cells are selected. *Pdgfrb*+ sub-populations can then be separated based on LY6C, CD9, and DPP4, expression.

c) Validation of the sorting strategy: qPCR analysis of the expression of genes identified by scRNA-seq as markers of P7 *Pdgfrb*+ sub-populations. n=3 for each group.

Exact p values and numbers of repetitions can be found in Supplementary Table 2.

**Extended Data Figure 4. Bulk-mRNA-seq reveals distinct global transcriptomes of P7 eWAT PDGFRβ+ subpopulations.**

a) Bar graph depicting the relative frequency of individual PDGFRβ+ subpopulations amongst total eWAT PDGFRβ+ cells based on flow cytometry analysis. n=8 for each group.

b) Principal component analysis (PCA) of global transcriptomes obtained by bulk-mRNA-seq analysis.

c) Sample clustering based on global transcriptomes obtained by bulk-mRNA-seq analysis.

d) Heatmap depicting the expression of top 10 signature genes defining each P7 PDGFRβ+ sub-populations. Expression normalized by z-score.

**Extended Data Figure 5. Pro-inflammatory responses of P7 FIPS.**

a) GSEA reveals gene signatures/pathways differentially expressed between P7 APCs and P7 FIPS. Pathways of statistical significance (Pval < 0.05) are shown. NES = Normalized Enrichment Score.

b) mRNA levels of indicated proinflammatory genes in cultured P7 APCs and P7 FIPs treated with PBS or LPS (100ng/ml) for 2 hours. n=3 for each group. Bars represent ± SEM. * denotes p<0.05 by student t-test, ** denotes p<0.01, *** denotes p<0.001.

c) mRNA levels of indicated proinflammatory genes in P7 FIPs and adult (5 weeks-old) FIPs treated with PBS or TNF (20ng/ml) for 2 hours. n=3 for each group. Bars represent ± SEM. * denotes p<0.05 by student t-test, ** denotes p<0.01, *** denotes p<0.001.

Exact p values and numbers of repetitions can be found in Supplementary Table 2.

**Supplemental Table 1: Sequences of qPCR primers used in this study**

| Gene | Forward (5' -3') | Reverse (5' -3') |
|---|---|---|
| *Adipoq* | AGATGGCACTCCTGGAGAGAA | TTCTCCAGGCTCTCCTTTCCT |
| *Cfd* | CTACATGGCTTCCGTGCAAGT | AGTCGTCATCCGTCACTCCAT |
| *Fabp4* | GATGAAATCACCGCAGACGAC | ATTCCACCACCAGCTTGTCAC |
| *Ccl2* | CCACAACCACCTCAAGCACTTC | AAGGCATCACAGTCCGAGTCAC |
| *Col3a1* | ATTCTGCCACCCCGAACTCAA | ACAGTCATGGGGCTGGCATTT |
| *Cxcl1* | CTGGGATTCACCTCAAGAACATC | CAGGGTCAAGGCAAGCCTC |
| *Cxcl10* | CTCAGGCTCGTCAGTTCTAAGT | CCCTTGGGAAGATGGTGGTTAA |
| *Cxcl2* | ACTAGCTACATCCCACCCACAC | GCACACTCCTTCCATGAAAGCC |
| *Icam1* | GTGATGCTCAGGTATCCATCCA | CACAGTTCTCAAAGCACAGCG |
| *Vcam1* | AGTTGGGGATTCGGTTGTTCT | CCCCTCATTCCTTACCACCC |
| *Il6* | AAGCCAGAGTCCTTCAGAGAGA | ACTCCTTCTGTGACTCCAGCTT |
| *Pparg2* | GCATGGTGCCTTCGCTGA | TGGCATCTCTGTGTCAACCATG |
| *Pparg*$^{TG}$ | TCAGGCAGATCGTCACAGAG | TTTGCCCCTCCATATAACA |
| *Rps18* | CATGCAAACCCACGACAGTA | CCTCACGCAGCTTGTTGTCTA |
| *Acta2* | TGACGCTGAAGTATCCGATAGA | GTACGTCCAGAGGCATAGAGG |
| *Tgfbi* | TTTAGGAAGGACCTGGGTTGG | TGTTGGTTGTAGAGGGCAAGG |
| *Hif1a* | GTCCCAGCTACGAAGTTACAGC | CAGTGCAGGATACACAAGGTTT |
| *Tnfa* | CCTGTAGCCCACGTCGTAG | GGGAGTAGACAAGGTACAACCC |
| *Lox* | TCGCTACACAGGACATCATGC | ATGTCCAAACACCAGGTACGG |
| *Mmp11* | CCGGAGAGTCACCGTCATC | GCAGGACTAGGGACCCAATG |
| *Mmp14* | ACCCACACACAACGCTCAC | GCCTGTCACTTGTAAACCATAGA |
| *Timp1* | CTTGGTTCCCTGGCGTACTC | ACCTGATCCGTCCACAAACAG |
| *Agt* | GTTCTGGGCAAAACTCAGTGC | GAGGCTCTGCTGCTCATCATT |
| *Apoe* | CTCCCAAGTCACACAAGAACTG | CCAGCTCCTTTTTGTAAGCCTTT |
| *Fndc5* | TTGCCATCTCTCAGCAGAAGA | GGCCTGCACATGGACGATA |
| *Ly6c* | ACTGTGCCTGCAACCTTGTCT | GGCCACAAGAAGAATGAGCAC |

| | | |
|---|---|---|
| *Lims2* | GCGGATTCTGTGGTGAATTTGT | CTGGCAGATGAATTTGCCCA |
| *Mfap5* | TCAACGCGGAGATGATGTGC | TCAGCCAGAGCTGTATCGTCT |
| *Fmo2* | AGCATCTACCGCTCTGTCATT | CAGGAGTTTAGAGTTGTGCAGG |
| *Fxdy6* | GTGCAAGTGCAGTTTCAATCAG | GCGTTTGTAGTGATGAGGTTCT |
| *Msln* | CTTGGGTGGATACCACGTCTG | GTCCCCGGAGTGTAATGTTCT |
| *Upk3b* | GCTTGGCCAACTTAACCTCCT | TGCTGCGTTCTCTGAAGTCTG |
| *Krt8* | GAATGGCCACTGAAGTCCTTG | AGTTCCCTGCACTCTGCCATA |

**Supplemental Table 2: Statistical data (exact p values and sample/cohort sizes for each dataset in the study).**

| Figure | N(sample size) | Statistical test method | # of Times Experiment was Performed | Description | | *p*-value |
|---|---|---|---|---|---|---|
| Figure 3b | Day 0: (P7 FIPs) n=3; (P7 APCs) n=3 | Unpaired two-tailed Student's t test | 3 independent trials | *Pparg2* | Day 0: P7 APCs vs P7 FIPs | 2.16716E-06 |
| | | | | | Day 6 Insulin only: P7 APCs vs P7 FIPs | 0.000717546 |
| | | | | | Day 6 DMI + Rosi: P7 APCs vs P7 FIPs | 0.602732433 |
| | | | | *Fabp4* | Day 0: P7 APCs vs P7 FIPs | 1.68761E-05 |
| | | | | | Day 6 Insulin only: P7 APCs vs P7 FIPs | 8.44799E-05 |
| | Day 6 Insulin only: (P7 FIPs) n=3; (P7 APCs) n=3 | | | | Day 6 DMI + Rosi: P7 APCs vs P7 FIPs | 0.01538233 |
| | | | | *Adipoq* | Day 0: P7 APCs vs P7 FIPs | 0.000254745 |
| | | | | | Day 6 Insulin only: P7 APCs vs P7 FIPs | 0.000183963 |
| | | | | | Day 6 DMI + Rosi: P7 APCs vs P7 FIPs | 0.250503785 |
| | Day 6 DMI + Rosi: (P7 FIPs) n=3; (P7 APCs) n=3 | | | *Cfd* | Day 0: P7 APCs vs P7 FIPs | 4.03364E-05 |
| | | | | | Day 6 Insulin only: P7 APCs vs P7 FIPs | 0.000341353 |
| | | | | | Day 6 DMI + Rosi: P7 APCs vs P7 FIPs | 0.168505852 |
| Figure 5b | | Unpaired two-tailed Student's t test | 2 independent trials | *Ccl2* | LPS: P7 FIPs vs Adult FIPs | 0.00029766 |
| | LPS ( P7 FIPs) n=3; | | | *Cxcl1* | | 9.03455E-05 |
| | LPS ( Adult FIPs) n=3; | | | *Cxcl2* | | 0.002111 |
| | Vehicle ( P7 FIPs) n=3; | | | *Cxcl10* | | 0.011274 |
| | Vehicle (Adult FIPs) n=3; | | | *Il6* | | 0.000810 |

| | | | | | | |
|---|---|---|---|---|---|---|
| | | | | *Icam1* | | 0.000326 |
| Figure 5d | | Unpaired two-tailed Student's t test | 2 independent trials | *Ccl2* | *Pdgfrb-Ikk2*$^{CA}$: P7 FIPs vs Adult FIPs | 0.002426135 |
| | *Pdgfrb-Ikk2*$^{CA}$( P7 FIPs) n=3; | | | *Cxcl1* | | 0.000287902 |
| | *Pdgfrb-Ikk2*$^{CA}$( Adult FIPs) n=3; | | | *Cxcl2* | | 0.001072 |
| | Control ( P7 FIPs) n=3; | | | *Cxcl10* | | 0.036203 |
| | Control ( Adult FIPs) n=3; | | | *Il6* | | 0.042594 |
| | | | | *Icam1* | | 0.040140 |
| Extended Data Figure 2c | P7 APCs n=3 | | 3 independent trials | *Agt* | P7 APCs vs P7 FIPs/SMCs/MLCs | |
| | | | | *Apoe* | | |
| | | | | *Fndc5* | | |
| | P7 FIPs n=3 | | | *Ly6c* | P7 FIPs vs P7 APCs/SMCs/MLCs | |
| | | | | *Lims2* | | |
| | | | | *Mfap5* | | |
| | P7 SMCs n=3 | | | *Acta2* | P7 SMCs vs P7 APCs/FIPs/MLCs | |
| | | | | *Fmo2* | | |
| | | | | *Fxyd6* | | |
| | P7 MLCs n=3 | | | *Msln* | P7 SMLCs vs P7 APCs/FIPs/SMCs | |
| | | | | *Upk3b* | | |
| | | | | *Krt8* | | |
| Extended Data Figure 3a | P7 APCs | | 3 independent trials | Frequency of PDGFRb+ cells | | |
| | P7 FIPs | | | | | |
| | P7 SMCs | | | | | |
| | P7 MLCs | | | | | |
| Extended Data Figure 4b | Control APCs (DoxP0.5-P7.5) n=4 | | 3 independent trials | *Adipoq* | Dox P0.5-P7.5: Control vs PpargTG | 0.250928256 |
| | | | | *Cfd* | | 0.269367455 |
| | *Pparg*$^{TG}$ APCs (DoxP0.5-P7.5) n=4 | | | *Cebpa* | | 0.904338906 |

**Figure 1**

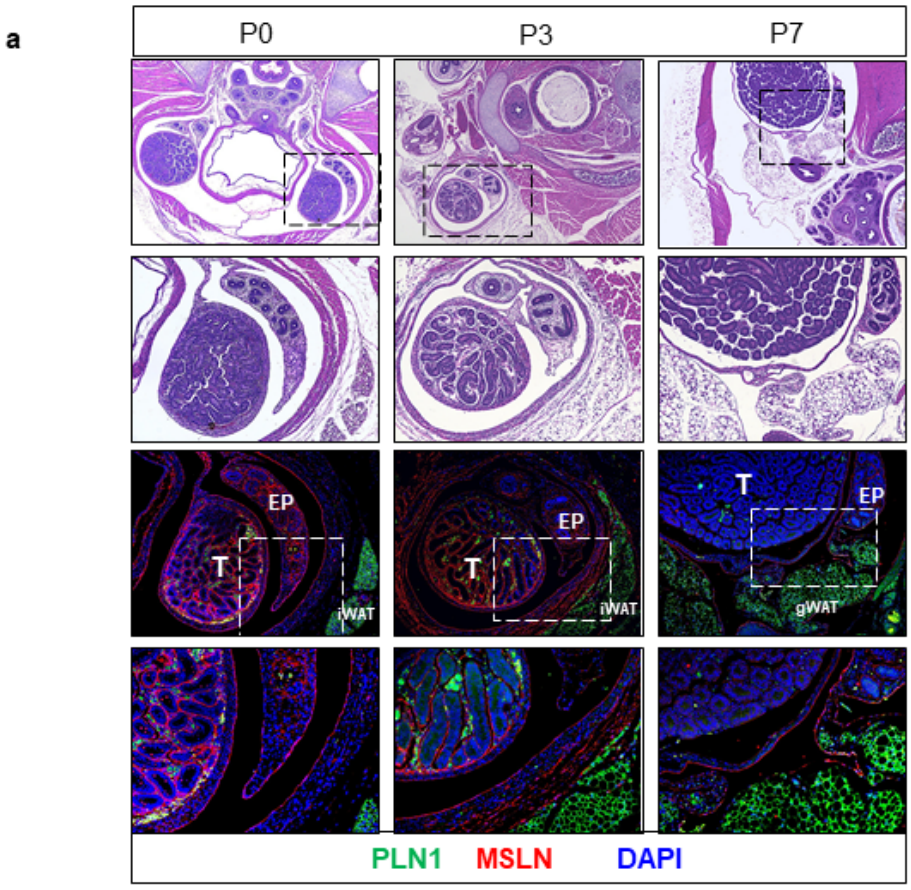
a
P0
P3
P7
EP
T
iWAT
gWAT
PLN1
MSLN
DAPI
b
Pdgfrb
rtTA
TRE
Cre
loxP
m-tdTomato
m-GFP
c
Dox P0-P28
tdTomato
GFP
Merge

**Figure 2**

a

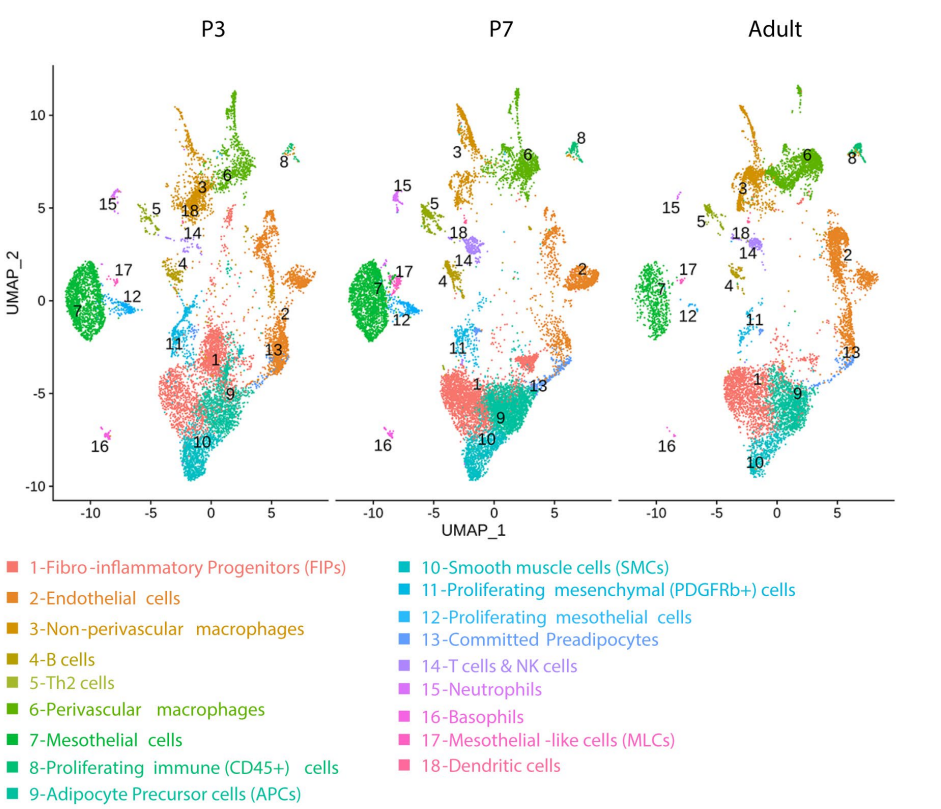
P3
P7
Adult
UMAP_2
UMAP_1
1-Fibro-inflammatory Progenitors (FIPs)
2-Endothelial cells
3-Non-perivascular macrophages
4-B cells
5-Th2 cells
6-Perivascular macrophages
7-Mesothelial cells
8-Proliferating immune (CD45+) cells
9-Adipocyte Precursor cells (APCs)
10-Smooth muscle cells (SMCs)
11-Proliferating mesenchymal (PDGFRb+) cells
12-Proliferating mesothelial cells
13-Committed Preadipocytes
14-T cells & NK cells
15-Neutrophils
16-Basophils
17-Mesothelial -like cells (MLCs)
18-Dendritic cells

b

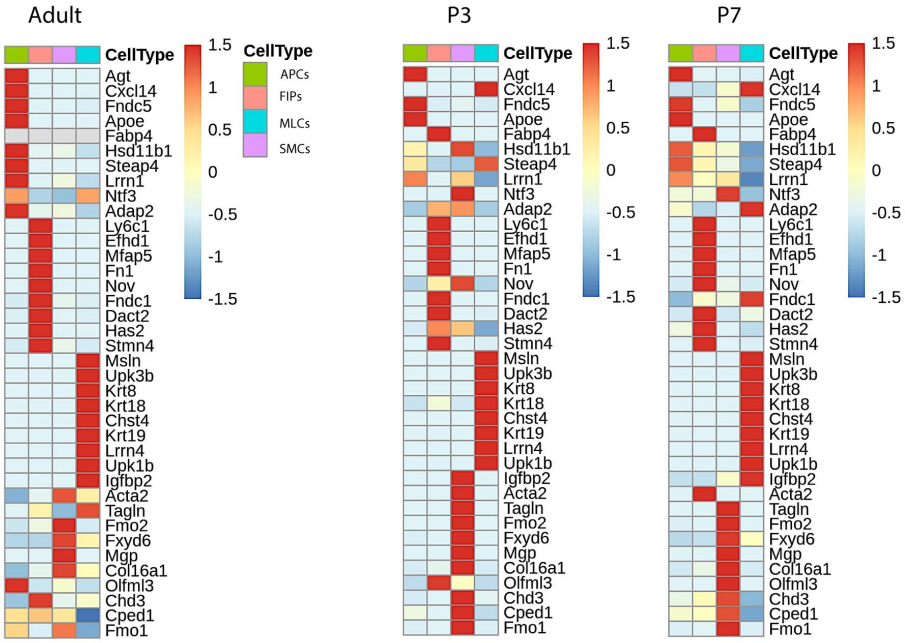
Adult
P3
P7
CellType
APCs
FIPs
MLCs
SMCs
Agt
Cxcl14
Fndc5
Apoe
Fabp4
Hsd11b1
Steap4
Lrrn1
Ntf3
Adap2
Ly6c1
Efhd1
Mfap5
Fn1
Nov
Fndc1
Dact2
Has2
Stmn4
Msln
Upk3b
Krt8
Krt18
Chst4
Krt19
Lrrn4
Upk1b
Igfbp2
Acta2
Tagln
Fmo2
Fxyd6
Mgp
Col16a1
Olfml3
Chd3
Cped1
Fmo1

**Figure 3**

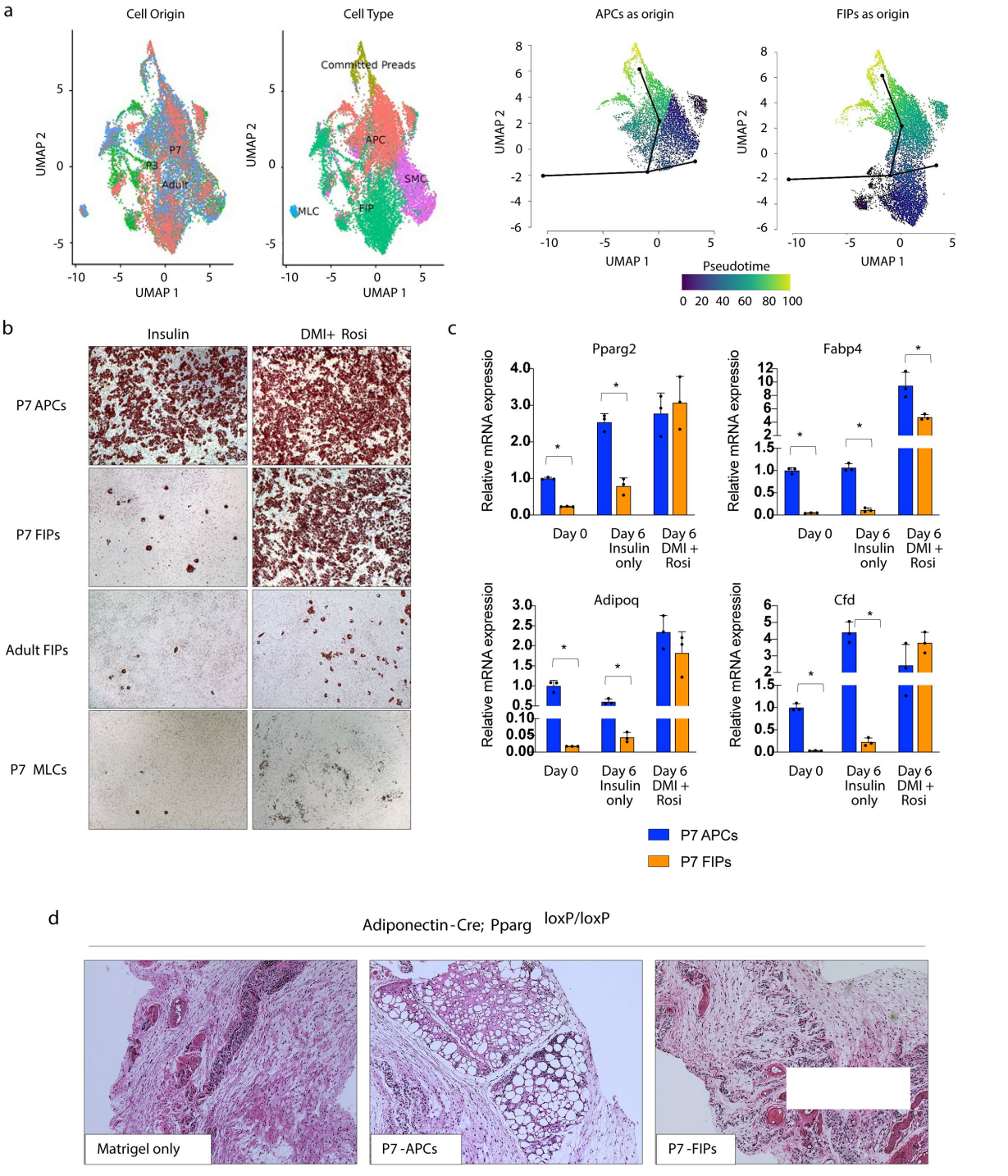
a
Cell Origin
Cell Type
APCs as origin
FIPs as origin
UMAP 1
UMAP 2
P7
P3
Adult
Committed Preads
APC
SMC
MLC
FIP
Pseudotime
0 20 40 60 80 100
b
Insulin
DMI+ Rosi
P7 APCs
P7 FIPs
Adult FIPs
P7 MLCs
c
Pparg2
Fabp4
Adipoq
Cfd
Relative mRNA expressio
Day 0
Day 6 Insulin only
Day 6 DMI + Rosi
P7 APCs
P7 FIPs
d
Adiponectin-Cre; Pparg loxP/loxP
Matrigel only
P7 -APCs
P7 -FIPs

**Figure 4**

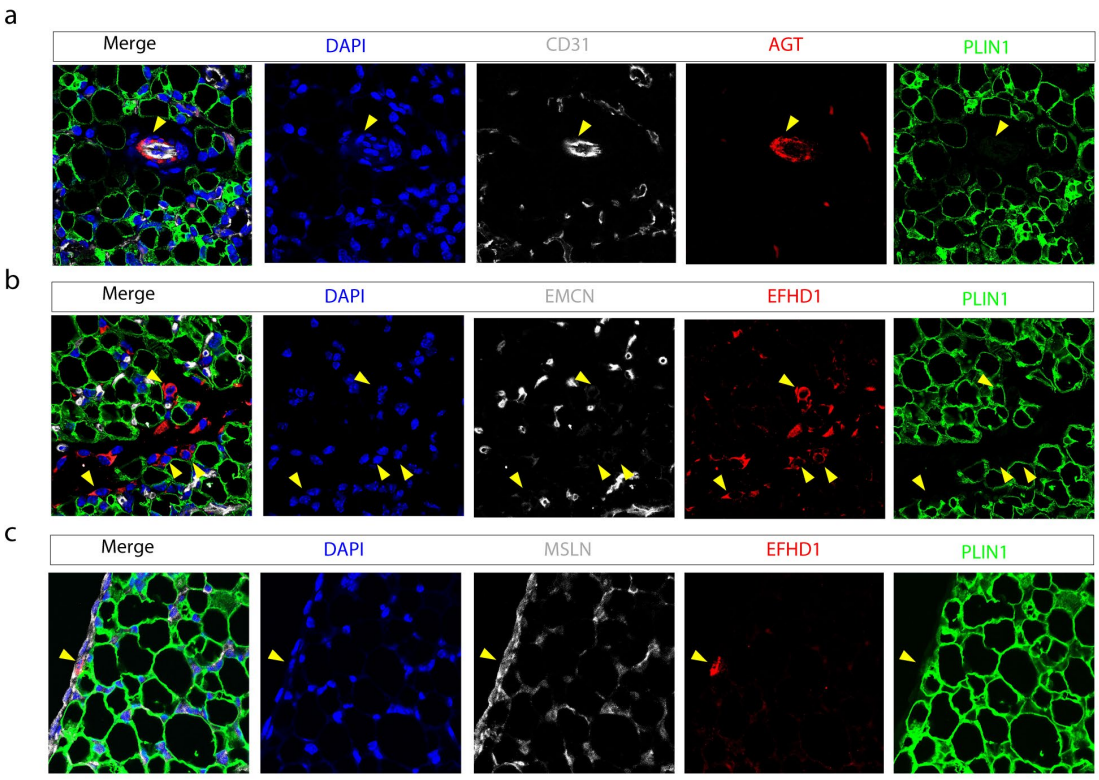
a
Merge
DAPI
CD31
AGT
PLIN1
b
Merge
DAPI
EMCN
EFHD1
PLIN1
c
Merge
DAPI
MSLN
EFHD1
PLIN1

# Figure 5

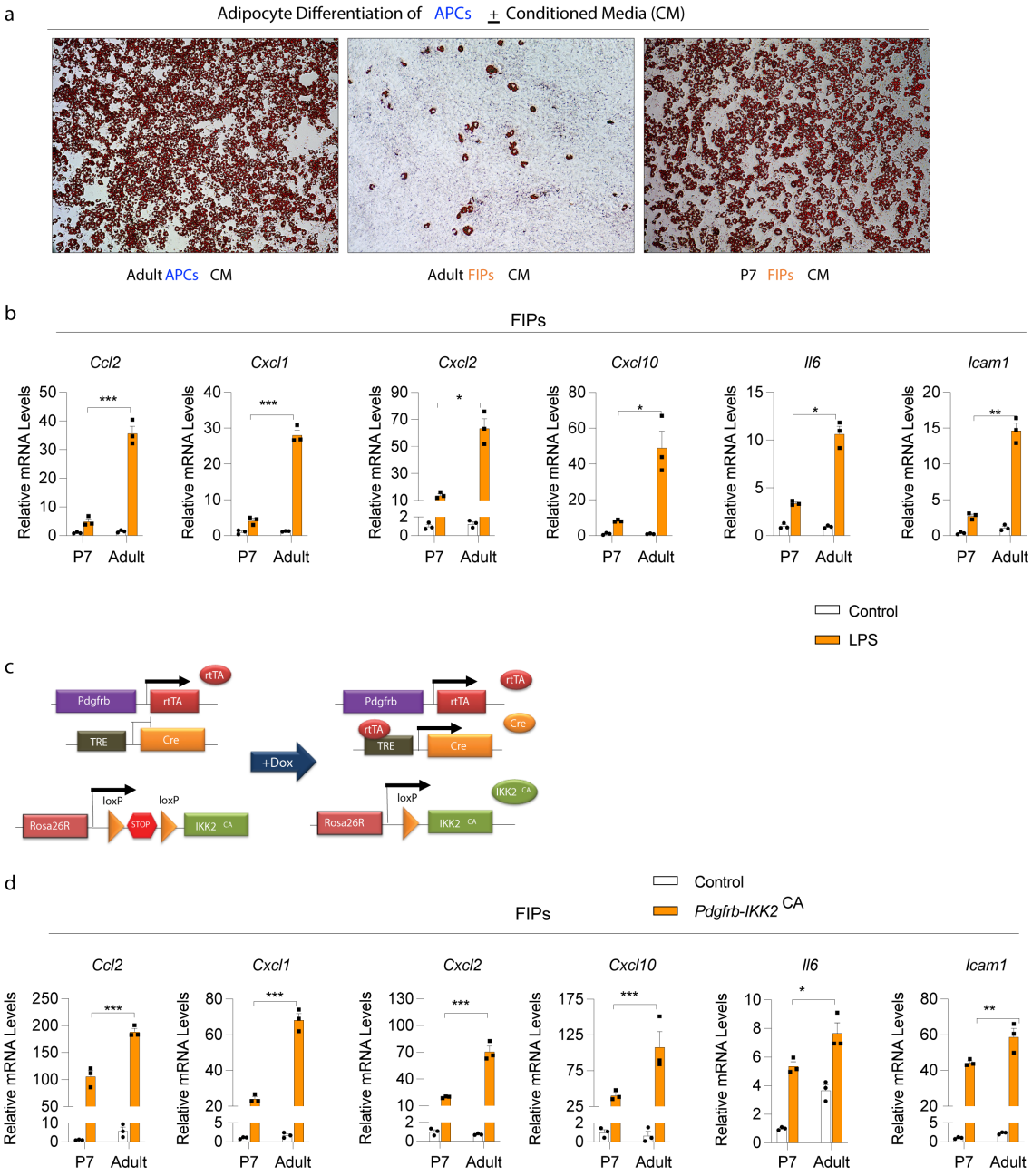
a
Adipocyte Differentiation of APCs ± Conditioned Media (CM)
Adult APCs CM
Adult FIPs CM
P7 FIPs CM
b
FIPs
Ccl2
Cxcl1
Cxcl2
Cxcl10
Il6
Icam1
Relative mRNA Levels
P7
Adult
Control
LPS
c
Pdgfrb
rtTA
TRE
Cre
+Dox
loxP
STOP
Rosa26R
IKK2 CA
d
FIPs
Control
Pdgfrb-IKK2 CA

**Extended Data Figure 1**

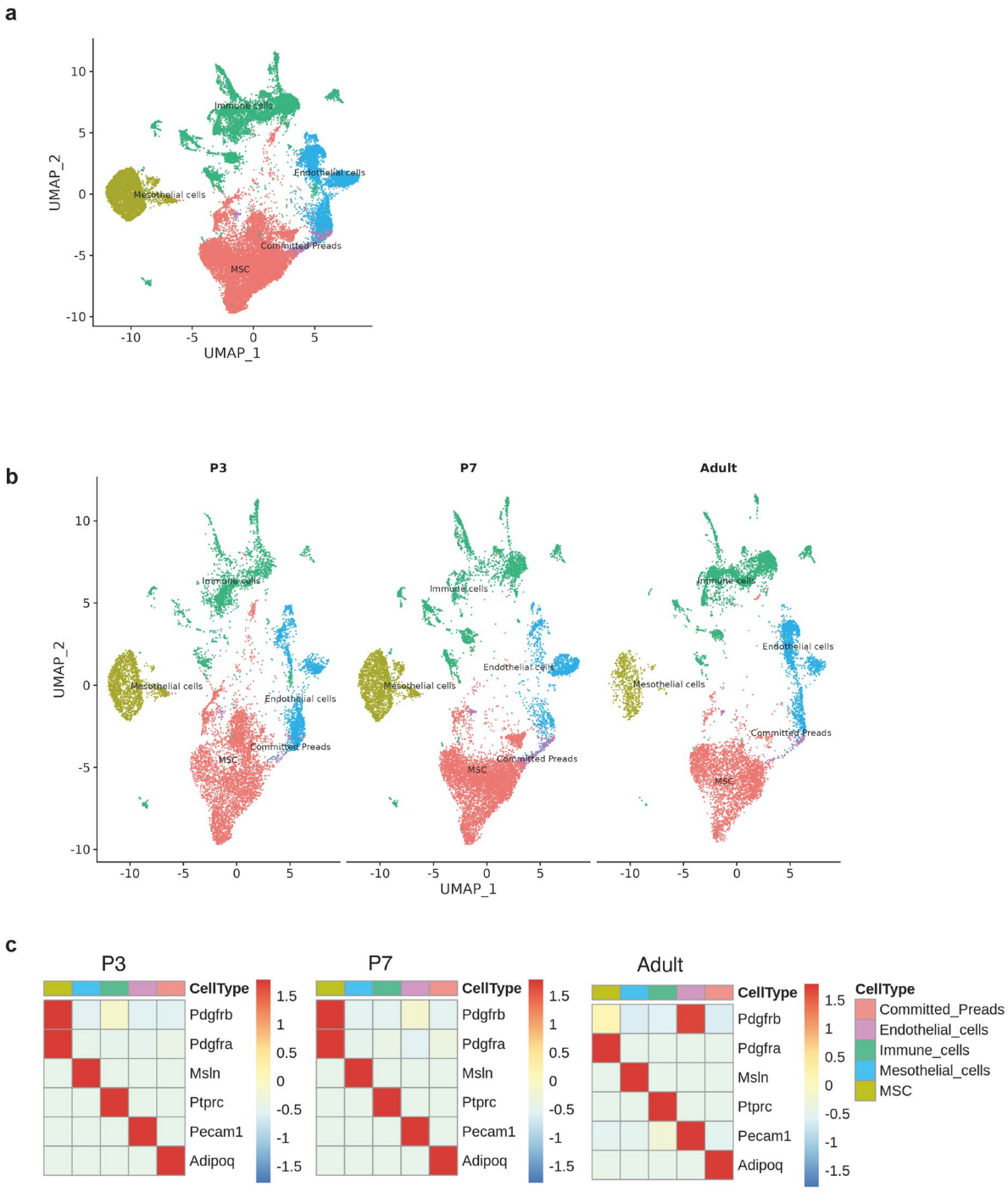

## Extended Data Figure 2

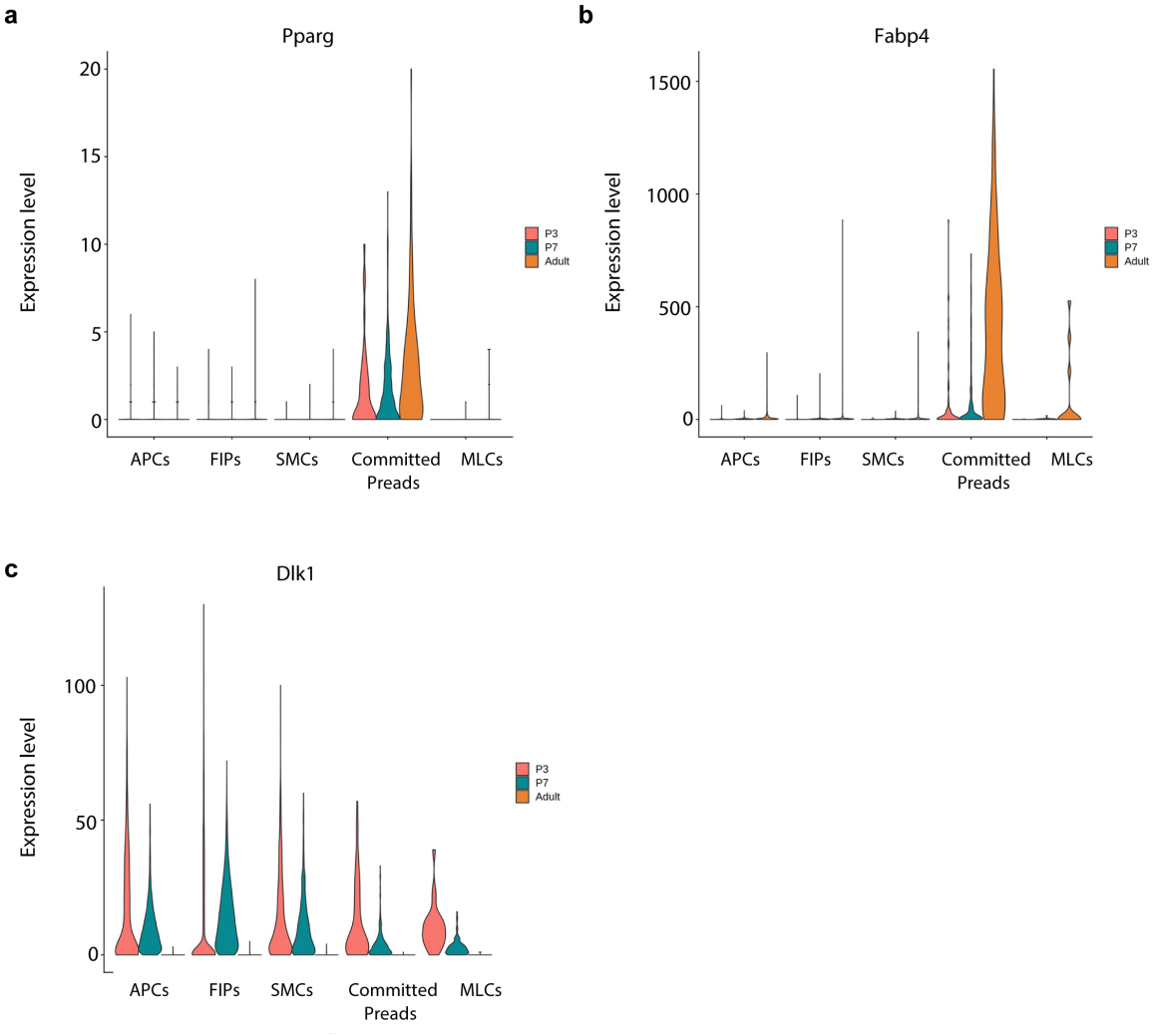

## Extended Data Figure 3

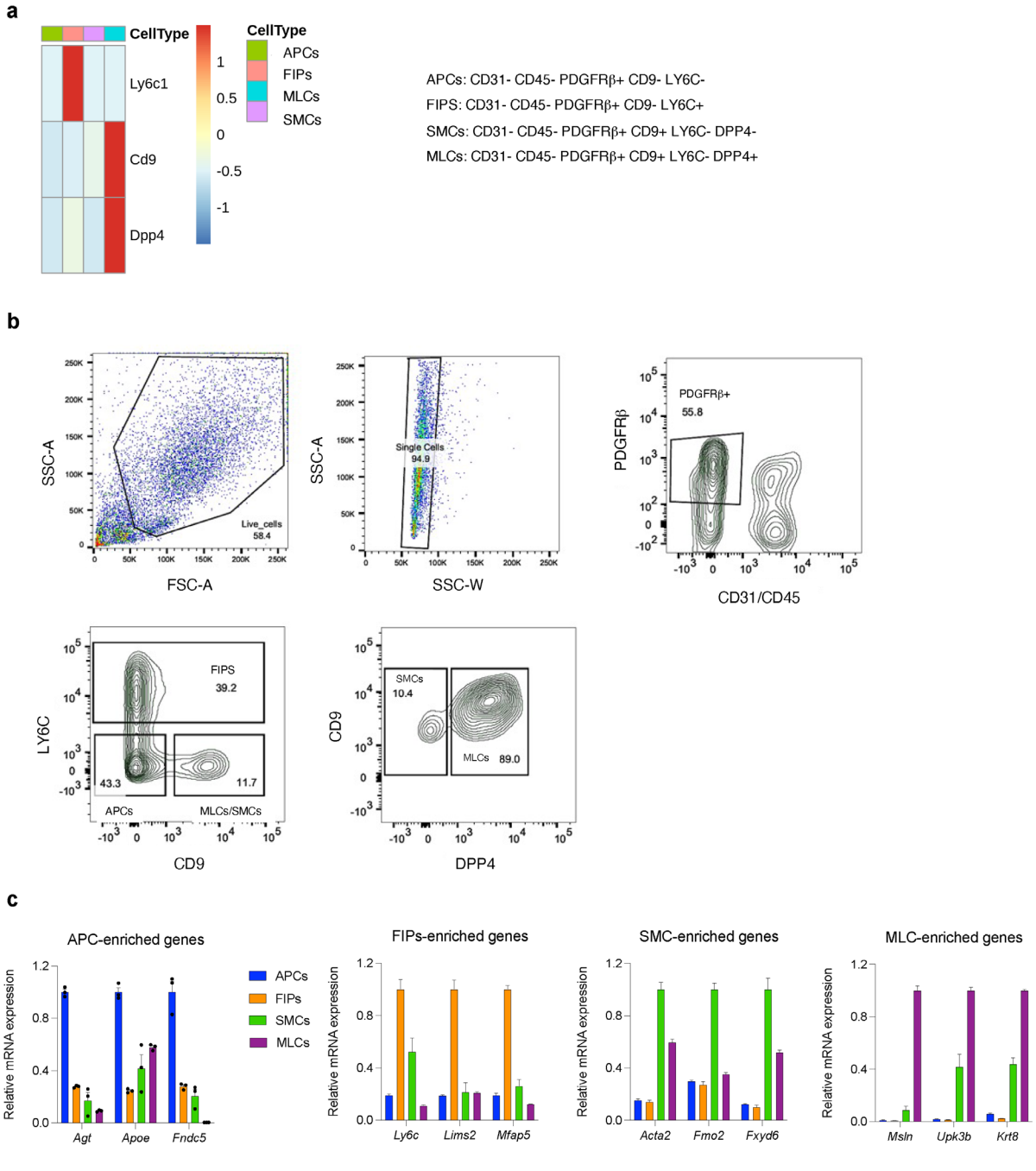

## Extended Data Figure 4

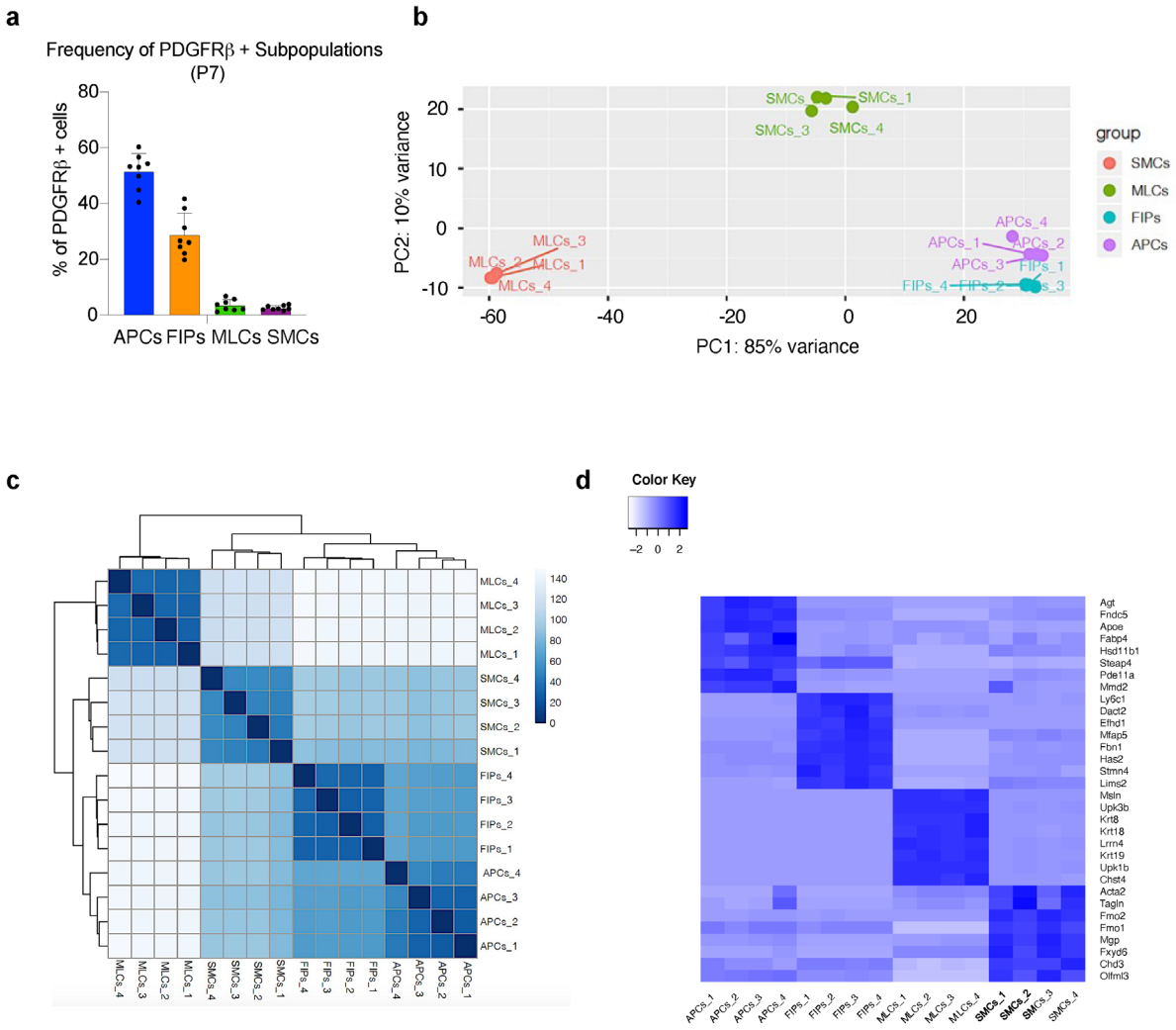

## Extended Data Figure 5

**a**

Enriched in P7 FIPs

| Pathway | pval | NES |
|---|---|---|
| HALLMARK_ALLOGRAFT_REJECTION | 0.001 | 1.85241 |
| HALLMARK_IL6_JAK_STAT3_SIGNALING | 0.001 | 1.84715 |
| HALLMARK_INFLAMMATORY_RESPONSE | 0.001 | 1.82571 |
| HALLMARK_KRAS_SIGNALING_UP | 0.001 | 1.75306 |
| HALLMARK_COAGULATION | 0.001 | 1.68419 |
| HALLMARK_TNFA_SIGNALING_VIA_NFKB | 0.001 | 1.63536 |
| HALLMARK_INTERFERON_GAMMA_RESPONSE | 0.001 | 1.5427 |
| HALLMARK_INTERFERON_ALPHA_RESPONSE | 0.006 | 1.44354 |
| HALLMARK_IL2_STAT5_SIGNALING | 0.001 | 1.44332 |
| HALLMARK_COMPLEMENT | 0.001 | 1.42759 |
| HALLMARK_APICAL_JUNCTION | 0.001 | 1.4269 |
| HALLMARK_APOPTOSIS | 0.033 | 1.27973 |
| HALLMARK_ESTROGEN_RESPONSE_EARLY | 0.024 | 1.247 |

Enriched in P7 APCs

| Pathway | pval | NES |
|---|---|---|
| HALLMARK_PANCREAS_BETA_CELLS | 0.0024 | 1.346 |
| HALLMARK_UV_RESPONSE_DN | 0.0080 | 1.233 |
| HALLMARK_APICAL_SURFACE | 0.0152 | 1.321 |
| HALLMARK_ADIPOGENESIS | 0.0170 | 1.202 |
| HALLMARK_EPITHELIAL_MESENCHYMAL_TRANSITION | 0.0220 | 1.167 |
| HALLMARK_XENOBIOTIC_METABOLISM | 0.0250 | 1.173 |
| HALLMARK_ANDROGEN_RESPONSE | 0.047 | 1.197 |
| HALLMARK_COAGULATION | 0.049 | 1.241 |

**b**

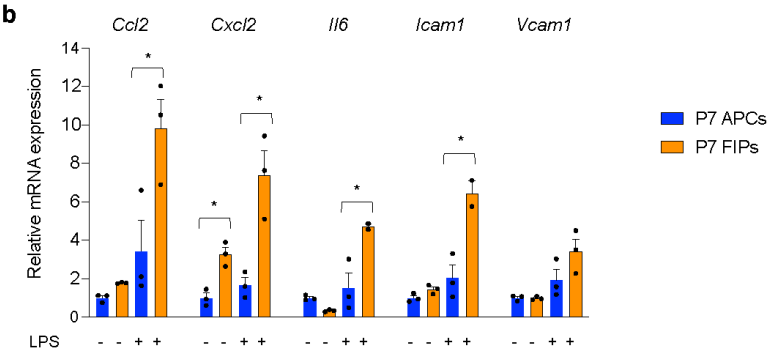


**c**

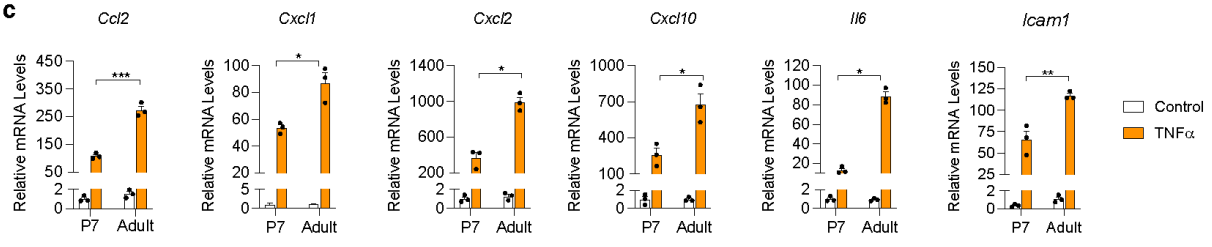

# CHAPTER THREE

## Transient Perinatal Manipulation in Pdgfrβ+ Cells Have Long-Term Consequences on Progenitor Cell Plasticity

*(This section contains content from a manuscript in revision at Nature Metabolism)*


SUMMARY

The observed differences in the functional properties of adult vs. perinatal PDGFRβ+ progenitor subpopulations prompted us to ask whether increasing the adipogenic capacity of PDGFRβ+ precursors specifically during the perinatal period would impact adipose tissue development and expandability in adulthood. We found that transient overexpression of *Pparg* in PDGFRβ+ cells only during postnatal day 0.5 to 7.5 leads to hyperplastic WAT development, durable progenitor cell reprogramming, and protection against pathologic WAT remodeling and glucose intolerance in adult-onset obesity. Thus, factors that alter the adipogenic capacity of perinatal adipose progenitors can have long-lasting effects on progenitor plasticity, tissue expandability, and metabolic health into adulthood.

# INTRODUCTION

The prevailing hypothesis in the field is that the recruitment of adipocytes from adipose progenitors in the setting of caloric excess is a protective mechanism to ensure safe energy storage in expanding adipose tissue. As proof of concept, we previously induced adipocyte hyperplasia in mice undergoing high fat diet feeding by inducing overexpressing the master regulator of adipogenesis, *Pparg,* in PDGFRβ+ cells. These *Pparg* transgenic mice ($Pparg^{TG}$) mice had improved insulin sensitivity, and their adipose tissues were less fibrotic and less inflamed (Shao, Vishvanath et al. 2018). This study highlighted the protective role of adipogenesis against pathologic adipose adipose tissue remodeling in obesity and revealed the significant contribution of PDGFRβ+ progenitors during the process.

In the previous chapter, we showed conclusively the unique functional properties of perinatal adipose progenitor subpopulations in murine eWAT. Specifically, we revealed important molecular and functional differences between postnatal day 7 (P7) and adult progenitor cell subpopulations. With this novel knowledge, we utilized the well-established *Pparg* overexpression genetic model and demonstrated that transient perinatal exposure to pro-adipogenic stimuli can exert long-lasting effects on progenitor plasticity and tissue cellularity into adulthood.

# RESULTS

**Perinatal *Pparg* overexpression in PDGFRβ+ cells have long-term consequences on progenitor cell plasticity.**

We previously described a model in which the adipogenic capacity of PDGFRβ+ progenitors can be increased through Dox-inducible overexpression of *Pparg*. (*Pdgfrb*$^{rtTA}$; *TRE-Pparg*, herein "*Pparg*$^{TG}$" mice) (Fig. 1a) (Shao, Vishvanath et al. 2018). Inducing PPARγ overexpression in adult *Pparg*$^{TG}$ mice at the onset of high fat diet (HFD) led to a doubling of the amount of de novo adipogenesis that normally occurs in the gonadal WAT depot in association with HFD feeding (Shao, Vishvanath et al. 2018). This observed increase in de novo adipogenesis was associated with healthy WAT remodeling; eWAT accumulated smaller and more numerous fat cells, relatively fewer pro-inflammatory macrophages, and maintained local insulin sensitivity. Importantly, inducible PPARγ overexpression in adult PDGFRβ+ precursors was not sufficient to drive de novo adipogenesis in adult chow-fed mice (Shao, Vishvanath et al. 2018).

The observed differences in the functional properties of adult vs. perinatal PDGFRβ+ progenitor subpopulations prompted us to ask whether increasing the adipogenic capacity of PDGFRβ+ precursors specifically during the perinatal period would impact adipose tissue development and expandability in adulthood. Newborn littermate Control (carrying *Pdgfrb*$^{rtTA}$ only) and *Pparg*$^{TG}$ pups were transiently exposed to doxycycline from P0.5 to P7.5 through postpartum feeding of lactating mothers with DOX-Chow. After P7.5, lactating

mice were switched back to standard chow diet without Dox until the time of weaning and harvesting (P28) (Fig. 1b). I confirmed by gene expression analysis that the *Pparg* transgene mRNA levels were induced to comparable levels in both APCs and FIPs following seven days of perinatal Dox exposure (Fig. 1c). Importantly, by P28 (3 weeks after Dox washout), transgene expression was turned off with mRNA levels returning to baseline levels. I did not observe any effect of transient perinatal *Pparg* overexpression in PDGFRβ+ cells on P28 body weights (Fig. 1d). Moreover, the frequency of eWAT APCs and FIPs at P28 was also not impacted by perinatal *Pparg* overexpression (Fig. 1e). I isolated APCs and FIPs from eWAT depots of both P28 Control and $Pparg^{TG}$ mice to test their differentiation potential *in vitro*. APCs from Control and $Pparg^{TG}$ mice underwent differentiation to a similar degree (Extended Data Figure 1a,b); however, transient *Pparg* overexpression only between P0.5-P.7.5 had a striking and durable pro-adipogenic impact on the differentiation capacity of FIPs (Fig. 1f,g). P28 FIPs from $Pparg^{TG}$ mice underwent adipocyte differentiation to a much greater extent than Control P28 FIPs upon induction. Histological analysis of P28 eWAT sections revealed the presence of smaller and more numerous adipocytes (Fig. 1h,i). To investigate whether the presence of smaller adipocytes is a matter of beiging, I put 5-weeks old Control and $Pparg^{TG}$ mice in 6°C for one week (Extended Data Figure 1c) and found no significant elevation of thermogenesis genes especially *Ucp1*(Extended Data Figure 1d), and no significant amount of emerging beige adipocytes in eWAT(Extended Data Figure 1d). Taken together, my data indicate a hyperplastic eWAT development in response to transient *Pparg* overexpression during the first week of life.

I also asked whether transient *Pparg* overexpression in PDGFRβ+ cells at a later stage of life can exert the same long-lasting effects. I weaned Control and *Pparg*$^{TG}$ mice at P21 and placed them directly on a Dox-chow diet for one week (P21-P28) (Fig. 1b). This is a period considered to represent murine adolescence (Holtrup, Church et al. 2017). Three weeks after Dox diet was removed (P49), body weights of *Pparg*$^{TG}$ mice were indistinguishable from Controls (Fig. 1d). Moreover, transient expression of *Pparg* did not impact the frequency of APCs and FIPs or the adipogenic capacity of FIPs (Fig. 1e-g). Histological analysis of eWAT sections revealed that transient *Pparg* overexpression from P21-P28 also did not impact the cellularity of tissue at P49 (Fig. 1h,i). Taken together, these data suggest that the early perinatal period (P0.5-7.5) is a unique window for adipose progenitor plasticity.

**Transient perinatal *Pparg* overexpression have prolong impact on functional properties of PDGFRβ+ cells after adult-onset obesity.**

I next engaged to decipher the roles of PDGFRβ+ subpopulations in the long-term impact of obese transient *Pparg*$^{TG}$ mice. Technical limitations prevented investigation of APCs and FIPs independently *in vivo*, but I managed to isolate the two populations post-HFD and conducted a series of *in vitro* experiments.

After 12 weeks of HFD feeding, APCs and FIPs from control and *Pparg*$^{TG}$ mice with dox from P0.5-P7.5 as described above were isolated by FACS using the same strategy as in Hepler et. al (Hepler, Shan et al. 2018). Frequency of total PDGFRβ+ cells out of all live cells were not changed between control and *Pparg*$^{TG}$ mice, frequency of APCs and FIPs out

of total PDGFRβ+ cells were also not altered (figure 2a); however, quantitative real-time PRC showed lower expression levels of several key pro-inflammatory cytokines in freshly isolated FIPs from *Pparg*$^{TG}$ mice compared to control (figure 2b). Moreover, post-12w HFD FIPs from *Pparg*$^{TG}$ mice also responded less to lps stimulation (figure 2c). Strikingly, post-12w HFD FIPs from *Pparg*$^{TG}$ mice were still capable of adipocyte differentiation upon induction, while control FIPs could not differentiate, being consistent with when they were at p28 (figure 2d,e). Post-12w HFD APCs from both control and *Pparg*$^{TG}$ mice remained spontaneous differentiation capacity with no detectable difference (extended data figure 2a). Notably, expression of *pparg2* was significantly elevated in post-12w HFD FIPs from *Pparg*$^{TG}$ mice upon induction, but *pparg* transgene remained off with mRNA level remaining at baseline (extended data figure 2b). Taken together, *Pparg*$^{TG}$ (dox P0.5-P7.5) FIPs maintained their functional property differences that were observed at P28 in chow mice, even after 12 weeks HFD feeding and now in obese mice.

The adipocyte fractions of eWAT were also collected for examination. Quantitative real-time PCR of fibrogenesis and pro-inflammatory gene signatures suggested that adipocytes from *Pparg*$^{TG}$ mice were also healthier (extended data figure 2c,d), consistent with eWAT whole tissue level observations.

**Transient perinatal *Pparg* overexpression in PDGFRβ+ cells impact WAT plasticity in adult-onset obesity.**

The hyperplastic eWAT phenotype observed following perinatal *Pparg* overexpression prompted us to ask how these *Pparg*$^{TG}$ mice would ultimately adapt to high-

fat diet feeding in adulthood. I treated Control and *Pparg*$^{TG}$ mice with Dox from P0.5-P7.5 as described above, and then placed animals on a standard chow diet until 6 weeks of age. At 6 weeks of age, mice were then placed on a HFD (60% kcal) for up to 12 weeks (Fig. 3a). During the 12 weeks of HFD feeding, Control and *Pparg*$^{TG}$ mice did not significantly differ in body weights (Fig. 3b). After 12 weeks of HFD, WAT mass was also comparable between the controls and transgenic mice (Fig. 3c); however, eWAT depots from HFD-fed *Pparg*$^{TG}$ mice contained fewer MAC-2+ inflammatory cells and few crown-like structures (Fig. 3d,e). This correlated with lower mRNA levels of pro-inflammatory genes and fibrogenic genes assayed across whole depots (Fig. 3f,g). Moreover, eWAT from HFD-fed *Pparg*$^{TG}$ mice maintained smaller and more numerous adipocytes after the 12 weeks of HFD feeding (Fig. 3h-j). The healthy eWAT phenotype correlated with systemic improvements in metabolic health. Obese *Pparg*$^{TG}$ mice exhibit better glucose tolerance than Control animals (Fig. 3k,l). Moreover, serum levels of ADIPONECTIN are higher in obese *Pparg*$^{TG}$ mice, further reflective of preserved WAT function (Fig. 3m). Furthermore, serum triglyceride levels were lower in obese *Pparg*$^{TG}$ mice (Fig. 3n). Taken together, these data highlight the long-term impact of modulating the adipogenic capacity of adipose progenitors during the perinatal stage.

# DISCUSSION

My data here highlight the long-term impact of modulating the adipogenic capacity of adipose progenitors specifically during the perinatal stage. Transient overexpression of *Pparg* in PDGFRβ+ cells during the first week of life led to healthy hyperplastic eWAT development that can be observed at weaning and even after HFD feeding in adulthood. Remarkably, PPARγ expression during this perinatal window exerted a long-lasting impact on the adipogenic capacity of FIPs. These phenotypes were not observed when PPARγ was instead transiently expressed for the same duration in P21-P28 mice, suggesting a unique plasticity to perinatal progenitors. The differences between perinatal vs. adult adipose progenitors in molecular markers (e.g. *Dlk1*) and lineage plasticity may have implications for the study of adipogenesis in mice. The use of gain and loss of function animals that lack temporal control (e.g. constitutively active transgenes) may make it difficult to discriminate between perinatal vs. adult effects on progenitor activity.

It is increasingly apparent that maternal obesity and maternal environmental factors influence energy balance and nutrient homeostasis of offspring through durable reprograming of cells (Rando and Simmons 2015). Going forward, it will be important to examine how maternal nutrition and energy balance impact the distinct progenitor subpopulations of adipose tissues, and whether long-term changes in these cell populations underly any of the long-term effects on offspring physiology. Moreover, gaining deeper insight into the molecular mechanisms underlying the observed differences between perinatal and adult FIPs may identify strategies to enhance adipogenesis and healthy WAT remodeling in adulthood.

# MATERIALS AND METHODS

## Animals and diets

All animal experiments were performed according to procedures approved by the UTSW Animal Care and Use Committee. *Pdgfrb*$^{rtTA}$ transgenic mice (C57BL/6-Tg(Pdgfrb-rtTA)58Gpta/J; JAX 028570) have been described previously. *TRE-Pparg2* transgenic mice were derived by the UTSW transgenic core facility. Postnatal day 7 (P7), 4-6 weeks and 18 weeks old male mice were used in this study.

Mice were maintained on a 12 hr light/dark cycle in a temperature-controlled environment (22˚C) and given free access to water and diets as indicated in the manuscript. For cold exposure, mice were housed at room temperature until 5 weeks of age and then switched to cold housing chambers (6ºC) for the indicated times. Diet utilized include, standard rodent chow diet, or doxycyline-containing chow diet (Dox-Chow, 600 mg/kg doxycycline, Bio-Serv, S4107), or HFD (HFD; 60% kcal fat; Research Diets no. D12492i).

## Histological analysis

Adipose tissues were fixed in 4% paraformaldehyde for 24h and maintained in 50% ethanol solution. Paraffin embedding, perinatal tissue sectioning and H&E staining was performed by the Molecular Pathology Core Facility at UTSW. Brightfield and fluorescent images were acquired using a Keyence BZ-X710 microscope. Indirect immunofluorescence was performed as previously described (Vishvanath, MacPherson et al. 2016). Primary

antibodies used for immunofluorescence include: guinea pig anti-PERILIPIN 1:1000 (Fitzgerald #20R-PP004) and rabbit anti-MAC-2 1:500 (Cedarlane #CL8942AP).

**Gene expression analysis by qPCR**

RNA was isolated using RNAqueous-Micro Total RNA Isolation Kit (Thermo Fisher Scientific). cDNA was synthesized using M-MLV Reverse Transcriptase (Invitrogen) and Random Primers (Invitrogen). Relative mRNA levels were determined by quantitative PCR using SYBR Green PCR Master Mix (Applied Biosystems). Values were normalized to *Rps18* levels using the 2-$Ct^{\Delta\Delta}$ method. Unpaired Student's t-test was used to evaluate statistical significance. All primer sequences are listed within Supplementary Table 1.

**Isolation of adipose SVF and flow cytometry**

Adipose tissue from five P7 pups or one 6-8 weeks or one 18 weeks old male mouse were combined and minced with scissors in a 1.5 mL tube containing 100ul of digestion buffer (1X HBSS, 1.5% BSA, and 1 mg/mL collagenase D) and then transferred to a 50 mL Falcon tube containing 5 mL digestion buffer. The mixture was incubated in a 37˚C shaking water bath for 30 mins or 1h. The solution of digested tissue was passed through a 100 μm cell strainer, diluted to 30 mL with 2% FBS/PBS, and centrifuged at 500 x g for 5 min. The supernatant was aspirated, and cells were washed once with 2% FBS/PBS and resuspended in blocking buffer (2% FBS/PBS containing anti-mouse CD16/CD32 Fc Block (1:200)). Primary antibodies were added to the cells in blocking buffer for 15 mins at 4˚C in the dark. After incubation, the cells were washed once with 2% FBS/PBS and resuspended in 200 μl of

2% FBS/PBS for sorting. Cells were sorted for collection into 100% FBS using a BD Biosciences FACSAria cytometer (UTSW Flow Cytometry Core Facility). Flow cytometry plots were generated using FlowJo.

Primary antibodies and the working concentrations were as follows: CD45–PerCP/Cyanine 5.5 1:400 (Biolegend, clone 30-F11, no. 103132), CD31–PerCP/Cyanine 5.5 1:400 (Biolegend, clone 390, no. 102420), PDGFRβ-PE 1:75 (Biolegend, clone APB5, no. 136006), LY6C–APC/Cyanine7 1:400 (Biolegend, clone HK1.4, no. 128026), CD9–FITC 1:400 (Biolegend, clone MZ3, no. 124808), CD26(DPP4)-APC 1:400 (Biolegend, clone H194-112, #137807).

**Cell culture and cellular assays**

Sorted PDGFRβ+ sub-populations cells were plated at a density of 4 x $10^4$ cells/ well in a 48-well plate or 2 x $10^4$ cells/ well in a 96-well plate containing 2% ITS growth media [consisting of 60% low-glucose DMEM, 40% MCDB-201 medium, 2% FBS, 1% ITS premix (Insulin–Transferrin–Selenium) (BD Biosciences, no. 354352), 0.1 mM l-ascorbic acid-2-2phosphate (Sigma, no. A8960-5G), 10 ng ml–1 FGF basic (R&D systems, no.3139-FB-025/CF), penicillin–streptomycin and gentamicin] and incubated at 37˚C in 10% $CO_2$.

For in vitro adipocyte differentiation assay, cells were grown to confluence in 2% ITS growth media and switched to induction media (growth media supplemented with 1 mM dexamethasone, 0.5 mM isobutylmethyxanthine, ±1 mM rosiglitazone) for 48 hrs. After 48 hrs., cultures were maintained in 2% ITS growth media. Media were changed every two days until harvesting.

For LPS treatment, cells were grown to confluence and starved overnight with serum-free ITS medium. Cells were then treated with 100ng/ml LPS or PBS for 2 hrs. prior to harvest.

**Oil red O staining**

Cells were pre-fixed in 4% PFA for 15 min at room temperature and then washed twice with ddH2O. Following 1 hour of additional fixation, cells were rinsed with ddH2O six times and then incubated in Oil Red O working solution (2 g Oil red O in 60% isopropanol) for 10 minures. Stained cells were then washed three times with ddH2O and then bright field images were acquired using Keyence BZ-X710 Microscope.

**Glucose tolerance tests.**

For glucose tolerance tests, overnight fasted mice were injected i.p. with glucose (Sigma, no. G7021) at the dose of 1 g per kg (body weight). Blood glucose concentrations were determined using Bayer Contour glucometers.

**Serum measurements.**

Serum levels of ADIPONECTIN and TG were measured using the mouse adiponectin ELISA (Millipore, no. EZMADP-60K) and TG kit, respectively. Assays were performed according to manufacturer instructions.

**Statistical analysis**

Statistical methods were not used to predetermine sample size. The experiments were not randomized, and the investigators were not blinded. All data were expressed as the mean ±SEM. GraphPad Prism 9.1.2 (GraphPad Software, Inc., La Jolla, CA, USA) were used to perform the statistical analyses. For comparisons between two independent groups, unpaired Student's t-test was used and $p<0.05$ was considered statistically significant. All statistical analyses were performed using Microsoft Excel or GraphPad Prism 9.1.2 (GraphPad Software). All statistical information, including P values, samples sizes and repetitions, are provided in the Source Data associated with each figure.

## ACKNOWLEDGEMENTS

The authors are grateful to members of the UTSW Touchstone Diabetes Center for critical reading of the manuscript and B. Evers for useful discussions. The authors thank C. Lee, the UTSW Animal Resource Center, Metabolic Phenotyping Core, Pathology Core, Live Cell Imaging Core, Flow Cytometry Core, and McDermott Sequencing Center for excellent guidance and assistance with experiments performed here. This study and/or personnel were supported in part by the NIH NIDDK R01 DK104789, R01 DK119163, and RC2 DK118620 to R.K.G., the American Heart Association postdoctoral fellowship 16POST26420136 and Career Development Award 19CDA34670007 from the American Heart Association and the Harry S. Moss Heart Trust to M.S.

FIGURE LEGENDS

**Figure 1. Transient perinatal *Pparg* overexpression in PDGFRβ+ cells has long-term consequences on progenitor cell plasticity.**

a) *Pparg*$^{TG}$ mice (Bi-transgenic *Pdgfrb*$^{rtTA}$; *TRE-Pparg2*) are generated by breeding the *Pdgfrb*$^{rtTA}$ transgenic mice to animals expressing *Pparg2* under the control of the tet-response element (*TRE- Pparg2*). Littermates carrying only *Pdgfrb*$^{rtTA}$ or *TRE-Pparg2* alleles were used as the control animals.

b) Experimental Design: Transient perinatal *Pparg* overexpression was achieved by exposing newborn pups to doxycycline from P0.5-P7.5 via lactating mothers fed a Dox-containing chow diet (600 mg/kg). Animals were then maintained on standard chow diet (- Dox) until harvest at P28 for analysis. Transient adolescent *Pparg* overexpression was achieved by directly feeding animals Dox-containing chow diet from P21-P28. Animals were then maintained on standard chow diet (- Dox) until harvest at P49 for analysis.

c) mRNA levels of *Pparg2* transgene levels (transgene-specific primers) in isolated APCs and FIPs at the 7$^{th}$ day of Dox treatment and 3 weeks after the removal of Dox (washout). n=3-5 for each group. Bars represent ± SEM. ** denotes $p<0.01$ by student t-test, *** denotes $p<0.001$.

d) Body weights of Control and *Pparg*$^{TG}$ 3 weeks after the indicated Dox-treatment periods (left: Dox from P0.5-P7.5; right: Dox from P21-P28). n=5-11 for each group. Bars represent ± SEM. N.S. denotes $p>0.5$ by student t-test.

e) Frequency of APCs and FIPs in eWAT of Control and *Pparg*$^{TG}$ 3 weeks after the indicated Dox-treatment periods (left: Dox from P0.5-P7.5; right: Dox from P21-P28). n=5-6 for each group. Bars represent ± SEM. N.S. denotes $p>0.5$ by student t-test.

f) Representative 10x brightfield image of lipid accumulation in differentiated cultures of FIPs derived from Control and *Pparg*$^{TG}$. FIPs were isolated 3 weeks after the indicated periods of Dox-treatment and transient *Pparg* expression. Cells were induced to undergo adipogenesis with induction media containing dexamethasone, IMBX, insulin, and

rosiglitazone. Oil Red O staining of lipid accumulation and imaging was performed 6 days following the induction of differentiation.

g) mRNA levels of adipocyte-selective genes in differentiated cultures of FIPs corresponding to panel f. n=3 for each group. Bars represent ± SEM. * denotes $p<0.05$ by student t-test, *** denotes $p<0.001$.

h) Representative 10x brightfield images of H&E stained eWAT obtained from Control and *Pparg*$^{TG}$ 3 weeks after the indicated period of Dox-treatment and transient *Pparg* expression.

i) Adipocyte size distribution in eWAT of Control and *Pparg*$^{TG}$ 3 weeks after the indicated period of Dox-treatment and transient *Pparg* expression. n = 4 for each group. Bars represent ± SEM. * denotes $p<0.05$ by student t-test, ** denotes $p<0.01$, *** denotes $p<0.001$.

Exact p values and numbers of repetitions can be found in Supplemental Table 2.

**Figure 2. Transient perinatal *Pparg* overexpression has prolong impact on functional properties of PDGFRβ+ cells after adult-onset obesity.**

a) Frequency of total PDGFRβ+ cells, APCs, FIPs isolated from eWAT of Control and *Pparg*$^{TG}$ mice after 12 weeks of HFD feeding.

b) mRNA levels of indicated proinflammatory genes in FIPs freshly isolated from eWAT of Control and *Pparg*$^{TG}$ mice after 12 weeks of HFD feeding. n=4 for each group. Bars represent ± SEM. * denotes $p<0.05$ by student t-test.

c) mRNA levels of indicated proinflammatory genes in FIPs isolated from eWAT of Control and *Pparg*$^{TG}$ mice after 12 weeks of HFD feeding. FIPs treated with PBS or LPS (100ng/ml) for 2 hours. n=4 for each group. Bars represent ± SEM. * denotes $p<0.05$ by student t-test, ** denotes $p<0.01$.

d) Representative 10x brightfield image of lipid accumulation in differentiated cultures of FIPs derived from Control and *Pparg*$^{TG}$ after 12 weeks of HFD feeding. Cells were induced to undergo adipogenesis with induction media containing dexamethasone, IMBX, insulin, and rosiglitazone. Oil Red O staining of lipid accumulation and imaging was performed 6 days following the induction of differentiation.

e) mRNA levels of adipocyte-selective genes in differentiated cultures of FIPs corresponding to panel d. n=4 for each group. Bars represent ± SEM. * denotes $p<0.05$ by student t-test, *** denotes $p<0.001$.

Exact p values and numbers of repetitions can be found in Supplemental Table 2.

**Figure 3. Transient perinatal *Pparg* overexpression in PDGFRβ+ cells impacts eWAT plasticity in adult-onset obesity.**

a) Experimental design: Transient perinatal *Pparg* overexpression from P0.5-P7.5 was induced by exposing newborn pups to doxycycline via lactating mothers fed a Dox-containing chow diet (600 mg/kg). Lactating animals were then switched to a standard chow diet (- Dox) until weaning. 6 weeks-old Control and $Pparg^{TG}$ offspring then administrated a high-fat-diet (HFD) (60% kcal) for 12 weeks prior to analysis.

b) Weekly body weights of Control and $Pparg^{TG}$ mice during the HFD feeding period. n=7 for each group.

c) Tissue weights of Control and $Pparg^{TG}$ mice after 12 weeks of HFD feeding. n=7 for each group. Bars represent ± SEM. N.S. denotes $p>0.5$ by student t-test.

d) Representative 10x immunofluorescence image of PERILIPIN (red) and MAC-2 (green) expression in eWAT sections of Control and $Pparg^{TG}$ mice after 12 weeks of HFD feeding. Nuclei counterstained with DAPI.

e) Frequency of MAC-2 crown-like structures (Mac-2 positive) per 10x field in eWAT sections of Control and $Pparg^{TG}$ mice after 12 weeks of HFD feeding. n=7 for each group. Bars represent ± SEM. *** denotes $p<0.001$ by student t-test.

f) mRNA levels of indicated proinflammatory genes in eWAT from Control and $Pparg^{TG}$ mice after 12 weeks of HFD feeding. n=7 for each group. Bars represent ± SEM. * denotes $p<0.05$ by student t-test, ** denotes $p<0.01$, *** denotes $p<0.001$.

g) mRNA levels of indicated fibrogenesis genes in eWAT from Control and $Pparg^{TG}$ mice after 12 weeks of HFD feeding. n=7 for each group. Bars represent ± SEM. * denotes $p<0.05$ by student t-test, ** denotes $p<0.01$, *** denotes $p<0.001$.

h) Adipocyte size distribution in eWAT from Control and $Pparg^{TG}$ mice after 12 weeks of HFD feeding. n=7 for each group. Bars represent ± SEM. * denotes $p<0.05$ by student t-test, ** denotes $p<0.01$, *** denotes $p<0.001$.

i) Mean adipocyte size in eWAT from Control and *Pparg*$^{TG}$ mice after 12 weeks of HFD feeding. n=7 for each group. Bars represent ± SEM. * denotes $p<0.05$ by student t-test.

j) Adipocyte counts per 10x field in H&E stained sections of eWAT from Control and *Pparg*$^{TG}$ mice after 12 weeks of HFD feeding. n=7 for each group. Bars represent ± SEM. ** denotes $p<0.01$ by student t-test.

k) Glucose tolerance tests of Control and *Pparg*$^{TG}$ mice after 11 weeks of HFD feeding. n = 7 for each group.

l) Area under curve measurements of glucose tolerance tests shown in k. Bars represent ± SEM. *** denotes $p<0.001$ by student t-test.

m) Serum adiponectin levels in Control and *Pparg*$^{TG}$ mice after 12 weeks of HFD feeding. n=7 for each group. Bars represent ± SEM. ** denotes $p<0.01$ by student t-test.

n) Serum triglyceride (TG) levels in Control and *Pparg*$^{TG}$ mice after 12 weeks of HFD feeding. n=7 for each group. Bars represent ± SEM. ** denotes $p<0.01$ by student t-test.

Exact p values and numbers of repetitions can be found in Supplemental Table 2.

**Extended Data Figure 1. Transient perinatal *Pparg* overexpression has no apparent long-term effect on APCs differentiation capacity in vitro.**

a) Representative 10x brightfield image of adipocyte cultures derived from APCs obtained from P28 Control and *Pparg*$^{TG}$ mice treated with doxycycline (Dox) from P0.5-P7.5. Cultures are stained with oil red-O to visualize lipid accumulation.

b) mRNA levels of adipocyte-selective genes in differentiated cultures of APCs corresponding to panel a. n=4 for each group. Bars represent ± SEM.

c) Experimental design: Transient perinatal *Pparg* overexpression from P0.5-P7.5 was induced by exposing newborn pups to doxycycline via lactating mothers fed a Dox-containing chow diet (600 mg/kg). Lactating animals were then switched to a standard chow diet (- Dox) until weaning. 5 weeks-old Control and *Pparg*$^{TG}$ offspring then housed at 6°C for one week prior to analysis.

Exact p values and numbers of repetitions can be found in Supplemental Table 2.

**Extended Data Figure 2. Transient perinatal *Pparg* overexpression has no apparent long-term effect on APCs differentiation capacity in vitro but improved mature adipocytes behavior after adult-onset obesity.**

a) Representative 10x brightfield image of adipocyte cultures derived from APCs isolated from eWAT of Control and *Pparg*$^{TG}$ mice after 12 weeks of HFD feeding.

b) mRNA levels of *Pparg2* and *Pparg2_transgene* levels (transgene-specific primers) in differentiated cultures of FIPs corresponding to Figure 3-panel d. n=4 for each group. Bars represent ± SEM. * denotes $p<0.05$ by student t-test, ** denotes $p<0.01$.

c) mRNA levels of indicated proinflammatory genes in mature adipocytes from Control and *Pparg*$^{TG}$ mice after 12 weeks of HFD feeding. n=4 for each group. Bars represent ± SEM. * denotes $p<0.05$ by student t-test, ** denotes $p<0.01$, *** denotes $p<0.001$.

d) mRNA levels of indicated fibrogenesis genes in mature adipocytes from Control and *Pparg*$^{TG}$ mice after 12 weeks of HFD feeding. n=4 for each group. Bars represent ± SEM. * denotes $p<0.05$ by student t-test, ** denotes $p<0.01$, *** denotes $p<0.001$.

Exact p values and numbers of repetitions can be found in Supplemental Table 2.

**Supplemental Table 1: Sequences of qPCR primers used in this study**

| Gene | Forward (5' -3') | Reverse (5' -3') |
|---|---|---|
| *Adipoq* | AGATGGCACTCCTGGAGAGAA | TTCTCCAGGCTCTCCTTTCCT |
| *Cfd* | CTACATGGCTTCCGTGCAAGT | AGTCGTCATCCGTCACTCCAT |
| *Fabp4* | GATGAAATCACCGCAGACGAC | ATTCCACCACCAGCTTGTCAC |
| *Ccl2* | CCACAACCACCTCAAGCACTTC | AAGGCATCACAGTCCGAGTCAC |
| *Col3a1* | ATTCTGCCACCCCGAACTCAA | ACAGTCATGGGGCTGGCATTT |
| *Cxcl1* | CTGGGATTCACCTCAAGAACATC | CAGGGTCAAGGCAAGCCTC |
| *Cxcl10* | CTCAGGCTCGTCAGTTCTAAGT | CCCTTGGGAAGATGGTGGTTAA |
| *Cxcl2* | ACTAGCTACATCCCACCCACAC | GCACACTCCTTCCATGAAAGCC |
| *Icam1* | GTGATGCTCAGGTATCCATCCA | CACAGTTCTCAAAGCACAGCG |
| *Vcam1* | AGTTGGGGATTCGGTTGTTCT | CCCCTCATTCCTTACCACCC |
| *Il6* | AAGCCAGAGTCCTTCAGAGAGA | ACTCCTTCTGTGACTCCAGCTT |
| *Pparg2* | GCATGGTGCCTTCGCTGA | TGGCATCTCTGTGTCAACCATG |
| *Pparg*$^{TG}$ | TCAGGCAGATCGTCACAGAG | TTTGCCCCTCCATATAACA |
| *Rps18* | CATGCAAACCCACGACAGTA | CCTCACGCAGCTTGTTGTCTA |
| *Acta2* | TGACGCTGAAGTATCCGATAGA | GTACGTCCAGAGGCATAGAGG |
| *Tgfbi* | TTTAGGAAGGACCTGGGTTGG | TGTTGGTTGTAGAGGGCAAGG |
| *Hif1a* | GTCCCAGCTACGAAGTTACAGC | CAGTGCAGGATACACAAGGTTT |
| *Tnfa* | CCTGTAGCCCACGTCGTAG | GGGAGTAGACAAGGTACAACCC |
| *Lox* | TCGCTACACAGGACATCATGC | ATGTCCAAACACCAGGTACGG |
| *Mmp11* | CCGGAGAGTCACCGTCATC | GCAGGACTAGGGACCCAATG |
| *Mmp14* | ACCCACACACAACGCTCAC | GCCTGTCACTTGTAAACCATAGA |
| *Timp1* | CTTGGTTCCCTGGCGTACTC | ACCTGATCCGTCCACAAACAG |
| *Cox8b* | TGCTGGAACCATGAAGCCAAC | AGCCAGCCAAAACTCCCACTT |
| *Cidea* | TCCTATGCTGCACAGATGACG | TGCTCTTCTGTATCGCCCAGT |
| *Dio2* | CATTGATGAGGCTCACCCTTC | GGTTCCGGTGCTTCTTAACCT |
| *Elovl3* | GTGTGCTTTGCCATCTACACG | CTCCCAGTTCAACAACCTTGC |

| | | |
|---|---|---|
| *Prdm16* | ACACGCCAGTTCTCCAACCTGT | TGCTTGTTGAGGGAGGAGGTA |
| *Pgc1a* | AGGTTCCCTCTCTGCTGCTTT | GGTGCTTTAGAAATGCGGGGT |
| *Ucp1* | TCTCAGCCGGCTTAATGACTG | GGCTTGCATTCTGACCTTCAC |
| *Cd11b* | GGCTCCGGTAGCATCAACAA | ATCTTGGGCTAGGGTTTCTCT |

**Supplemental Table 2: Statistical data (exact p values and sample/cohort sizes for each dataset in the study).**

| Figure | N(sample size) | Statistical test method | # of Times Experiment was Performed | Description | | *p*-value |
|---|---|---|---|---|---|---|
| Figure 1c | Control (+Dox APCs) n=3; | Unpaired two-tailed Student's t test | 2 independent trials | *Pparg_tg* | Dox APCs: Control vs *Pparg*$^{TG}$ | 0.000184 |
| | Control (+Dox FIPs) n=3; | | | | | |
| | Control (-Dox washout APCs) n=4; | | | | Dox FIPs: Control vs *Pparg*$^{TG}$ | 0.001614 |
| | Control (-Dox washout FIPs) n=4; | | | | | |
| | *Pparg*$^{TG}$ (+Dox APCs) n=5; | | | | Dox washout APCs: Control vs *Pparg*$^{TG}$ | 0.429952 |
| | *Pparg*$^{TG}$ (+Dox FIPs) n=5; | | | | | |
| | *Pparg*$^{TG}$ (-Dox washout APCs) n=3; | | | | Dox washout FIPs: Control vs *Pparg*$^{TG}$ | 0.932471 |
| | *Pparg*$^{TG}$ (-Dox washout FIPs) n=3; | | | | | |
| Figure 1d | Control (DoxP0.5-P7.5) n=11 | Unpaired two-tailed Student's t test | Pulled samples from 2 independent trials | Body Weight | Dox P0.5-P7.5: Control vs *Pparg*$^{TG}$ | 0.558127 |
| | *Pparg*$^{TG}$ (DoxP0.5-P7.5) n=10 | | | | | |
| | Control (DoxP21-P28) n=5 | | | | Dox P21-P28: Control vs *Pparg*$^{TG}$ | 0.686808 |
| | *Pparg*$^{TG}$ (DoxP21-P28) n=7 | | | | | |
| Figure 1e | Control APCs (DoxP0.5-P7.5) n=6 | Unpaired two-tailed Student's t test | Pulled samples from 2 independent trials | Cell Frequency | Dox P0.5-P7.5 APCs: Control vs *Pparg*$^{TG}$ | 0.953671 |
| | *Pparg*$^{TG\ APCs}$ (DoxP0.5-P7.5) n=7 | | | | | |
| | Control APCs (DoxP21-P28) n=5 | | | | Dox P21-P28 APCs: Control vs *Pparg*$^{TG}$ | 0.658209 |
| | *Pparg*$^{TG\ APCs}$ (DoxP21-P28) n=5 | | | | | |
| | Control FIPs | | | | Dox P0.5- | 0.398517 |

| | | | | | | |
|---|---|---|---|---|---|---|
| | (DoxP0.5-P7.5) n=6 | | | | P7.5 FIPs: Control vs *Pparg*$^{TG}$ | |
| | *Pparg*$^{TG}$ $^{FIPs}$(DoxP0.5-P7.5) n=7 | | | | | |
| | Control FIPs(DoxP21-P28) n=5 | | | | Dox P21-P28 FIPs: Control vs *Pparg*$^{TG}$ | 0.859028 |
| | *Pparg*$^{TG}$ $^{FIPs}$(DoxP21-P28) n=5 | | | | | |
| Figure 1g | Control FIPs (DoxP0.5-P7.5) n=3 | Unpaired two-tailed Student's t test | 3 independent trials | *Adipoq* | *Pparg*$^{TG}$: Dox P0.5-P7.5 vs Dox P21-P28 | 0.043734 |
| | *Pparg*$^{TG}$ FIPs (DoxP0.5-P7.5) n=3 | | | *Cfd* | *Pparg*$^{TG}$: Dox P0.5-P7.5 vs Dox P21-P28 | 0.013175 |
| | Control FIPs(DoxP21-P28) n=3 | | | *Fabp4* | *Pparg*$^{TG}$: Dox P0.5-P7.5 vs Dox P21-P28 | 0.003194 |
| | *Pparg*$^{TG}$ FIPs(DoxP21-P28) n=3 | | | | | |
| Figure 1i | | Unpaired two-tailed Student's t test | 2 independent trials | Precent of Adipocyte counts | size 0-1000 um$^2$:Control vs PpargTG | 0.00009 |
| | | | | | size 1001-2000 um$^2$:Control vs PpargTG | 0.021131 |
| | Control (DoxP0.5-P7.5) n=3 (2 mice pulled as one) | | | | size 2001-4000 um$^2$:Control vs PpargTG | 0.00576 |
| | *Pparg*$^{TG}$ (DoxP0.5-P7.5) n=4 (2 mice pulled as one) | | | | size 4001-6400 um$^2$:Control vs PpargTG | 0.000006 |
| | Control (DoxP21-P28) n=4 (2 mice pulled as one) | | | | size 0-1000 um$^2$:Control vs PpargTG | 0.329577 |
| | *Pparg*$^{TG}$ (DoxP21-P28) n=4 (2 mice pulled as one) | | | | size 1001-2000 um$^2$:Control vs PpargTG | 0.975349 |
| | | | | | size 2001- | 0.633365 |

| | | | | | | |
|---|---|---|---|---|---|---|
| | | | | | 4000 um$^2$:Control vs PpargTG | |
| | | | | | size 4001-6400 um$^2$:Control vs PpargTG | 0.579723 |
| Figure 2a | Control (DoxP0.5-P7.5) n=9 | Unpaired two-tailed Student's t test | 2 independent trials | Cell Frequency | Dox P0.5-P7.5 APCs: Control vs *Pparg*$^{TG}$ | |
| | *Pparg*$^{TG}$ (DoxP0.5-P7.5) n=4 | | | | Dox P0.5-P7.5 FIPs: Control vs *Pparg*$^{TG}$ | |
| Figure 2b | Control (DoxP0.5-P7.5) n=4 | Unpaired two-tailed Student's t test | 2 independent trials | *Ccl2* | FIPs: Control vs *Pparg*$^{TG}$ | 0.03789 |
| | | | | *Cxcl 2* | | 0.274641 |
| | | | | *Icam 1* | | 0.049247 |
| | *Pparg*$^{TG}$ (DoxP0.5-P7.5) n=4 | | | *Vcam 1* | | 0.047494 |
| | | | | *Cd11b* | | 0.01408 |
| | | | | *Tnfa* | | 0.707905 |
| Figure 2c | Control FIPs (DoxP0.5-P7.5) n=4 | Unpaired two-tailed Student's t test | 3 independent trials | *Cd11b* | LPS: Control vs *Pparg*$^{TG}$ | 0.0018647 |
| | | | | *Cxcl 10* | | 0.3387376 |
| | | | | *Icam 1* | | 0.0340104 |
| | *Pparg*$^{TG}$ FIPs (DoxP0.5-P7.5) n=4 | | | *Il6* | | 0.4155809 |
| | | | | *Vcam 1* | | 0.0449464 |
| | | | | *Tnfa* | | 0.0066155 |
| Figure 2e | Insulin: Control FIPs (DoxP0.5-P7.5) n=4 | Unpaired two-tailed Student's t test | 3 independent trials | *Adipoq* | DMIR: Control vs *Pparg*$^{TG}$ | 0.0060174 |
| | DMIR: Control FIPs (DoxP0.5-P7.5) n=4 | | | *Cfd* | | 0.0002731 |
| | Insulin*: Pparg*$^{TG}$ FIPs (DoxP0.5-P7.5) n=4 | | | *Fabp 4* | | 0.0089259 |
| | DMIR*: Pparg*$^{TG}$ FIPs (DoxP0.5-P7.5) n=4 | | | *Cd36* | | 0.0227093 |

| | | | | | | |
|---|---|---|---|---|---|---|
| Figure 3b | Control (DoxP0.5-P7.5) n=7 | two-way ANOVA | 3 independent trials | Body Weight | Dox P0.5-P7.5: Control vs PpargTG | 0.788632 |
| | *Pparg*$^{TG}$ (DoxP0.5-P7.5) n=7 | | | | | |
| Figure 3c | Control (DoxP0.5-P7.5) n=7 | Unpaired two-tailed Student's t test | 3 independent trials | iWAT weight | Dox P0.5-P7.5: Control vs PpargTG | 0.510685 |
| | *Pparg*$^{TG}$ (DoxP0.5-P7.5) n=7 | | | gWAT weight | | 0.605399 |
| | | | | rWAT weight | | 0.81082 |
| Figure 3e | Control (DoxP0.5-P7.5) n=7 | Unpaired two-tailed Student's t test | 3 independent trials | CLS counts | Dox P0.5-P7.5: Control vs PpargTG | 0.000398 |
| | *Pparg*$^{TG}$ (DoxP0.5-P7.5) n=7 | | | | | |
| Figure 3f | | Unpaired two-tailed Student's t test | 3 independent trials | *Ccl2* | Dox P0.5-P7.5: Control vs *Pparg*TG | 0.929153 |
| | | | | *Cxcl 2* | | 0.032983 |
| | Control (DoxP0.5-P7.5) n=7 | | | *Cxcl 10* | | 0.065065 |
| | *Pparg*$^{TG}$ (DoxP0.5-P7.5) n=7 | | | *Il6* | | 0.040822 |
| | | | | *Icam 1* | | 0.019333 |
| | | | | *Vcam 1* | | 0.001426 |
| | | | | *Tnfa* | | 0.02267 |
| Figure3 g | | Unpaired two-tailed Student's t test | 3 independent trials | *Acta 2* | Dox P0.5-P7.5: Control vs *Pparg*TG | 0.040114 |
| | | | | *Tgfbi* | | 0.427921 |
| | Control (DoxP0.5-P7.5) n=7 | | | *Col3a1* | | 0.312451 |
| | *Pparg*$^{TG}$ (DoxP0.5-P7.5) n=7 | | | *Hif1a* | | 0.004457 |
| | | | | *Lox* | | 0.012058 |
| | | | | *Mmp 11* | | 0.002796 |
| | | | | *Mmp 14* | | 0.014602 |

| | | | | | | |
|---|---|---|---|---|---|---|
| | | | | *Timp 1* | | 0.042168 |
| Figure 3h | | Unpaired two-tailed Student's t test | 3 independent trials | Precent of Adipocyte counts | size <=1500 $um^2$:Control vs PpargTG | 0.000006 |
| | Control (DoxP0.5-P7.5) n=7 | | | | size 1501-5100 $um^2$:Control vs PpargTG | 0.518934 |
| | *Pparg*$^{TG}$ (DoxP0.5-P7.5) n=7 | | | | size 5101-9100 $um^2$:Control vs PpargTG | 0.007714 |
| | | | | | size 9101-11300 $um^2$:Control vs PpargTG | 0.04376 |
| Figure 3i | Control (DoxP0.5-P7.5) n=7 | Unpaired two-tailed Student's t test | 3 independent trials | Cell Area ($um^2$) | Dox P0.5-P7.5: Control vs PpargTG | 0.034914 |
| | *Pparg*$^{TG}$ (DoxP0.5-P7.5) n=7 | | | | | |
| Figure 3j | Control (DoxP0.5-P7.5) n=7 | Unpaired two-tailed Student's t test | 3 independent trials | Cell counts per 10x field | Dox P0.5-P7.5: Control vs PpargTG | 0.006626 |
| | *Pparg*$^{TG}$ (DoxP0.5-P7.5) n=7 | | | | | |
| Figure 3l | Control (DoxP0.5-P7.5) n=7 | Unpaired two-tailed Student's t test | 3 independent trials | GTT area under curve | Dox P0.5-P7.5: Control vs *Pparg*TG | 0.000755 |
| | *Pparg*$^{TG}$ (DoxP0.5-P7.5) n=7 | | | | | |
| Figure 3m | Control (DoxP0.5-P7.5) n=7 | Unpaired two-tailed Student's t test | 3 independent trials | Serum ADIPONECTIN level | Dox P0.5-P7.5: Control vs *Pparg*TG | 0.037065 |
| | *Pparg*$^{TG}$ (DoxP0.5-P7.5) n=7 | | | | | |
| Figure 3n | Control (DoxP0.5-P7.5) n=7 | Unpaired two-tailed Student's t test | 3 independent trials | Serum TG level | Dox P0.5-P7.5: Control vs *Pparg*TG | 0.020797 |
| | *Pparg*$^{TG}$ (DoxP0.5-P7.5) n=7 | | | | | |
| Extended Data Figure 1b | Control APCs (DoxP0.5-P7.5) n=4 | Unpaired two-tailed Student's t test | 3 independent trials | *Adipoq* | Control vs *Pparg*TG | 0.250928 |
| | *Pparg*$^{TG}$ APCs (DoxP0.5-P7.5) | | | *Cfd* | | 0.269367 |

| | | | | | | |
|---|---|---|---|---|---|---|
| | n=3 | | | | | |
| | | | | *Cebpa* | | 0.904339 |
| Extended Data Figure 1d | RT: Control (DoxP0.5-P7.5) n=3 | Unpaired two-tailed Student's t test | 3 independent trials | *Cox8b* | CE: Control vs *Pparg*TG | 0.033640 |
| | RT*: Pparg*$^{TG}$ (DoxP0.5-P7.5) n=4 | | | *Cidea* | | 0.512131 |
| | | | | *Dio2* | | 0.062943 |
| | CE: Control (DoxP0.5-P7.5) n=4 | | | *Elovl3* | | 0.043894 |
| | | | | *Prdm16* | | 0.266905 |
| | CE*: Pparg*$^{TG}$ (DoxP0.5-P7.5) n=4 | | | *Pgc1a* | | 0.458328 |
| | | | | *Ucp1* | | 0.983535 |
| Extended Data Figure 2b | Insulin: Control FIPs (DoxP0.5-P7.5) n=4 | Unpaired two-tailed Student's t test | 3 independent trials | *Pparg2* | DMIR: Control vs *Pparg*$^{TG}$ | 0.012764 |
| | DMIR: Control FIPs (DoxP0.5-P7.5) n=4 | | | | | |
| | Insulin*: Pparg*$^{TG}$ FIPs (DoxP0.5-P7.5) n=4 | | | *Pparg_tg* | | 0.779945 |
| | DMIR*: Pparg*$^{TG}$ FIPs (DoxP0.5-P7.5) n=4 | | | | | |
| Extended Data Figure 2c | | Unpaired two-tailed Student's t test | 2 independent trials | *Ccl2* | Adipocytes: Control vs *Pparg*TG | 0.002057 |
| | Adipocytes: Control (DoxP0.5-P7.5) n=4 | | | *Cxcl2* | | 0.013374 |
| | Adipocytes: *Pparg*$^{TG}$ (DoxP0.5-P7.5) n=4 | | | *Il6* | | 0.049653 |
| | | | | *Icam1* | | 0.859773 |
| | | | | *Il1b* | | 0.130859 |
| | | | | *Cd11b* | | 0.230664 |
| Extended Data Figure 2c | Adipocytes: Control (DoxP0.5-P7.5) n=4 | Unpaired two-tailed Student's t test | 2 independent trials | *Col1a1* | Adipocytes: Control vs *Pparg*TG | 0.002538 |
| | | | | *Col3a1* | | 0.026387 |
| | | | | *Hif1a* | | 0.003094 |
| | | | | *Mmp* | | 0.000133 |

| | | | | | | |
|---|---|---|---|---|---|---|
| | | | | *9* | | |
| | Adipocytes: *Pparg*$^{TG}$ (DoxP0.5-P7.5) n=4 | | | *Mmp 10* | | 0.001459 |
| | | | | *Mmp 14* | | 0.039892 |
| | | | | *Timp 1* | | 0.002531 |

# Figure 1

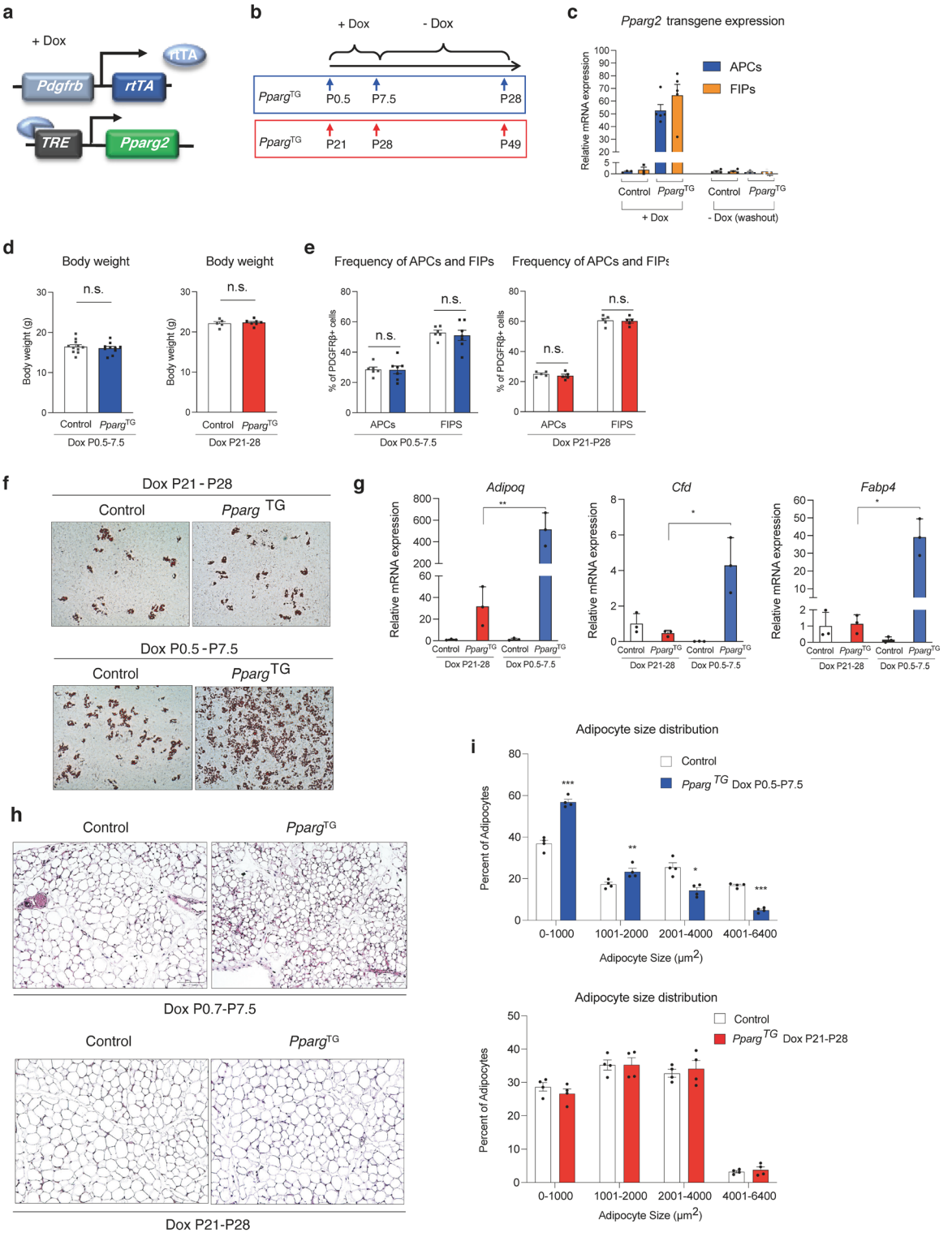
a
+ Dox
rtTA
Pdgfrb
rtTA
TRE
Pparg2
b
+ Dox
- Dox
PpargTG
P0.5
P7.5
P28
PpargTG
P21
P28
P49
c
Pparg2 transgene expression
Relative mRNA expression
APCs
FIPs
Control
PpargTG
Control
PpargTG
+ Dox
- Dox (washout)
d
Body weight
Body weight
n.s.
n.s.
Body weight (g)
Control
PpargTG
Dox P0.5-7.5
Dox P21-28
e
Frequency of APCs and FIPs
Frequency of APCs and FIPs
% of PDGFRβ+ cells
n.s.
n.s.
n.s.
n.s.
APCs
FIPS
Dox P0.5-7.5
Dox P21-P28
f
Dox P21 - P28
Control
Pparg TG
Dox P0.5 - P7.5
Control
PpargTG
g
Adipoq
Cfd
Fabp4
Relative mRNA expression
Control
PpargTG
Dox P21-28
Dox P0.5-7.5
h
Control
PpargTG
Dox P0.7-P7.5
Control
PpargTG
Dox P21-P28
i
Adipocyte size distribution
Control
Pparg TG Dox P0.5-P7.5
Percent of Adipocytes
0-1000
1001-2000
2001-4000
4001-6400
Adipocyte Size (μm2)
Adipocyte size distribution
Control
PpargTG Dox P21-P28
Percent of Adipocytes
0-1000
1001-2000
2001-4000
4001-6400
Adipocyte Size (μm2)

**Figure 2**

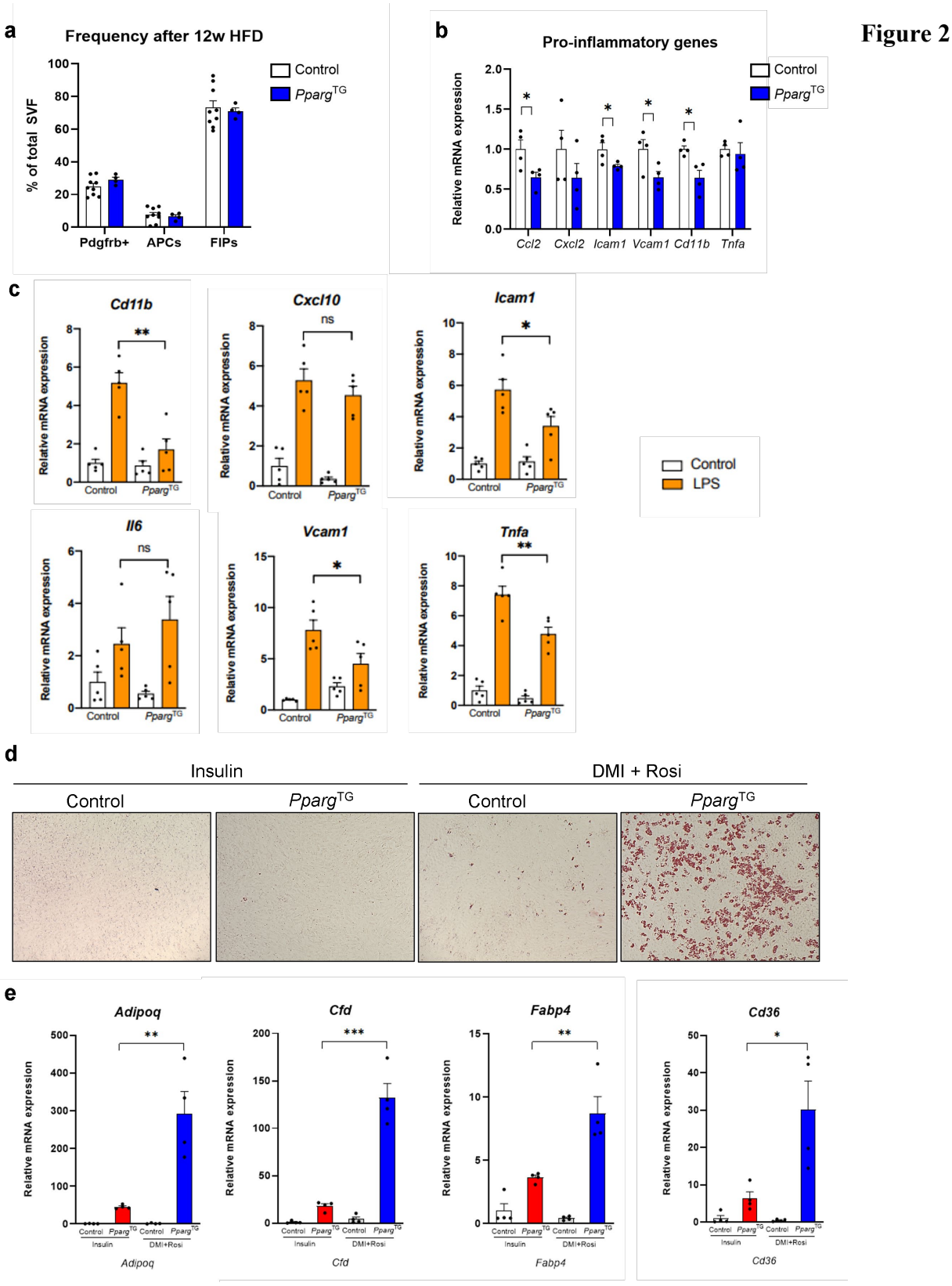
a
Frequency after 12w HFD
% of total SVF
Control
Pparg^TG
Pdgfrb+
APCs
FIPs
b
Pro-inflammatory genes
Relative mRNA expression
Ccl2
Cxcl2
Icam1
Vcam1
Cd11b
Tnfa
c
Cd11b
Cxcl10
Icam1
Il6
Vcam1
Tnfa
ns
Control
LPS
d
Insulin
DMI + Rosi
e
Adipoq
Cfd
Fabp4
Cd36
Insulin
DMI+Rosi

**Figure 3**

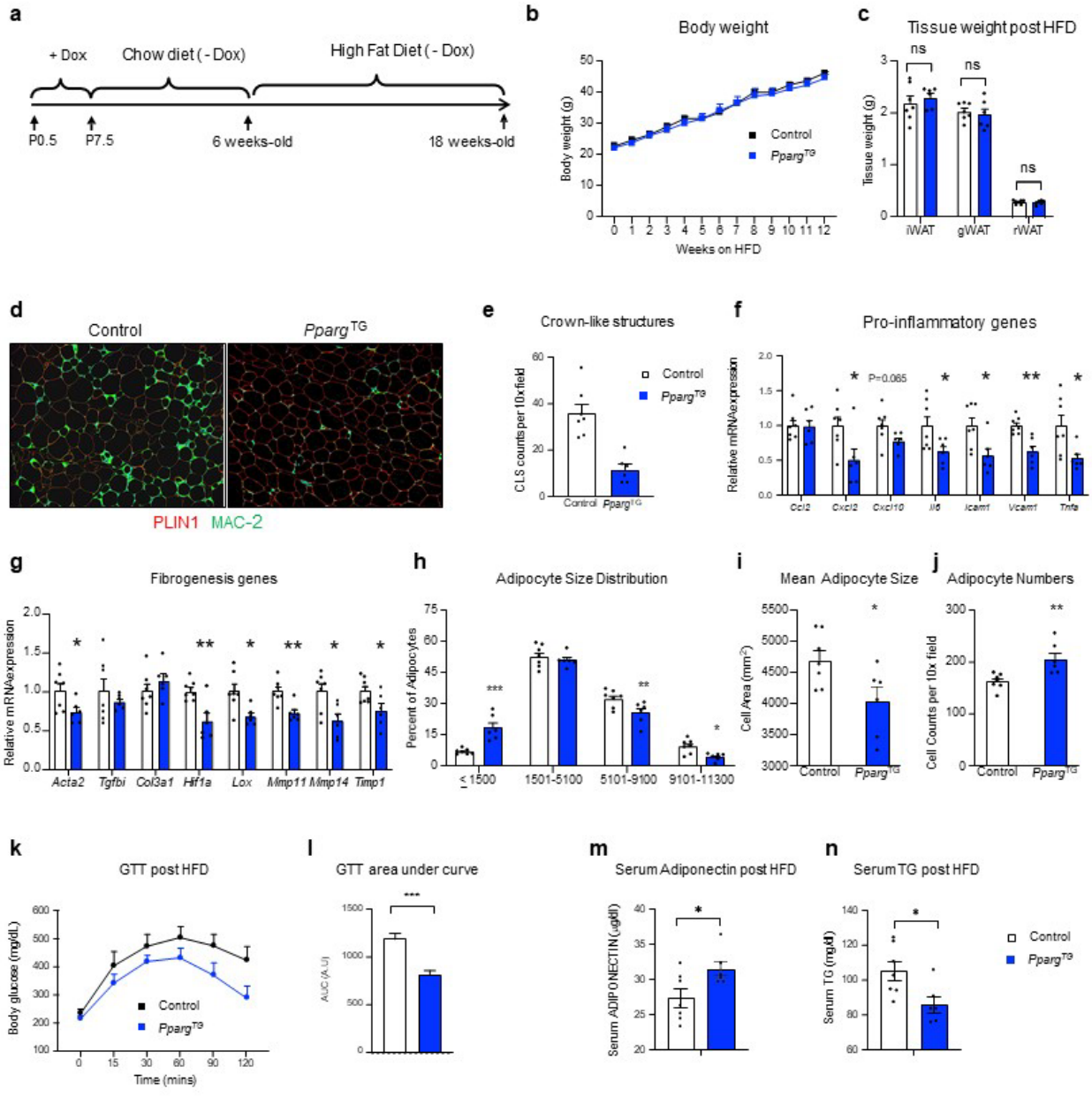
a
+ Dox
Chow diet ( - Dox)
High Fat Diet ( - Dox)
P0.5
P7.5
6 weeks-old
18 weeks-old
b
Body weight
Body weight (g)
Weeks on HFD
Control
Pparg^TG
c
Tissue weight post HFD
Tissue weight (g)
ns
iWAT
gWAT
rWAT
d
Control
Pparg^TG
PLIN1 MAC-2
e
Crown-like structures
CLS counts per 10x field
f
Pro-inflammatory genes
Relative mRNA expression
P=0.065
Ccl2
Cxcl2
Cxcl10
Il6
Icam1
Vcam1
Tnfa
g
Fibrogenesis genes
Relative mRNA expression
Acta2
Tgfbi
Col3a1
Hif1a
Lox
Mmp11
Mmp14
Timp1
h
Adipocyte Size Distribution
Percent of Adipocytes
≤ 1500
1501-5100
5101-9100
9101-11300
i
Mean Adipocyte Size
Cell Area (mm^2)
j
Adipocyte Numbers
Cell Counts per 10x field
k
GTT post HFD
Body glucose (mg/dL)
Time (mins)
l
GTT area under curve
AUC (A.U)
m
Serum Adiponectin post HFD
Serum ADIPONECTIN (µg/dl)
n
Serum TG post HFD
Serum TG (mg/dl)

**Extended Data Figure 1**

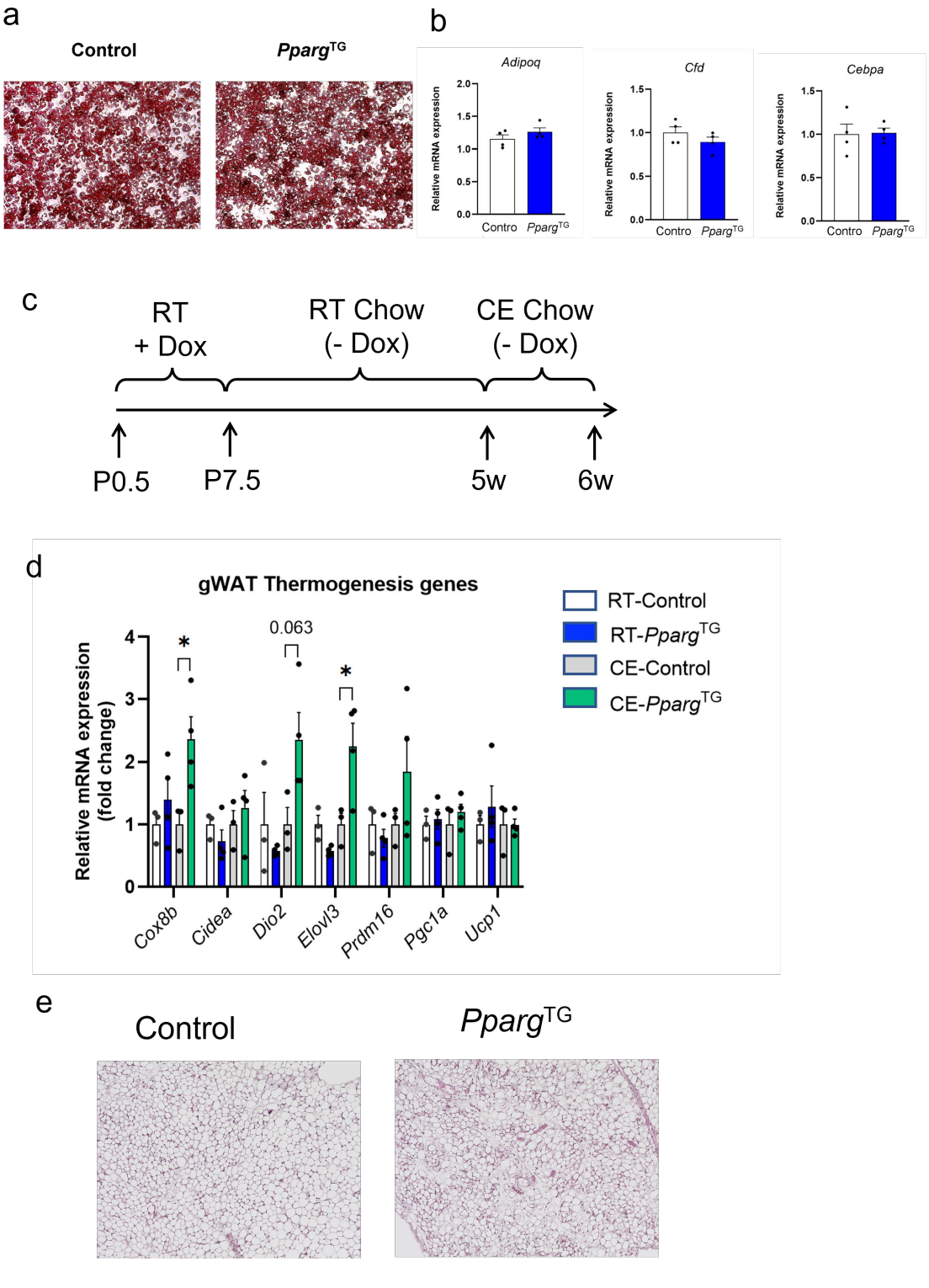

**Extended Data Figure 2**

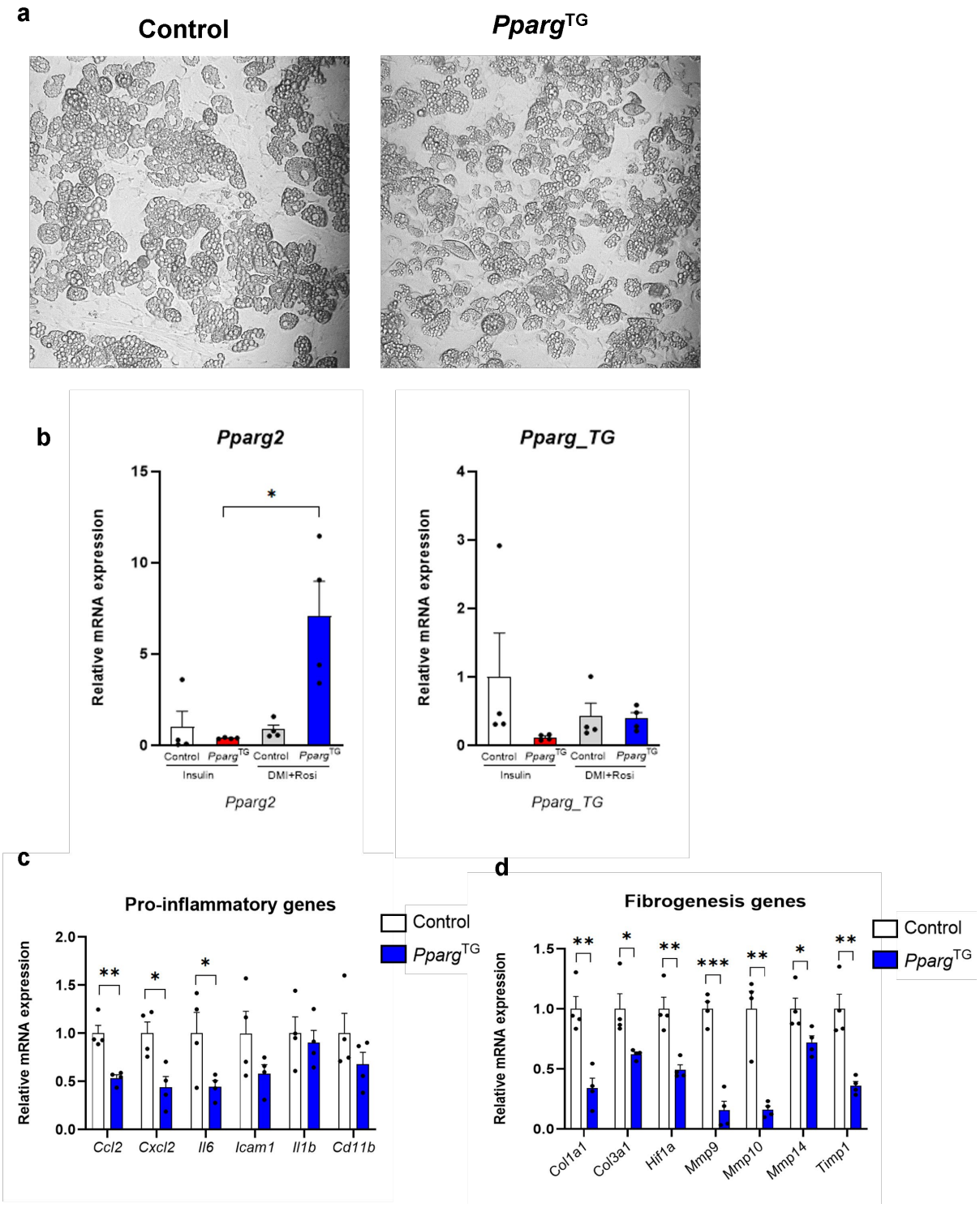

# CHAPTER FOUR

## CONCLUSION

Adipocytes are generally organized into anatomically distinct tissues which are also called “depots”. The murine perigonadal WAT depot is of particular interest to adipose tissue biologists. The perigonadal WAT depot of male mice (epididymal WAT, or “eWAT”) is a well characterized site of immune cell residence, adipose progenitor heterogeneity, and robust tissue remodeling and expansion in obesity. As such, the eWAT depot of mice offers a model for many aspects of adipose tissue remodeling observed in human obesity. In recent years, single-cell/nucleus RNA sequencing has helped reveal the remarkable cellular heterogeneity of adipose tissue, including the sex and depot differences in adipose progenitor cell heterogeneity. Our own efforts have focused on two functionally distinct fibro-inflammatory and adipogenic PDGFRβ-expressing cell subpopulations within adult eWAT (Hepler, Shan et al. 2018, Shan, Shao et al. 2020). The LY6C- CD9- PDGFRβ+ subpopulation in eWAT represents functional adipose precursor cells (APCs). These cells are enriched in the expression of *Pparg*, encoding the “master regulator” of adipocyte differentiation, and possess robust adipogenic capacity both *in vitro* and *in vivo* (Hepler, Shan et al. 2018). De novo differentiation from PDGFRβ+ APCs drives adipocyte recruitment in the setting of diet-induced obesity and ensures healthy tissue remodeling and proper lipid storage in WAT (Shao, Vishvanath et al. 2018, Vishvanath and Gupta 2019, Shao, Hepler et al. 2021). In contrast, LY6C+ PDGFRβ+ cells represent fibro-inflammatory precursors, or “FIPs.” FIPs exert strong pro-inflammatory, fibrogenic, and anti-adipogenic

phenotypes (Hepler, Shan et al. 2018). These cells are activated upon high-fat diet (HFD) feeding and play an important role in controlling pro-inflammatory macrophage accrual and tissue collagen deposition associated with obesity (Shan, Shao et al. 2020, Joffin, Paschoal et al. 2021, Shao, Hepler et al. 2021).

Given my strong interest in developmental biology, I became intrigued by the important questions that remain unknown: when and where do these functionally distinct adipose progenitor subpopulations emerge development? Where are they localized? Do the molecular and functional properties of these distinct cell subpopulations change over time? As such, I conducted a series of experiments to define the developmental origin of murine eWAT and the unique functional properties of perinatal adipose progenitor subpopulations. My scRNA-seq results indicated that molecularly distinct PDGFRβ+ progenitor cell subpopulations (APCs, FIPs, MLCs and SMCs) emerged as early as postnatal day 3, prior to the formation of parenchymal adipocytes. Using a combination of *in vitro* functional analyses and genetic mouse models, I identified a subpopulation of PDGFRβ+ cells within postnatal day 7 (P7) eWAT that exhibits a strong commitment to the adipocyte lineage. This population of APCs appears similar (functionally and molecularly) to the corresponding APC population previously identified in adult eWAT (Hepler, Shan et al. 2018). I also identified cells in P7 eWAT that shared molecular similarity to adult FIPs; however, P7 FIPs differed from adult FIPs in notable way. P7 FIPs showed latent adipogenic potential, were less pro-inflammatory, and lacked the notable anti-adipogenic activity of adult FIPs. Taken together, my data indicate that distinct adipose tissue progenitor subpopulations emerge early in tissue development, even before the appearance of differentiated adipocytes. This work sets the

stage for future studies to unravel the developmental signaling mechanisms controlling the formation of these distinct cell subpopulations.

I investigated whether altering the functional properties of perinatal progenitors can have lasting effects into adulthood. Using a genetic mouse model, I showed that overexpressing *Pparg2* in PDGFRβ+ progenitor cells for only the first week of life (P0.5 to P7.5) could impact the plasticity of adipose tissue in adulthood. Transient perinatal *Pparg* during this early period resulted in a significant level of adipocyte hyperplasia in eWAT by the time the mice were 5 weeks of age. Notably, adult FIPs from these transgenic animals now possessed the ability to undergo adipocyte differentiation in vitro. As such, transient *Pparg* expression had a lasting effect on the lineage plasticity of perinatal FIPs. Indeed, the beneficial effects of transient *Pparg* activation in adipose progenitors persisted after 12 weeks of HFD feeding. FIPs from transient perinatal $Pparg^{TG}$ mice maintained on HFD retained their heightened *in vitro* adipogenic ability and were less responsive to pro-inflammatory stimuli. Transient perinatal $Pparg^{TG}$ mice maintained on HFD feeding did not differ from Control animals with respect to body weight or adiposity; however, obese perinatal $Pparg^{TG}$ mice exhibit an improved GTT, higher serum Adiponectin levels, and lower serum TG levels. Moreover, the eWAT expressed lower levels of fibrogenic and pro-inflammatory genes and maintained the hypercellular phenotype that appeared at 5 weeks of age (before the onset of HFD feeding). Taken together, these data highlight the long-term impact of modulating the adipogenic capacity of adipose progenitors during the perinatal stage. It is important to note that transient *Pparg* overexpression during a later period (P21-P28; chow diet) did not drive

adipogenesis. Thus, the perinatal period represents a unique period of adipose progenitor plasticity.

The stromal-vascular fraction of adult eWAT consists of a vast array of cell types, of which the fibroblast-like subpopulations are greatly involved in activities such as adipogenesis, immune cell regulation, and collagen deposition. My studies shed light into when these fibroblast-like subpopulations emerge during development and how their properties change over time. These findings can be valuable to efforts to understand how early life physiological and pathophysiological events (e.g., material obesity, gestational Diabetes, or perinatal exposure to “obesogens”) can impact metabolic health in the long term. Importantly, these findings provide proof of concept that targeting adipose progenitors early in life can elicit lasting benefits into adulthood, which may lead to strategies to prevent the development of metabolic disease.

# FUTURE DIRECTIONS

**Identify the origin of eWAT adipose tissue progenitors.**

One important question that remains is where the distinct PDGFRβ subpopulations emerge from during embryonic development. My in-silico cell trajectory analysis suggested APCs as the direct source of committed pre-adipocytes; however, this computational analysis did not provide evidence of lineage hierarchy amongst APCs, FIPs, MLCs, and SMCs, from the earliest observable timepoint (P3).

One of the existing hypotheses is the mesothelial origin of eWAT adipose tissue, given that eWAT adipose tissues are outlined by a layer of mesothelial cells. Using lineage tracing, Chau et al. observed that epididymal adipocytes descend from cells expressing *Wt1* (Wilms' tumor protein)(Chau, Bandiera et al. 2014). The enriched expression of *Wt1* in mesothelial cells during development suggests a mesothelial origin of adipocytes; however, we and others have observed that *Wt1* expression was not exclusive in mesothelial cells (Westcott, Emont et al. 2021). To test this hypothesis further, I conducted scRNA-seq analysis of dissociated eWAT mesothelium. The adipose mesothelium can be obtained upon gentle trypsin digestion of intact whole adipose depots from P3 and P7 mice. My scRNA-seq analysis revealed that the predominant cluster of cells (mGroup1, mGroup2) obtained from the isolated population express markers of classical mesothelial cells, including *Msln*, *Krt19*, and *Wt1*, with mGroup2 had a higher expression of proliferation hallmarks such as *Ki67*. A small portion of residential immune cells were also detected (mGroup3), as well as a subset of mesenchymal stromal cells that expressed *Pdgfrb* and *Acta2* (mGroup4) (Figure 1a, b).

Indeed, we observed *Wt1* expression within both mesothelial cells and mesenchymal stromal cells. This pattern of expression makes it difficult to exclude the contribution of mesenchymal stromal cells when using *Wt1* as a lineaging tracing tool (Figure 1c). I examined the differentiation potential of eWAT mesothelial cells directly by performing *in vitro* adipocyte differentiation assays Isolated cells in culture exhibited the cobblestone epithelial phenotype characteristic of classical mesothelial cells (Figure 1d). Notably, these cells, much like MLCs, failed to undergo adipocyte differentiation in response to the hormonal adipogenic cocktail containing dexamethasone, IBMX, insulin, and rosiglitazone (Figure 1e). As such, my analysis does not reveal evidence in support of the hypothesis that adipocytes emerge from mesothelial cells. Given the limitations of all approaches utilized, further studies will be needed to understand the complexity of eWAT development and the inductive signals that initiate tissue development during the perinatal period.

**Understand the mechanisms by which transient perinatal manipulation of adipose tissue progenitors drives long term changes in adipose tissue plasticity.**

The phenomenon of perinatal progenitor cell reprogramming that I report here is novel and interesting; however, it is undeniable that my studies have now raised more questions than it has answered. One of the remaining questions is the underlying mechanism by which *Pparg* overexpression drives stable long-term changes in the function of adipose progenitors. PPARγ has been shown to have important roles in adipose tissue other than driving adipogenesis per se. PPARγ regulates adipokine gene expression and broad inflammatory programs both in adipocytes and in immune cells (Rosen and Spiegelman 2001, Chalise,

Hashimoto et al. 2019). Pparγ in other tissues/organs can also crosstalk with adipose tissue (Liu, Bookout et al. 2014). Nevertheless, considering that PPARγ was only transiently overexpressed in PDGFRβ+ cells, and returned to normal level after P7, long term effects on the adipose progenitors are unlikely to be attributed to higher levels of PPARγ expression in stromal cells of other tissues.

I first investigated whether the frequency of PDGFRβ+ subpopulations were altered as consequence of transient *Pparg2* overexpression. In the transient *Pparg*$^{TG}$ model, differences in the frequency of APCs and FIPs between control and transgenic mice could not be observed in both young/lean and old/obese conditions. Therefore, the cellular identity of APCs and FIPs and their relative portion remained the same after transient perinatal manipulation.

I next considered whether the change in function of APCs/FIPs in the transient Pparg expression model were a result of epigenetic alterations. Indeed, the concept of "metabolic memory" has been long been considered to be a result of epigenetic regulation (Reddy, Zhang et al. 2015, Roh, Tsai et al. 2018). I conducted ChIP-seq of histone markers h3k27ac and h3k4me1 with freshly isolated FIPs from control and transient *Pparg*$^{TG}$ mice of 5 weeks old on chow diet. This was a very difficult experiment as 1 million cells were required per sample per antibody. Unfortunately, in both of my two attempts, I failed to get sufficient numbers of peaks for my control group, thus no comparison could be made. Going forward, this line of investigation should be pursued.

The long-term ability of FIPs to undergo adipogenesis *in vitro* after transient overexpression of *Pparg* is remarkable; however, the physiological significance of this

finding is still unclear. I conducted bulk mRNA-seq on confluent cultures of FIPs from control and transient *Pparg*$^{TG}$ mice, prior to the addition of the differentiation cocktail. Genes involved in early adipocyte lineage commitment such as *Cepbd*, *Cebpb* as well as adipocyte genes such as *Adipoq*, *Plin1* were all expressed of a higher level in transgenic FIPs (Figure 2a). GSEA also indicated an enrichment in adipogenesis and fatty acid metabolism (Figure 2b). Interestingly, adipogenesis genes were not expressed at higher levels in freshly isolated FIPs (prior to culture) (Figure 2c). As such, it is unclear whether FIPs in *Pparg*$^{TG}$ mice are indeed undergoing adipocyte differentiation in vivo. Specific lineage tracing of FIPs (not total PDGFRβ cells) using intersectional Cre-loxp systems will be needed to address this question. If FIPs are differentiating into adipocytes in vivo, then it raises the intriguing possibility that FIPs-derived adipocytes exhibit different properties than APC-derived adipocytes. The use of Single nuclei sequencing and/or spatial transcriptomics may shed insight into this question.

**Explore human physiological/pathophysiological relevance of transient perinatal manipulation of adipose tissue progenitors.**

I choose to utilize *Pparg*$^{TG}$ mice as a tool to manipulate the adipogenic activity of perinatal adipocyte precursors in vivo; however, whether there is a physiological or pathophysiological human condition that mimics this action is still unclear. In rodents, subcutaneous WAT depots, such as interscapular and inguinal, form prior to visceral WAT depots, which include retroperitoneal, perigonadal and mesenteric WAT (Berry, Stenesen et al. 2013). Generally, subcutaneous WAT depots form prenatally, and are towards fully

developed at postnatal stage, while visceral WAT depots emerge postnatally. In human, adipose tissue development takes place at the beginning of the second trimester of gestation period in various sites (buccal, neck, shoulder, gluteal, perirenal) (G. Ailhaud, P. Grimaldi et al. 1992) and develops dynamically throughout fetus stage (Desoye and Herrera 2021). Therefore, the gestational and perinatal stages are important for adipose tissue development in both mouse and human. Moreover, mice during P0.5-P7.5 could roughly correspond to newborn infants to 8 months of age (Dutta and Sengupta 2016); this is a period when breast-milk or formula represent the predominant source of nutrition. It is tempting to speculate how maternal or perinatal factors during this period might impact adipocyte precursor biology.

For instance, there are also multiple clinical case reports linking maternal obesity and diabetes to increased risk of obesity, T2DM, cardiometabolic disease in children (Reece 2008, Tam, Ma et al. 2008, Anness, Clark et al. 2022, Longmore, Titmuss et al. 2022). This includes women presenting with obesity, diabetes, and hypertension at the onset of pregnancy, and those metabolically healthy women could also develop diseases such as Gestational Diabetes Melius (GDM) and preeclampsia, during pregnancy. The influence of maternal and paternal obesity on offspring health is increasingly studied in rodents. Maternal high fat feeding during the lactation-suckling period in rats leads to long-term eWAT expansion in offspring (Butruille, Marousez et al. 2019). The mechanisms underlying these long-term effects are not clear; however, an impact of adipose progenitors has been postulated.

It is noteworthy that women are recommended to stop medications during pregnancy, citing a risk (known or unknown) of pharmacological therapies to fetal development

(Bazargan, Foster et al. 2016). Rosiglitazone and pioglitazone are antidiabetic drugs in the thiazolidinedione (TZD) class. They promote insulin sensitization by binding to PPARγ in adipocytes and activating the expression of genes that directly or indirectly promote insulin responsiveness. Animal studies have not provided evidence of TZD-induced birth effects or miscarriage; however, it is recommended to discontinue TZDs as soon as pregnancy is confirmed. In 2004, there was a case report where the subject took rosiglitazone during undetected pregnancy till the 8$^{th}$ week of gestation with a normal pregnancy outcome (Yaris, Yaris et al. 2004). In 2005, another case was reported to be exposed to rosiglitazone between 13th and 17th gestational weeks and successfully delivered a healthy infant (Kalyoncu, Yaris et al. 2005). Besides its antidiabetic effect, many recent rodent studies have shown rosiglitazone to have protective or therapeutic potentials in face of pregnancy-induced hypertension, placenta inflammation, and can even reverse asthma in offspring (Liu, Sakurai et al. 2015, Bo, Chen et al. 2016, Wu, Ruan et al. 2017). Motivated by my findings in our transgenic mouse model, I treated newborn mice with rosiglitazone during from P0.5-P7.5 via gavage of lactating mothers. I harvested the mice at 5 week old as well as after 12-weeks of HFD feeding (Figure 3a), and observed no body weight difference (Figure 3b,c). In comparison with my transient *Pparg*$^{TG}$ model, TZD treatment during this period did not elicit the same long-term effects in eWAT (Figure 3d) nor the same systematic improvements after HFD feeding (Figure 3e,f) ; however, I did observe a lasting impact on beige adipocyte recruitment in the inguinal WAT depot at both 5 weeks old and after 12-weeks HFD feeding (Figure 3d, e). Therefore, existing drugs could be of beneficial effect for both mother and offspring; however, a careful evaluation of these drugs during pregnancy/lactation is needed.

The most widely used antidiabetic drug, metformin, has been used more often than rosiglitazone during pregnancy. It is used for the treatment of GDM. GDM is associated with substantial rates of maternal and perinatal complications and an increased risk of macrosomia (Caroline A. Crowther, Hiller et al. 2005, Tam, Ma et al. 2008, Sweeting, Wong et al. 2022), and increased long term risk of cardiometabolic diseases in offspring (Tam, Ching et al. 2017, Scholtens, Kuang et al. 2019). Traditionally, subcutaneous insulin was the preferred treatment for GDM (Metzger and Coustan 1998). Metformin treatment or metformin-insulin combination therapy later became widely used in pursue of better cost effectiveness, compliance, and acceptability (Ryu, Hays et al. 2014). (*Glyburide has also been applied to GDM in some cases, but were reported to have greater adverse effects compared to metformin ((Oliveira, Andrade et al. 2022)), thus is not as commonly used.*) Large up-to-date cohort studies indicated no increased long-term risk associated with pregnancy exposure to metformin (Landi, Radke et al. 2019, Anness, Clark et al. 2022, Brand, Saarelainen et al. 2022). Going forward, it may be interesting to evaluate the short-term and long-term effects of GDM and metformin use on adipose tissue plasticity and progenitor cell function.

**Figure 1. scRNA-seq analysis and differentiation capacity of dissociated P7 eWAT mesothelial cells.**

a) UMAP analysis of 4857 single cell transcriptomes obtained by scRNA-seq analysis of P7 eWAT mesothelium-associated cells.

b) Dot plot depicting the expression of indicated genes within cell clusters revealed by UMAP analysis. Expression levels are normalized by z-score.

c) 10x brightfield image of cultured eWAT-associated mesothelial cells at confluence.

d) 10x brightfield image of indicated cell subpopulations following adipocyte differentiation. P7 APCs were differentiated by maintaining cells in growth media containing insulin. P7 eWAT-associated mesothelial cells were induced to differentiate by maintaining cells in growth media containing insulin or by induction with dexamethasone, IMBX, insulin (DMI), and rosiglitazone. Cultures are stained with oil red-O to visualize lipid accumulation.

**Figure 2. Bulk-mRNA-seq reveals adipogenic capacity of *Pparg*$^{TG}$ FIPs after *in vitro* culture.**

a) Heatmap showing representative adipogenic genes from bulk-mRNA-seq of Control and *Pparg*$^{TG}$ FIPs after confluency in cell culture plates (n=4). Expression normalized by z-score.

b) GSEA reveals gene signatures/pathways differentially expressed between Control and *Pparg*$^{TG}$ FIPs. NES= Normalized Enrichment Score.

c) Heatmap showing representative adipogenic genes from bulk-mRNA-seq of freshly isolated Control and *Pparg*$^{TG}$ FIPs (n=5). Expression normalized by z-score.

**Figure 3. Transient perinatal Rosiglitazone treatment has lasting impact on beige adipocyte recruitment in iWAT.**

a) Experimental design: Transient perinatal Rosiglitazone treatment from P0.5-P7.5 was induced by gavaging lactating mothers daily with Rosiglitazone solution (10mg/kg). 5 weeks-old Control and Rosiglitazone treated offspring were harvested for analysis, or 8 weekes-old Control and Rosiglitazone treated offspring were administrated a high-fat-diet (HFD) (60% kcal) for 12 weeks prior to analysis.

b) Body weights of Control and Rosiglitazone treated mice at 5 weeks old. n=7 for each group.

c) Weekly body weights of Control and Rosiglitazone treated mice during the HFD feeding period. n=5 for each group.

d) Representative 10x brightfield images of H&E stained eWAT and iWAT obtained from Control and Rosiglitazone treated mice at 5 weeks old.

e) Glucose tolerance tests of Control and Rosiglitazone treated mice after 11 weeks of HFD feeding. n = 5 for each group.

f) Serum triglyceride (TG) levels in Control and Rosiglitazone treated mice after 12 weeks of HFD feeding. n=5 for each group. Bars represent ± SEM.

g) mRNA levels of indicated thermogenesis genes in iWAT from Control and Rosiglitazone treated mice at 5 weeks old. n=6 for each group. Bars represent ± SEM. * denotes $p<0.05$ by student t-test, ** denotes $p<0.01$, *** denotes $p<0.001$.

h) mRNA levels of indicated thermogenesis genes in iWAT from Control and Rosiglitazone treated mice after 12 weeks of HFD feeding. n=5 for each group. Bars represent ± SEM. * denotes $p<0.05$ by student t-test, ** denotes $p<0.01$, *** denotes $p<0.001$.

**Figure 1**

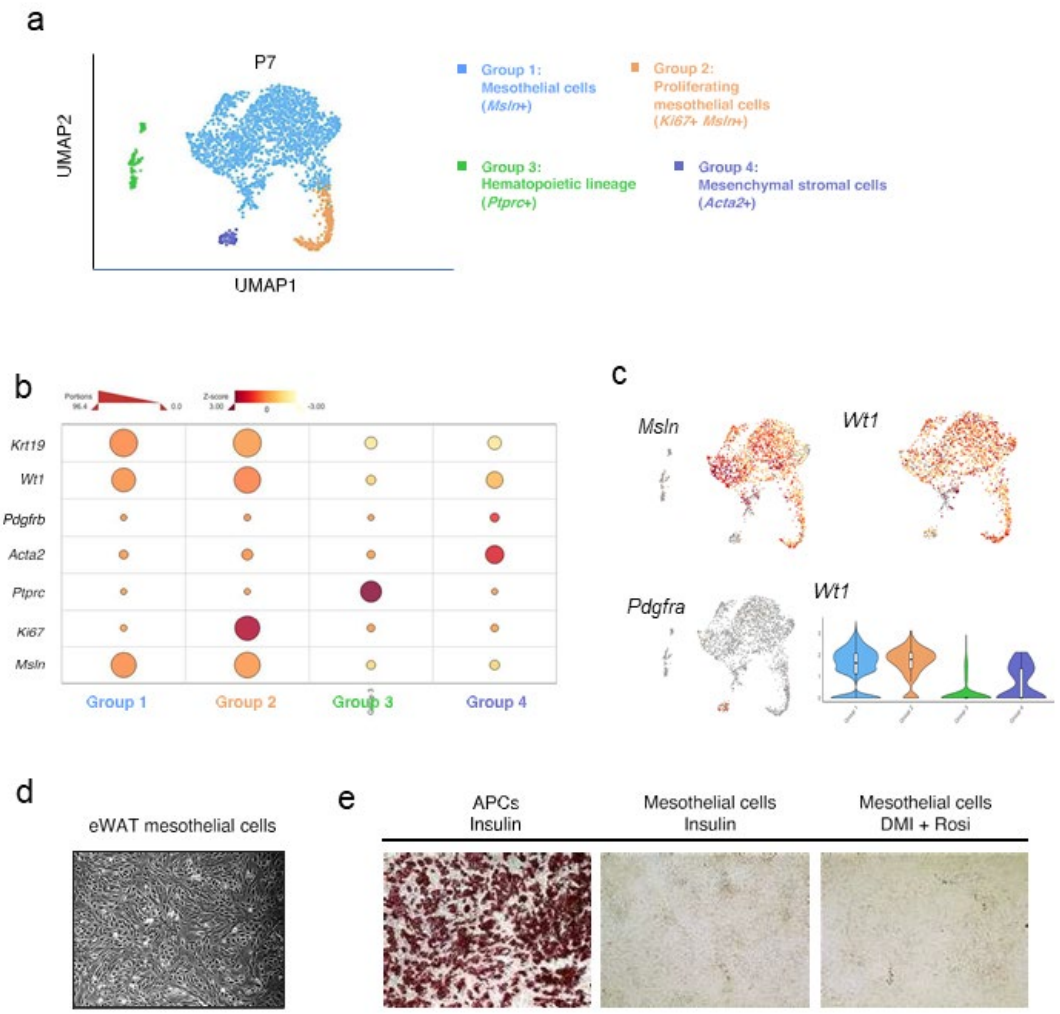
a
P7
UMAP2
UMAP1
Group 1: Mesothelial cells (Msln+)
Group 2: Proliferating mesothelial cells (Ki67+ Msln+)
Group 3: Hematopoietic lineage (Ptprc+)
Group 4: Mesenchymal stromal cells (Acta2+)
b
Krt19
Wt1
Pdgfrb
Acta2
Ptprc
Ki67
Msln
Group 1
Group 2
Group 3
Group 4
c
Msln
Wt1
Pdgfra
Wt1
d
eWAT mesothelial cells
e
APCs Insulin
Mesothelial cells Insulin
Mesothelial cells DMI + Rosi

**Figure 2**

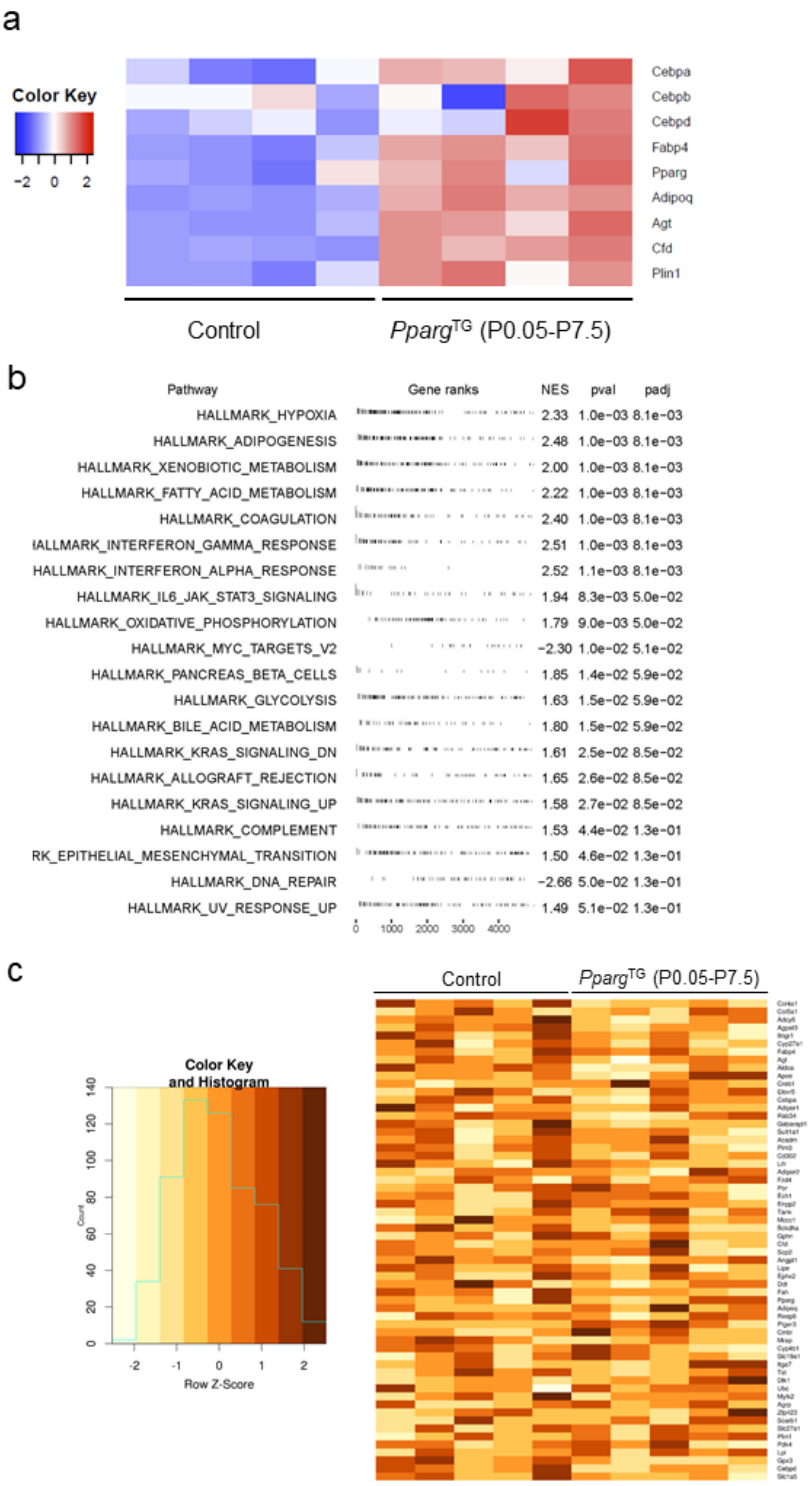
a
Color Key
−2 0 2
Cebpa
Cebpb
Cebpd
Fabp4
Pparg
Adipoq
Agt
Cfd
Plin1
Control
Pparg^TG (P0.05-P7.5)
b
Pathway
Gene ranks
NES pval padj
HALLMARK_HYPOXIA 2.33 1.0e−03 8.1e−03
HALLMARK_ADIPOGENESIS 2.48 1.0e−03 8.1e−03
HALLMARK_XENOBIOTIC_METABOLISM 2.00 1.0e−03 8.1e−03
HALLMARK_FATTY_ACID_METABOLISM 2.22 1.0e−03 8.1e−03
HALLMARK_COAGULATION 2.40 1.0e−03 8.1e−03
IALLMARK_INTERFERON_GAMMA_RESPONSE 2.51 1.0e−03 8.1e−03
HALLMARK_INTERFERON_ALPHA_RESPONSE 2.52 1.1e−03 8.1e−03
HALLMARK_IL6_JAK_STAT3_SIGNALING 1.94 8.3e−03 5.0e−02
HALLMARK_OXIDATIVE_PHOSPHORYLATION 1.79 9.0e−03 5.0e−02
HALLMARK_MYC_TARGETS_V2 −2.30 1.0e−02 5.1e−02
HALLMARK_PANCREAS_BETA_CELLS 1.85 1.4e−02 5.9e−02
HALLMARK_GLYCOLYSIS 1.63 1.5e−02 5.9e−02
HALLMARK_BILE_ACID_METABOLISM 1.80 1.5e−02 5.9e−02
HALLMARK_KRAS_SIGNALING_DN 1.61 2.5e−02 8.5e−02
HALLMARK_ALLOGRAFT_REJECTION 1.65 2.6e−02 8.5e−02
HALLMARK_KRAS_SIGNALING_UP 1.58 2.7e−02 8.5e−02
HALLMARK_COMPLEMENT 1.53 4.4e−02 1.3e−01
RK_EPITHELIAL_MESENCHYMAL_TRANSITION 1.50 4.6e−02 1.3e−01
HALLMARK_DNA_REPAIR −2.66 5.0e−02 1.3e−01
HALLMARK_UV_RESPONSE_UP 1.49 5.1e−02 1.3e−01
0 1000 2000 3000 4000
c
Color Key and Histogram
Count
0 20 40 60 80 100 120 140
-2 -1 0 1 2
Row Z-Score
Control
Pparg^TG (P0.05-P7.5)

**Figure 3**

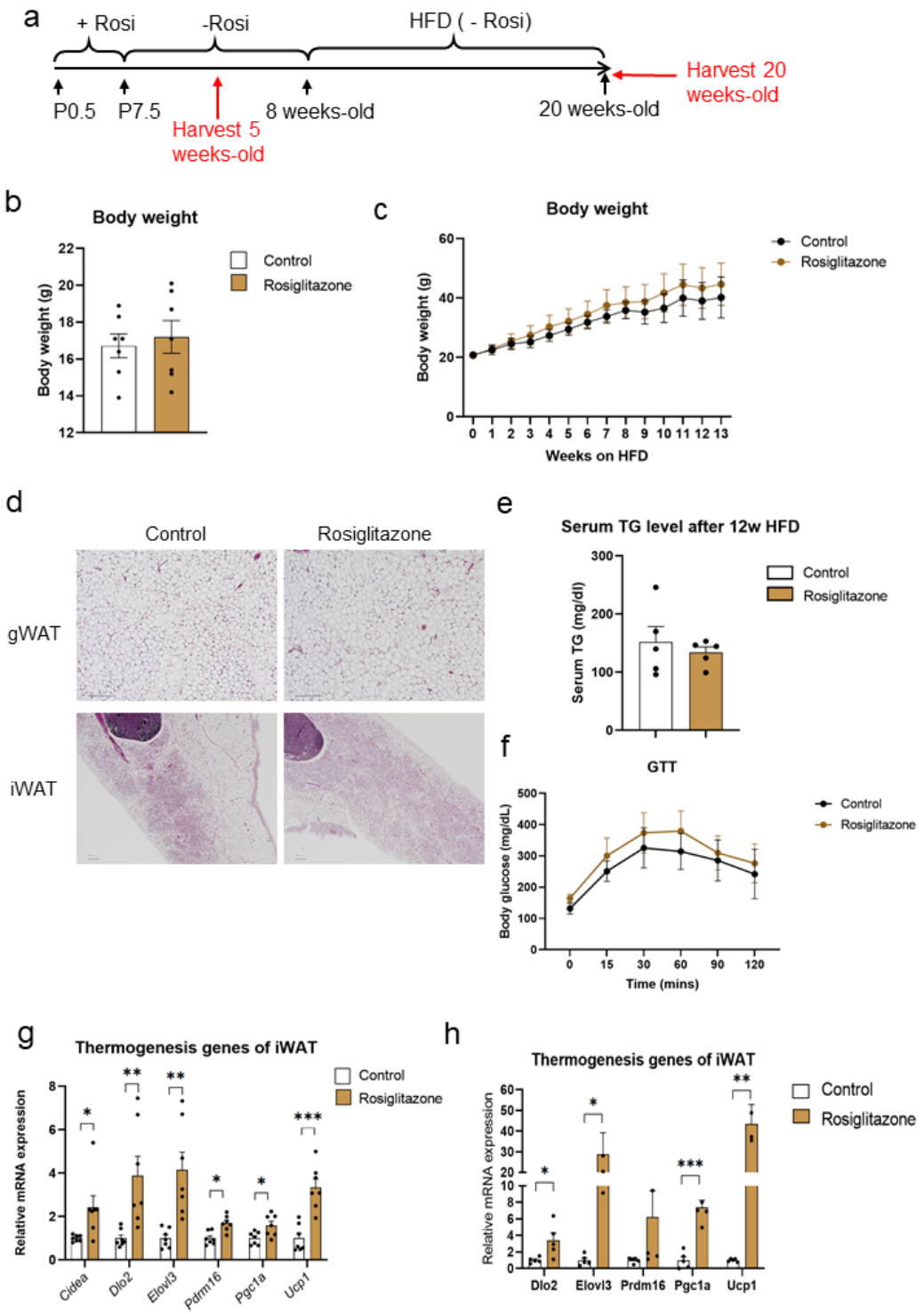
a
+ Rosi
-Rosi
HFD ( - Rosi)
P0.5
P7.5
Harvest 5 weeks-old
8 weeks-old
20 weeks-old
Harvest 20 weeks-old
b
Body weight
Body weight (g)
Control
Rosiglitazone
c
Body weight
Body weight (g)
Weeks on HFD
Control
Rosiglitazone
d
Control
Rosiglitazone
gWAT
iWAT
e
Serum TG level after 12w HFD
Serum TG (mg/dl)
Control
Rosiglitazone
f
GTT
Body glucose (mg/dL)
Time (mins)
Control
Rosiglitazone
g
Thermogenesis genes of iWAT
Relative mRNA expression
Cidea
Dio2
Elovl3
Prdm16
Pgc1a
Ucp1
Control
Rosiglitazone
h
Thermogenesis genes of iWAT
Relative mRNA expression
Dio2
Elovl3
Prdm16
Pgc1a
Ucp1
Control
Rosiglitazone

## BIBLIOGRAPHY

"<White fat progenitor cells reside in the adipose vasculature.pdf>."
Anness, A. R., A. Clark, K. Melhuish, F. M. T. Leone, M. W. Osman, D. Webb, T. Robinson, N. Walkinshaw, A. Khalil and H. A. Mousa (2022). "Maternal hemodynamics and neonatal birth weight in pregnancies complicated by gestational diabetes: new insights from novel causal inference analysis modeling." Ultrasound Obstet Gynecol.
Bass, R. and I. Eneli (2015). "Severe childhood obesity: an under-recognised and growing health problem." Postgrad Med J **91**(1081): 639-645.
Bazargan, M., D. J. Foster, B. S. Muhlhausler, J. L. Morrison, I. McMillen and A. K. Davey (2016). "Limited fetal metabolism of rosiglitazone: Elimination via the maternal compartment in the pregnant ewe." Reprod Toxicol **61**: 162-168.
Berry, D. C., Y. Jiang, R. W. Arpke, E. L. Close, A. Uchida, D. Reading, E. D. Berglund, M. Kyba and J. M. Graff (2017). "Cellular Aging Contributes to Failure of Cold-Induced Beige Adipocyte Formation in Old Mice and Humans." Cell Metab **25**(1): 166-181.
Berry, D. C., D. Stenesen, D. Zeve and J. M. Graff (2013). "The developmental origins of adipose tissue." Development **140**(19): 3939-3949.
Berry, R. and M. S. Rodeheffer (2013). "Characterization of the adipocyte cellular lineage in vivo." Nat Cell Biol **15**(3): 302-308.
Bo, Q.-L., Y.-H. Chen, Z. Yu, L. Fu, Y. Zhou, G.-B. Zhang, H. Wang, Z.-H. Zhang and D.-X. Xu (2016). "Rosiglitazone pretreatment protects against lipopolysaccharide-induced fetal demise through inhibiting placental inflammation." Molecular and Cellular Endocrinology **423**: 51-59.
Brand, K. M. G., L. Saarelainen, J. Sonajalg, E. Boutmy, C. Foch, M. Vaarasmaki, L. Morin-Papunen, J. Schlachter, C. S. Group, K. M. Hakkarainen and P. Korhonen (2022). "Metformin in pregnancy and risk of adverse long-term outcomes: a register-based cohort study." BMJ Open Diabetes Res Care **10**(1).
Brestoff, J. R., B. S. Kim, S. A. Saenz, R. R. Stine, L. A. Monticelli, G. F. Sonnenberg, J. J. Thome, D. L. Farber, K. Lutfy, P. Seale and D. Artis (2015). "Group 2 innate lymphoid cells promote beiging of white adipose tissue and limit obesity." Nature **519**(7542): 242-246.
Burl, R. B., V. D. Ramseyer, E. A. Rondini, R. Pique-Regi, Y. H. Lee and J. G. Granneman (2018). "Deconstructing Adipogenesis Induced by beta3-Adrenergic Receptor Activation with Single-Cell Expression Profiling." Cell Metab **28**(2): 300-309 e304.
Butruille, L., L. Marousez, C. Pourpe, F. Oger, S. Lecoutre, D. Catheline, S. Gors, C. C. Metges, C. Guinez, C. Laborie, P. Deruelle, J. Eeckhoute, C. Breton, P. Legrand, J. Lesage and D. Eberle (2019). "Maternal high-fat diet during suckling programs visceral adiposity and epigenetic regulation of adipose tissue stearoyl-CoA desaturase-1 in offspring." Int J Obes (Lond) **43**(12): 2381-2393.
Caroline A. Crowther, J. E. Hiller, J. R. Moss and J. S. Robinson (2005). "<Effect of Treatment of Gestational Diabetes Mellitus on Pregnancy Outcomes.pdf>."
Chalise, J. P., S. Hashimoto, G. Parajuli, S. Kang, S. K. Singh, Y. Gemechu, H. Metwally, K. K. Nyati, P. K. Dubey, M. M. Zaman, Y. Nagahama, H. Hamza, K. Masuda and T.

Kishimoto (2019). "Feedback regulation of Arid5a and Ppar-gamma2 maintains adipose tissue homeostasis." Proc Natl Acad Sci U S A **116**(30): 15128-15133.
Chau, Y. Y., R. Bandiera, A. Serrels, O. M. Martinez-Estrada, W. Qing, M. Lee, J. Slight, A. Thornburn, R. Berry, S. McHaffie, R. H. Stimson, B. R. Walker, R. M. Chapuli, A. Schedl and N. Hastie (2014). "Visceral and subcutaneous fat have different origins and evidence supports a mesothelial source." Nat Cell Biol **16**(4): 367-375.
Chawla, A. and M. A. Lazar (1994). "Peroxisome proliferator and retinoid signaling pathways co-regulate preadipocyte phenotype and survival." Proc Natl Acad Sci U S A **91**(5): 1786-1790.
Cohen, P. and B. M. Spiegelman (2016). "Cell biology of fat storage." Mol Biol Cell **27**(16): 2523-2527.
Corvera, S. (2021). "Cellular Heterogeneity in Adipose Tissues." Annu Rev Physiol **83**: 257-278.
Cypess, A. M. (2022). "Reassessing Human Adipose Tissue." N Engl J Med **386**(8): 768-779.
Darimont, C., O. Avanti, F. Blancher, S. Wagniere, R. Mansourian, I. Zbinden, P. Leone-Vautravers, A. Fuerholz, V. Giusti and K. Mace (2008). "Contribution of mesothelial cells in the expression of inflammatory-related factors in omental adipose tissue of obese subjects." Int J Obes (Lond) **32**(1): 112-120.
Desoye, G. and E. Herrera (2021). "Adipose tissue development and lipid metabolism in the human fetus: The 2020 perspective focusing on maternal diabetes and obesity." Prog Lipid Res **81**: 101082.
Dong, H., W. Sun, Y. Shen, M. Balaz, L. Balazova, L. Ding, M. Loffler, B. Hamilton, N. Kloting, M. Bluher, H. Neubauer, H. Klein and C. Wolfrum (2022). "Identification of a regulatory pathway inhibiting adipogenesis via RSPO2." Nat Metab **4**(1): 90-105.
Dutta, S. and P. Sengupta (2016). "Men and mice: Relating their ages." Life Sci **152**: 244-248.
Engin, A. (2017). The Definition and Prevalence of Obesity and Metabolic Syndrome. Obesity and Lipotoxicity. A. B. Engin and A. Engin. Cham, Springer International Publishing**:** 1-17.
Flynn, J. (2013). "The changing face of pediatric hypertension in the era of the childhood obesity epidemic." Pediatr Nephrol **28**(7): 1059-1066.
G. Ailhaud, P. Grimaldi and R. Negrel (1992). "CELLULAR AND MOLECULAR ASPECTS OF ADIPOSE TISSUE
DEVELOPMENT." Annu. Rev. Nutr.
Gao, Z., A. C. Daquinag, C. Fussell, Z. Zhao, Y. Dai, A. Rivera, B. E. Snyder, K. L. Eckel-Mahan and M. G. Kolonin (2020). "Age-associated telomere attrition in adipocyte progenitors predisposes to metabolic disease." Nat Metab **2**(12): 1482-1497.
Ghaben, A. L. and P. E. Scherer (2019). "Adipogenesis and metabolic health." Nat Rev Mol Cell Biol **20**(4): 242-258.
Gordon-Larsen, P., N. S. The and L. S. Adair (2010). "Longitudinal trends in obesity in the United States from adolescence to the third decade of life." Obesity (Silver Spring) **18**(9): 1801-1804.

Green, H. and M. Meuth (1974). "An established pre-adipose cell line and its differentiation in culture." Cell **3**: 127-133.
Gupta, O. T. and R. K. Gupta (2015). "Visceral Adipose Tissue Mesothelial Cells: Living on the Edge or Just Taking Up Space?" Trends Endocrinol Metab **26**(10): 515-523.
Gupta, R. K., Z. Arany, P. Seale, R. J. Mepani, L. Ye, H. M. Conroe, Y. A. Roby, H. Kulaga, R. R. Reed and B. M. Spiegelman (2010). "Transcriptional control of preadipocyte determination by Zfp423." Nature **464**(7288): 619-623.
Gupta, R. K., R. J. Mepani, S. Kleiner, J. C. Lo, M. J. Khandekar, P. Cohen, A. Frontini, D. C. Bhowmick, L. Ye, S. Cinti and B. M. Spiegelman (2012). "Zfp423 expression identifies committed preadipocytes and localizes to adipose endothelial and perivascular cells." Cell Metab **15**(2): 230-239.
Hafemeister, C. and R. Satija (2019). "Normalization and variance stabilization of single-cell RNA-seq data using regularized negative binomial regression." Genome Biol **20**(1): 296.
Hales, C. M., M. D. Carroll, C. D. Fryar and C. L. Ogden (2020). "Prevalence of Obesity and Severe Obesity Among Adults:
United States, 2017–2018." NCHS Data Brief.
Han, J., J. E. Lee, J. Jin, J. S. Lim, N. Oh, K. Kim, S. I. Chang, M. Shibuya, H. Kim and G. Y. Koh (2011). "The spatiotemporal development of adipose tissue." Development **138**(22): 5027-5037.
Hao, Y., S. Hao, E. Andersen-Nissen, W. M. Mauck, 3rd, S. Zheng, A. Butler, M. J. Lee, A. J. Wilk, C. Darby, M. Zager, P. Hoffman, M. Stoeckius, E. Papalexi, E. P. Mimitou, J. Jain, A. Srivastava, T. Stuart, L. M. Fleming, B. Yeung, A. J. Rogers, J. M. McElrath, C. A. Blish, R. Gottardo, P. Smibert and R. Satija (2021). "Integrated analysis of multimodal single-cell data." Cell **184**(13): 3573-3587 e3529.
Hepler, C. and R. K. Gupta (2017). "The expanding problem of adipose depot remodeling and postnatal adipocyte progenitor recruitment." Mol Cell Endocrinol **445**: 95-108.
Hepler, C., B. Shan, Q. Zhang, G. H. Henry, M. Shao, L. Vishvanath, A. L. Ghaben, A. B. Mobley, D. Strand, G. C. Hon and R. K. Gupta (2018). "Identification of functionally distinct fibro-inflammatory and adipogenic stromal subpopulations in visceral adipose tissue of adult mice." Elife **7**.
Holtrup, B., C. D. Church, R. Berry, L. Colman, E. Jeffery, J. Bober and M. S. Rodeheffer (2017). "Puberty is an important developmental period for the establishment of adipose tissue mass and metabolic homeostasis." Adipocyte **6**(3): 224-233.
Hu, E., P. Liang and B. M. Spiegelman (1996). "AdipoQ is a novel adipose-specific gene dysregulated in obesity." J Biol Chem **271**(18): 10697-10703.
Jensen, M. D. (2008). "Role of body fat distribution and the metabolic complications of obesity." The Journal of clinical endocrinology and metabolism **93**(11 Suppl 1): S57-S63.
Joffin, N., V. A. Paschoal, C. M. Gliniak, C. Crewe, A. Elnwasany, L. I. Szweda, Q. Zhang, C. Hepler, C. M. Kusminski, R. Gordillo, D. Y. Oh, R. K. Gupta and P. E. Scherer (2021). "Mitochondrial metabolism is a key regulator of the fibro-inflammatory and adipogenic stromal subpopulations in white adipose tissue." Cell Stem Cell **28**(4): 702-717 e708.

Kalyoncu, N. I., F. Yaris, C. Ulku, M. Kadioglu, M. Kesim, M. Unsal, M. Dikici and E. Yaris (2005). "A case of rosiglitazone exposure in the second trimester of pregnancy." Reprod Toxicol **19**(4): 563-564.
Kloting, N., M. Fasshauer, A. Dietrich, P. Kovacs, M. R. Schon, M. Kern, M. Stumvoll and M. Bluher (2010). "Insulin-sensitive obesity." Am J Physiol Endocrinol Metab **299**(3): E506-515.
Kodani, S. D. and Y. H. Tseng (2021). "Narrating the story ARC of adipose tissue aging." Dev Cell **56**(10): 1359-1360.
Landi, S. N., S. Radke, S. M. Engel, K. Boggess, T. Sturmer, A. S. Howe and M. J. Funk (2019). "Association of Long-term Child Growth and Developmental Outcomes With Metformin vs Insulin Treatment for Gestational Diabetes." JAMA Pediatr **173**(2): 160-168.
Liu, C., A. L. Bookout, S. Lee, K. Sun, L. Jia, C. Lee, S. Udit, Y. Deng, P. E. Scherer, D. J. Mangelsdorf, L. Gautron and J. K. Elmquist (2014). "PPARgamma in vagal neurons regulates high-fat diet induced thermogenesis." Cell Metab **19**(4): 722-730.
Liu, J., R. Sakurai and V. K. Rehan (2015). "PPAR-gamma agonist rosiglitazone reverses perinatal nicotine exposure-induced asthma in rat offspring." Am J Physiol Lung Cell Mol Physiol **308**(8): L788-796.
Longmore, D. K., A. Titmuss, E. Barr, F. Barzi, A. Simmonds, I. L. Lee, E. Hawthorne, R. Derkenne, C. Connors, J. Boyle, P. Zimmet, K. O'Dea, J. Oats, H. D. McIntyre, A. Brown, J. Shaw and L. J. Maple-Brown (2022). "Breastfeeding and infant growth in offspring of mothers with hyperglycaemia in pregnancy: The pregnancy and neonatal diabetes outcomes in remote Australia study." Pediatr Obes: e12891.
Lotta, L. A., L. B. L. Wittemans, V. Zuber, I. D. Stewart, S. J. Sharp, J. Luan, F. R. Day, C. Li, N. Bowker, L. Cai, E. De Lucia Rolfe, K. T. Khaw, J. R. B. Perry, S. O'Rahilly, R. A. Scott, D. B. Savage, S. Burgess, N. J. Wareham and C. Langenberg (2018). "Association of Genetic Variants Related to Gluteofemoral vs Abdominal Fat Distribution With Type 2 Diabetes, Coronary Disease, and Cardiovascular Risk Factors." JAMA **320**(24): 2553-2563.
Macotela, Y., B. Emanuelli, M. A. Mori, S. Gesta, T. J. Schulz, Y. H. Tseng and C. R. Kahn (2012). "Intrinsic differences in adipocyte precursor cells from different white fat depots." Diabetes **61**(7): 1691-1699.
Mann, J. P. and D. B. Savage (2019). "What lipodystrophies teach us about the metabolic syndrome." J Clin Invest **129**(10): 4009-4021.
Merrick, D., A. Sakers, Z. Irgebay, C. Okada, C. Calvert, M. P. Morley, I. Percec and P. Seale (2019). "Identification of a mesenchymal progenitor cell hierarchy in adipose tissue." Science **364**(6438).
Metzger, B. E. and D. R. Coustan (1998). "Summary and recommendations of the Fourth International Workshop-Conference on Gestational Diabetes Mellitus. The Organizing Committee." Diabetes care **21 Suppl 2**: B161-167.
Nguyen, H. P., F. Lin, D. Yi, Y. Xie, J. Dinh, P. Xue and H. S. Sul (2021). "Aging-dependent regulatory cells emerge in subcutaneous fat to inhibit adipogenesis." Dev Cell **56**(10): 1437-1451 e1433.

Oliveira, M. M., K. F. O. Andrade, G. H. S. Lima and T. C. Rocha (2022). "Metformin versus glyburide in treatment and control of gestational diabetes mellitus: a systematic review with meta-analysis." Einstein (Sao Paulo) **20**: eRW6155.
Poznanski, W. J., I. Waheed and R. Van (1973). "Human fat cell precursors. Morphologic and metabolic differentiation in culture." Lab Invest **29**(5): 570-576.
Rando, O. J. and R. A. Simmons (2015). "I'm eating for two: parental dietary effects on offspring metabolism." Cell **161**(1): 93-105.
Reddy, M. A., E. Zhang and R. Natarajan (2015). "Epigenetic mechanisms in diabetic complications and metabolic memory." Diabetologia **58**(3): 443-455.
Reece, E. A. (2008). "Perspectives on obesity, pregnancy and birth outcomes in the United States: the scope of the problem." Am J Obstet Gynecol **198**(1): 23-27.
Rodeheffer, M. S., K. Birsoy and J. M. Friedman (2008). "Identification of white adipocyte progenitor cells in vivo." Cell **135**(2): 240-249.
Roh, H. C., L. T. Tsai, A. Lyubetskaya, D. Tenen, M. Kumari and E. D. Rosen (2017). "Simultaneous Transcriptional and Epigenomic Profiling from Specific Cell Types within Heterogeneous Tissues In Vivo." Cell Rep **18**(4): 1048-1061.
Roh, H. C., L. T. Y. Tsai, M. Shao, D. Tenen, Y. Shen, M. Kumari, A. Lyubetskaya, C. Jacobs, B. Dawes, R. K. Gupta and E. D. Rosen (2018). "Warming Induces Significant Reprogramming of Beige, but Not Brown, Adipocyte Cellular Identity." Cell Metab **27**(5): 1121-1137 e1125.
Rondini, E. A. and J. G. Granneman (2020). "Single cell approaches to address adipose tissue stromal cell heterogeneity." Biochem J **477**(3): 583-600.
Rosen, E. D. and B. M. Spiegelman (2001). "PPARgamma : a nuclear regulator of metabolism, differentiation, and cell growth." J Biol Chem **276**(41): 37731-37734.
Rosen, E. D. and B. M. Spiegelman (2014). "What we talk about when we talk about fat." Cell **156**(1-2): 20-44.
Ryu, R. J., K. E. Hays and M. F. Hebert (2014). "Gestational diabetes mellitus management with oral hypoglycemic agents." Semin Perinatol **38**(8): 508-515.
Sarvari, A. K., E. L. Van Hauwaert, L. K. Markussen, E. Gammelmark, A. B. Marcher, M. F. Ebbesen, R. Nielsen, J. R. Brewer, J. G. S. Madsen and S. Mandrup (2021). "Plasticity of Epididymal Adipose Tissue in Response to Diet-Induced Obesity at Single-Nucleus Resolution." Cell Metab **33**(2): 437-453 e435.
Scherer, P. E., S. Williams, M. Fogliano, G. Baldini and H. F. Lodish (1995). "A novel serum protein similar to C1q, produced exclusively in adipocytes." J Biol Chem **270**(45): 26746-26749.
Scholtens, D. M., A. Kuang, L. P. Lowe, J. Hamilton, J. M. Lawrence, Y. Lebenthal, W. J. Brickman, P. Clayton, R. C. Ma, D. McCance, W. H. Tam, P. M. Catalano, B. Linder, A. R. Dyer, W. L. Lowe, Jr., B. E. Metzger, H. F.-u. S. C. R. Group and H. F.-U. S. C. R. Group (2019). "Hyperglycemia and Adverse Pregnancy Outcome Follow-up Study (HAPO FUS): Maternal Glycemia and Childhood Glucose Metabolism." Diabetes Care **42**(3): 381-392.
Schwalie, P. C., H. Dong, M. Zachara, J. Russeil, D. Alpern, N. Akchiche, C. Caprara, W. Sun, K. U. Schlaudraff, G. Soldati, C. Wolfrum and B. Deplancke (2018). "A stromal cell

population that inhibits adipogenesis in mammalian fat depots." Nature **559**(7712): 103-108.
Sebo, Z. L. and M. S. Rodeheffer (2019). "Assembling the adipose organ: adipocyte lineage segregation and adipogenesis in vivo." Development **146**(7).
Shan, B., M. Shao, Q. Zhang, Y. A. An, L. Vishvanath and R. K. Gupta (2021). "Cold-responsive adipocyte progenitors couple adrenergic signaling to immune cell activation to promote beige adipocyte accrual." Genes Dev **35**(19-20): 1333-1338.
Shan, B., M. Shao, Q. Zhang, C. Hepler, V. A. Paschoal, S. D. Barnes, L. Vishvanath, Y. A. An, L. Jia, V. S. Malladi, D. W. Strand, O. T. Gupta, J. K. Elmquist, D. Oh and R. K. Gupta (2020). "Perivascular mesenchymal cells control adipose-tissue macrophage accrual in obesity." Nat Metab **2**(11): 1332-1349.
Shao, M., C. Hepler, Q. Zhang, B. Shan, L. Vishvanath, G. H. Henry, S. Zhao, Y. A. An, Y. Wu, D. W. Strand and R. K. Gupta (2021). "Pathologic HIF1alpha signaling drives adipose progenitor dysfunction in obesity." Cell Stem Cell **28**(4): 685-701 e687.
Shao, M., L. Vishvanath, N. C. Busbuso, C. Hepler, B. Shan, A. X. Sharma, S. Chen, X. Yu, Y. A. An, Y. Zhu, W. L. Holland and R. K. Gupta (2018). "De novo adipocyte differentiation from Pdgfrbeta(+) preadipocytes protects against pathologic visceral adipose expansion in obesity." Nat Commun **9**(1): 890.
Shungin, D., T. W. Winkler, D. C. Croteau-Chonka, T. Ferreira, A. E. Locke, R. Magi, R. J. Strawbridge, T. H. Pers, K. Fischer, A. E. Justice, T. Workalemahu, J. M. W. Wu, M. L. Buchkovich, N. L. Heard-Costa, T. S. Roman, A. W. Drong, C. Song, S. Gustafsson, F. R. Day, T. Esko, T. Fall, Z. Kutalik, J. Luan, J. C. Randall, A. Scherag, S. Vedantam, A. R. Wood, J. Chen, R. Fehrmann, J. Karjalainen, B. Kahali, C. T. Liu, E. M. Schmidt, D. Absher, N. Amin, D. Anderson, M. Beekman, J. L. Bragg-Gresham, S. Buyske, A. Demirkan, G. B. Ehret, M. F. Feitosa, A. Goel, A. U. Jackson, T. Johnson, M. E. Kleber, K. Kristiansson, M. Mangino, I. M. Leach, C. Medina-Gomez, C. D. Palmer, D. Pasko, S. Pechlivanis, M. J. Peters, I. Prokopenko, A. Stancakova, Y. J. Sung, T. Tanaka, A. Teumer, J. V. Van Vliet-Ostaptchouk, L. Yengo, W. Zhang, E. Albrecht, J. Arnlov, G. M. Arscott, S. Bandinelli, A. Barrett, C. Bellis, A. J. Bennett, C. Berne, M. Bluher, S. Bohringer, F. Bonnet, Y. Bottcher, M. Bruinenberg, D. B. Carba, I. H. Caspersen, R. Clarke, E. W. Daw, J. Deelen, E. Deelman, G. Delgado, A. S. Doney, N. Eklund, M. R. Erdos, K. Estrada, E. Eury, N. Friedrich, M. E. Garcia, V. Giedraitis, B. Gigante, A. S. Go, A. Golay, H. Grallert, T. B. Grammer, J. Grassler, J. Grewal, C. J. Groves, T. Haller, G. Hallmans, C. A. Hartman, M. Hassinen, C. Hayward, K. Heikkila, K. H. Herzig, Q. Helmer, H. L. Hillege, O. Holmen, S. C. Hunt, A. Isaacs, T. Ittermann, A. L. James, I. Johansson, T. Juliusdottir, I. P. Kalafati, L. Kinnunen, W. Koenig, I. K. Kooner, W. Kratzer, C. Lamina, K. Leander, N. R. Lee, P. Lichtner, L. Lind, J. Lindstrom, S. Lobbens, M. Lorentzon, F. Mach, P. K. Magnusson, A. Mahajan, W. L. McArdle, C. Menni, S. Merger, E. Mihailov, L. Milani, R. Mills, A. Moayyeri, K. L. Monda, S. P. Mooijaart, T. W. Muhleisen, A. Mulas, G. Muller, M. Muller-Nurasyid, R. Nagaraja, M. A. Nalls, N. Narisu, N. Glorioso, I. M. Nolte, M. Olden, N. W. Rayner, F. Renstrom, J. S. Ried, N. R. Robertson, L. M. Rose, S. Sanna, H. Scharnagl, S. Scholtens, B. Sennblad, T. Seufferlein, C. M. Sitlani, A. V. Smith, K. Stirrups, H. M. Stringham, J. Sundstrom, M. A.

Swertz, A. J. Swift, A. C. Syvanen, B. O. Tayo, B. Thorand, G. Thorleifsson, A. Tomaschitz, C. Troffa, F. V. van Oort, N. Verweij, J. M. Vonk, L. L. Waite, R. Wennauer, T. Wilsgaard, M. K. Wojczynski, A. Wong, Q. Zhang, J. H. Zhao, E. P. Brennan, M. Choi, P. Eriksson, L. Folkersen, A. Franco-Cereceda, A. G. Gharavi, A. K. Hedman, M. F. Hivert, J. Huang, S. Kanoni, F. Karpe, S. Keildson, K. Kiryluk, L. Liang, R. P. Lifton, B. Ma, A. J. McKnight, R. McPherson, A. Metspalu, J. L. Min, M. F. Moffatt, G. W. Montgomery, J. M. Murabito, G. Nicholson, D. R. Nyholt, C. Olsson, J. R. Perry, E. Reinmaa, R. M. Salem, N. Sandholm, E. E. Schadt, R. A. Scott, L. Stolk, E. E. Vallejo, H. J. Westra, K. T. Zondervan, A. D. Consortium, C. A. D. Consortium, C. K. Consortium, G. Consortium, G. Consortium, Glgc, Icbp, C. International Endogene, S. LifeLines Cohort, M. Investigators, T. C. Mu, P. Consortium, C. ReproGen, P. Amouyel, D. Arveiler, S. J. Bakker, J. Beilby, R. N. Bergman, J. Blangero, M. J. Brown, M. Burnier, H. Campbell, A. Chakravarti, P. S. Chines, S. Claudi-Boehm, F. S. Collins, D. C. Crawford, J. Danesh, U. de Faire, E. J. de Geus, M. Dorr, R. Erbel, J. G. Eriksson, M. Farrall, E. Ferrannini, J. Ferrieres, N. G. Forouhi, T. Forrester, O. H. Franco, R. T. Gansevoort, C. Gieger, V. Gudnason, C. A. Haiman, T. B. Harris, A. T. Hattersley, M. Heliovaara, A. A. Hicks, A. D. Hingorani, W. Hoffmann, A. Hofman, G. Homuth, S. E. Humphries, E. Hypponen, T. Illig, M. R. Jarvelin, B. Johansen, P. Jousilahti, A. M. Jula, J. Kaprio, F. Kee, S. M. Keinanen-Kiukaanniemi, J. S. Kooner, C. Kooperberg, P. Kovacs, A. T. Kraja, M. Kumari, K. Kuulasmaa, J. Kuusisto, T. A. Lakka, C. Langenberg, L. Le Marchand, T. Lehtimaki, V. Lyssenko, S. Mannisto, A. Marette, T. C. Matise, C. A. McKenzie, B. McKnight, A. W. Musk, S. Mohlenkamp, A. D. Morris, M. Nelis, C. Ohlsson, A. J. Oldehinkel, K. K. Ong, L. J. Palmer, B. W. Penninx, A. Peters, P. P. Pramstaller, O. T. Raitakari, T. Rankinen, D. C. Rao, T. K. Rice, P. M. Ridker, M. D. Ritchie, I. Rudan, V. Salomaa, N. J. Samani, J. Saramies, M. A. Sarzynski, P. E. Schwarz, A. R. Shuldiner, J. A. Staessen, V. Steinthorsdottir, R. P. Stolk, K. Strauch, A. Tonjes, A. Tremblay, E. Tremoli, M. C. Vohl, U. Volker, P. Vollenweider, J. F. Wilson, J. C. Witteman, L. S. Adair, M. Bochud, B. O. Boehm, S. R. Bornstein, C. Bouchard, S. Cauchi, M. J. Caulfield, J. C. Chambers, D. I. Chasman, R. S. Cooper, G. Dedoussis, L. Ferrucci, P. Froguel, H. J. Grabe, A. Hamsten, J. Hui, K. Hveem, K. H. Jockel, M. Kivimaki, D. Kuh, M. Laakso, Y. Liu, W. Marz, P. B. Munroe, I. Njolstad, B. A. Oostra, C. N. Palmer, N. L. Pedersen, M. Perola, L. Perusse, U. Peters, C. Power, T. Quertermous, R. Rauramaa, F. Rivadeneira, T. E. Saaristo, D. Saleheen, J. Sinisalo, P. E. Slagboom, H. Snieder, T. D. Spector, K. Stefansson, M. Stumvoll, J. Tuomilehto, A. G. Uitterlinden, M. Uusitupa, P. van der Harst, G. Veronesi, M. Walker, N. J. Wareham, H. Watkins, H. E. Wichmann, G. R. Abecasis, T. L. Assimes, S. I. Berndt, M. Boehnke, I. B. Borecki, P. Deloukas, L. Franke, T. M. Frayling, L. C. Groop, D. J. Hunter, R. C. Kaplan, J. R. O'Connell, L. Qi, D. Schlessinger, D. P. Strachan, U. Thorsteinsdottir, C. M. van Duijn, C. J. Willer, P. M. Visscher, J. Yang, J. N. Hirschhorn, M. C. Zillikens, M. I. McCarthy, E. K. Speliotes, K. E. North, C. S. Fox, I. Barroso, P. W. Franks, E. Ingelsson, I. M. Heid, R. J. Loos, L. A. Cupples, A. P. Morris, C. M. Lindgren and K. L. Mohlke (2015). "New genetic loci link adipose and insulin biology to body fat distribution." Nature **518**(7538): 187-196.

Smith, G. I., B. Mittendorfer and S. Klein (2019). "Metabolically healthy obesity: facts and fantasies." J Clin Invest **129**(10): 3978-3989.
Spallanzani, R. G., D. Zemmour, T. Xiao, T. Jayewickreme, C. Li, P. J. Bryce, C. Benoist and D. Mathis (2019). "Distinct immunocyte-promoting and adipocyte-generating stromal components coordinate adipose tissue immune and metabolic tenors." Sci Immunol **4**(35).
Stefan, N., A. L. Birkenfeld and M. B. Schulze (2021). "Global pandemics interconnected - obesity, impaired metabolic health and COVID-19." Nat Rev Endocrinol **17**(3): 135-149.
Stefkovich, M., S. Traynor, L. Cheng, D. Merrick and P. Seale (2021). "Dpp4+ interstitial progenitor cells contribute to basal and high fat diet-induced adipogenesis." Mol Metab **54**: 101357.
Street, K., D. Risso, R. B. Fletcher, D. Das, J. Ngai, N. Yosef, E. Purdom and S. Dudoit (2018). "Slingshot: cell lineage and pseudotime inference for single-cell transcriptomics." BMC Genomics **19**(1): 477.
Sun, K., C. M. Kusminski and P. E. Scherer (2011). "Adipose tissue remodeling and obesity." J Clin Invest **121**(6): 2094-2101.
Sweeting, A., J. Wong, H. R. Murphy and G. P. Ross (2022). "A clinical update on Gestational Diabetes Mellitus." Endocr Rev.
Tam, W. H., R. Ching, Wan Ma and J. C. N. Chan (2017). "<In Utero Exposure to Maternal Hyperglycemia Increases Childhood Cardiometabolic Risk in Offspring.pdf>."
Tam, W. H., R. C. Ma, X. Yang, G. T. Ko, P. C. Tong, C. S. Cockram, D. S. Sahota, M. S. Rogers and J. C. Chan (2008). "Glucose intolerance and cardiometabolic risk in children exposed to maternal gestational diabetes mellitus in utero." Pediatrics **122**(6): 1229-1234.
Tang, Q.-Q., T. C. Otto and M. D. Lane (2004). "<Commitment of C3H10T12 pluripotent stem cells to the adipocyte lineage.pdf>." PNAS.
Tang, W., D. Zeve, J. M. Suh, D. Bosnakovski, M. Kyba, R. E. Hammer, M. D. Tallquist and J. M. Graff (2008). "White fat progenitor cells reside in the adipose vasculature." Science **322**(5901): 583-586.
Tchkonia, T., N. Giorgadze, T. Pirtskhalava, T. Thomou, M. DePonte, A. Koo, R. A. Forse, D. Chinnappan, C. Martin-Ruiz, T. von Zglinicki and J. L. Kirkland (2006). "Fat depot-specific characteristics are retained in strains derived from single human preadipocytes." Diabetes **55**(9): 2571-2578.
Tontonoz, P., E. Hu and B. M. Spiegelman (1994). "Stimulation of adipogenesis in fibroblasts by PPAR gamma 2, a lipid- activated transcription factor." Cell **79**(7): 1147-1156.
Unger, R. H. (2005). "Longevity, lipotoxicity and leptin: the adipocyte defense against feasting and famine." Biochimie **87**(1): 57-64.
Van, R. L., C. E. Bayliss and D. A. Roncari (1976). "Cytological and enzymological characterization of adult human adipocyte precursors in culture." J Clin Invest **58**(3): 699-704.

Van Robin, L. and D. A. Roncari (1977). "Isolation of fat cell precursors from adult rat adipose tissue." Cell and tissue research **181**(2): 197-203.
Vishvanath, L. and R. K. Gupta (2019). "Contribution of adipogenesis to healthy adipose tissue expansion in obesity." J Clin Invest **129**(10): 4022-4031.
Vishvanath, L., K. A. MacPherson, C. Hepler, Q. A. Wang, M. Shao, S. B. Spurgin, M. Y. Wang, C. M. Kusminski, T. S. Morley and R. K. Gupta (2016). "Pdgfrbeta+ Mural Preadipocytes Contribute to Adipocyte Hyperplasia Induced by High-Fat-Diet Feeding and Prolonged Cold Exposure in Adult Mice." Cell Metab **23**(2): 350-359.
Wang, F., S. E. Mullican, J. R. DiSpirito, L. C. Peed and M. A. Lazar (2013). "Lipoatrophy and severe metabolic disturbance in mice with fat-specific deletion of PPARgamma." Proc Natl Acad Sci U S A **110**(46): 18656-18661.
Wang, Q. A., C. Tao, R. K. Gupta and P. E. Scherer (2013). "Tracking adipogenesis during white adipose tissue development, expansion and regeneration." Nat Med **19**(10): 1338-1344.
Wang, W., J. Ishibashi, S. Trefely, M. Shao, A. J. Cowan, A. Sakers, H. W. Lim, S. O'Connor, M. T. Doan, P. Cohen, J. A. Baur, M. T. King, R. L. Veech, K. J. Won, J. D. Rabinowitz, N. W. Snyder, R. K. Gupta and P. Seale (2019). "A PRDM16-Driven Metabolic Signal from Adipocytes Regulates Precursor Cell Fate." Cell Metab **30**(1): 174-189 e175.
Westcott, G. P., M. P. Emont, J. Li, C. Jacobs, L. Tsai and E. D. Rosen (2021). "Mesothelial cells are not a source of adipocytes in mice." Cell Rep **36**(2): 109388.
Wolins, N. E., B. K. Quaynor, J. R. Skinner, A. Tzekov, C. Park, K. Choi and P. E. Bickel (2006). "OP9 mouse stromal cells rapidly differentiate into adipocytes: characterization of a useful new model of adipogenesis." J Lipid Res **47**(2): 450-460.
Wu, Y., Y. Ruan, L. Shen and Q. Gong (2017). "<Protective effects of PPAR-γ against pregnancy-induced hypertension by differential ETR expression in rat models.pdf>."
Yaris, F., E. Yaris, M. Kadioglu, C. Ulku, M. Kesim and N. I. Kalyoncu (2004). "Normal pregnancy outcome following inadvertent exposure to rosiglitazone, gliclazide, and atorvastatin in a diabetic and hypertensive woman." Reprod Toxicol **18**(4): 619-621.